UNIVERSITÀ DI TRENTO
Department of Industrial Engineering
XXXII cycle

Doctoral School in Materials, Mechatronics and Systems Engineering

Numerical models for the simulation of shot peening induced residual stress fields: from flat to notched targets

Michelangelo Marini

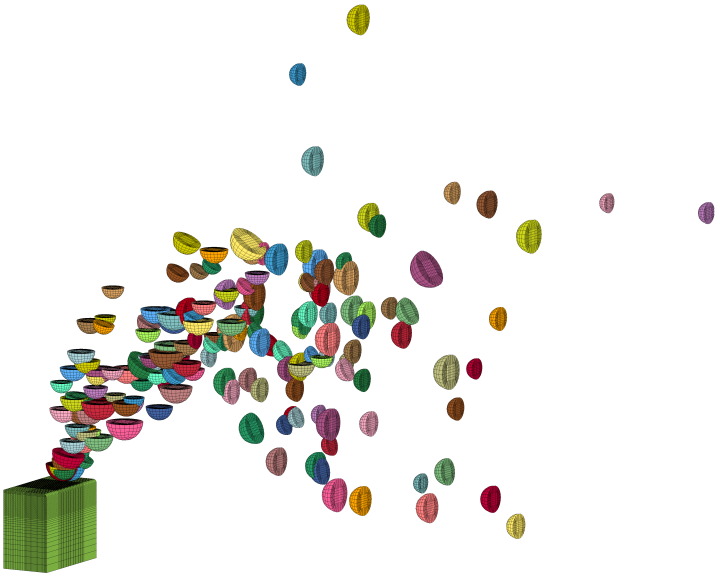

10th June 2020

Numerical models for the simulation of shot peening induced residual stress fields: from flat to notched targets

Michelangelo Marini

e-mail: m.marini@unitn.it

Approved by:

Prof. Vigilio Fontanari, advisor
Department of Industrial Engineering
University of Trento, Italy.

Prof. Matteo Benedetti, advisor
Department of Industrial Engineering
University of Trento, Italy.

Ph.D Commission:

Prof. Alberto Molinari,
Department of Industrial Engineering
University of Trento, Italy

Prof. Leonardo Bertini,
Department of Mechanical, Nuclear and Production Engineering
Pisa University, Italy

Prof. Filippo Berto,
Department of Mechanical and Industrial Engineering
Norwegian University of Science and Technology (NTNU), Norway

University of Trento,
Department of Industrial Engineering

10^{th} June 2020

University of Trento - Department of Industrial Engineering

Doctoral Thesis

Michelangelo Marini - 2020
Published in Trento (Italy) - by University of Trento

A chi lo sa

Abstract

Shot peening is a cold-working surface treatment, basically consisting in pelting the surface of the to-be-treated component with a high number of small hard particles blown at relatively high velocity. This causes the plasticization of the surface layer of the substrate, and the generation of a compressive residual stress field beneath the component surface. The surface topology modification can be beneficial for coating adhesion, and the work hardening enhances the fretting resistance of components, but the most commonly appreciated advantage of the process is the increased fatigue resistance in the treated component, due to the compressive residual stress which inhibits the nucleation and propagation of fatigue cracks. In spite of its widespread use, the mechanisms underlying the shot peening process are not completely clear. Many process parameters are involved (material, dimension, velocity of the shots, coverage, substrate mechanical behavior) and their complex mutual interaction affects the success of the process as well as the jeopardizing of any beneficial effect due to the increased surface roughness. Experimental measurements are excessively expensive and time-costly to deal with the wide variability of the process parameters, and their feasibility is not always granted. The effect of shot peening is indeed particularly effective where geometrical details (e.g. notches or grooves) act as stress raisers and where the direct measurement of residual stresses is very difficult. Nonetheless, the knwoledge of the effects of the treatment in this crictical locations would be extremely useful for the quantitative assessment of the effect of shot peening and, ultimately, for the optimization fo the process as well as its complete integration in the design process.

The implementation of the finite element method for the simulation of shot peening has been studied since many years. In this thesis the simulation of shot peening is studied, in order to progress towards a simulation approach to be used in the industrial practice. Specifically, the B120 micro shot peening treatment performed with micrometric ceramic beads is studied, which has proven to be very effective of aluminum alloys, such as the aeronautical grade Al7075-T651 alloy considered in this work.

The simulation of shot peening on a flat surface is addressed at first.

The nominal process parameters are used, to include stochastic variability of the shot dimensions and velocity. A MatLab routine based on the linearization of the impact dent dimension, on the shot dimension and velocity is used to assess the coverage level prior to the simulation and predict the number of shots to full coverage. To best reproduce the hardening phenomena of the substrate material under repeated impacts, the Lemaitre-Chaboche model is tuned on cyclic strain tests. Explicit dynamic finite element simulations are carried out and the statistical nature of the peening treatment is taken into account. The results extracted from the numerical analyses are the final surface roughness and residual stresses, which are compared to the experimentally measured values. A specific novel procedure is devised to account for the effect of surface roughness and radiation penetration in the in-depth residual stress profile. In addition, a static finite element model is devised to assess the concentration effect exerted by the increased surface roughness on an external stress.
The simulation of shot peening on an edge is then addressed as a first step towards more complex geometries. Since the true peening conditions are not known in this locations, a synergistic discrete element - finite element method approach is chosen for the correct modelization of the process. A discrete element model of the peening process on a flat surface is used to tune the simulation on the nominal process parameters, i.e. mass flow rate and average shot velocity, and to assess the nozzle translational velocity. Discrete element simulations are used to simulate the process when the nozzle turns around the edge tip. To lower the computing cost, the process is linearized into static-nozzle simulations at different tilting angles. The number of impacting shots and their impact velocity distribution are used to set up the finite element simulations, from which the resulting residual stress field is obtained. In addition to the realistic simulation, two simplified simulation approaches for the practical industrial use are devised. The resulting residual stress fields are compared with the reference residual stress field computed using thermal fields in a finite element simulation, tuned with experimental XRD measurements. The effect of the dimension of the fillet on the edge tip is studied by modifying the finite element model of shot peening on an edge. 3 different fillet radii (up to 40 µm) are considered, on the basis of experimental observations. The resulting residual stress field are compared to analyze

the effect of the precise geometry of the substrate. Lastly, the simplified simulation approach devised in the case of the edge is used to simulate shot peening on the root of a notch. The resulting residual stress field is again compared to the reconstructed reference one.

Contents

Chapter 1

Introduction

1.1 Shot peening

Shot peening (SP) is a cold-working surface finishing treatment, widely used in many applications of the industrial, automotive, energy and biomedical fields, mainly to enhance fatigue resistance of mechanical component. The original hammering process is known since ancient times of the human craftmanship [1] to shape metallic manufacts and relieve residual stresses (RSs) after their manufacturing. SP is an advanced version of hammering, which basically consists in blowing small hard particles at relatively high velocity onto the surface of the component to be treated [2], [3] (Figure 1.1).

Figure 1.1: Dome tank segment of the ESA Ariane 5 during SP treatment, picture from [4]

As in the case of hammering, the impacts cause the plastic deformation of a layer on the surface of the component, which, in the case

of SP, is relatively thin. The underneath material is only elastically deformed, so that, when the impacting body bounces off, tends towards a spring back compensation[5], as schematichally represented in Figure 1.2. Therefore, SP produces two main effects in the treated

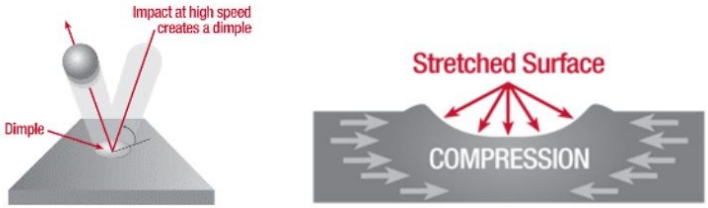

Figure 1.2: Schematic representation of the RS generation mechanism in SP, picture from [6]

component: a modification of the surface layer and the generations of a RS field. Surface layer modification include increased roughness due to indentations, increased surface hardness due to work hardening of the hardness, and a finer microstructure. The RSs do cause an intense compression in a thin layer directly under the surface, having its maximum magnitude slightly under the impacted surface, and slight residual tensile stress in a deeper still thicker layer [7], [8] (Figure 1.3).

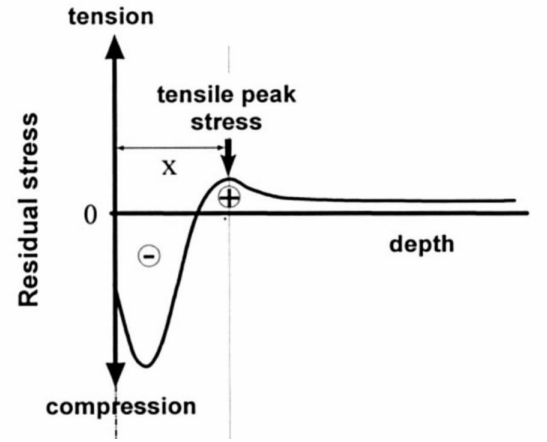

Figure 1.3: In-depth RS profile caused by the SP treatment.

The combinaton of the RS field in the substrate [9], [10], the in-

creased hardness and the finer grain microstructure in the surface layer [11], [12] enhances the fatigue resistance of the treated components (Figure 1.4) by inhibiting the nucleation of fatigue cracks and the propagation of the existing ones. The effectiveness of SP in improving the fatigue resistance of mechanical parts through this mechanism is the reason why this process has become so popular in a few years after its invention.

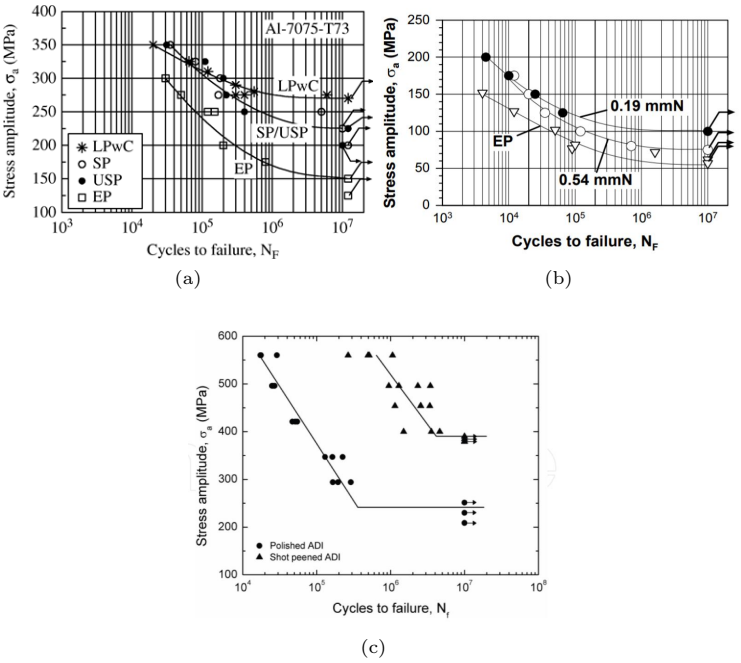

Figure 1.4: Effect of different SP treatments on the fatigue resistance of (a) aluminum alloy [13], (b) titanium alloy [14] and (c) austempered ductile iron [15].

Nowadays, many variants of the conventional SP process are used to promote specific desirable effects of the treatment in a variety of applications [16]. The most widely used processes are known as ultrasonic shot peening (USSP) [17], sandblasting and annealing [18], high energy shot peening (HESP) [19], severe shot peening (SSP) [12], [20], surface nanocrystallization and hardening (SNC, SNH) [21], [22], sur-

face mechanical attrition treatment (SMAT) [23], ultrasonic impact treatment (UIT) [24], ultrasonic impact peening (UIP)[25], and laser peening (LP)[26]. It is worth noting that all these treatments rely basically on the same principle (plasticize the surface to modify its morphology and introduce RSs) and some of them do share also the same process setup. The main differences are in the specific results they are aimed at obtaining.

On the other hand, as said, impacts do modify the surface morphology and increase the surface roughness. This effects may be negligible in some applications [27] or even desirable for some cases; an increased surface roughness, in fact, can enhance the adesion of coatings [28], [29] or biological tissue on the component surface, as in case of orthopaedic protheses [30], [31]. Nevertheless, SP is performed most of the times to the aim of improving the fatigue resistance of mechanical parts under fatigue loads, and in this case surface roughness is well known to be detrimental for the fatigue behavior of mechanical parts. Beyond surface roughening, the effects of SP on the surface can be far heavier. Repeated impacts on the peened surface do cause severe work hardening of the surface layer [10], and intense treatments with very high coverage may also lead to deep microstructural modifications of the substrate surface, up to grain recrystallization [32], [33]. In any case, even when a standard SP process is performed, a delicate balancing of the effects of the treatment is to be pursued. Gentler peening may indeed be more effective in enhancing the fatigue resistance than a stronger one, according to the substrate material [34], [35]. In some cases, SP may even exert a detrimental effect of the fatigue life of treated components [9], [36]–[40]. This is probably due, above other factors, to the increase in the surface roughness [41], which is detrimental for the fatigue resistance since it promotes stress concentration in some locations on the surface, which can act as preferential nucleation points for cracks. The RS field generated by SP in components, under suitable loading conditions, may cause the crack to initiate in the subsurface layer of the component [42]–[46] which causes very dangerous situations since it make impossible to early detect cracks through visual inspection or similar methods. Thus, for correctly performing an effective and fitting SP treatment, the correct choice of the process parameters is *extremely* important.

1.2 SP simulation

When SP is appropriately set up and performed, the complex interaction of the the phenomena occurring in the substrate, explained in some more detail in Section 2.1, may exert beneficial effects on the fatigue resistance, corrosion cracking resistance and wear performances of the treated components. Howbeit, despite the wide diffusion and longtime usage of SP in the industrial practice, neither the effect of each process parameter on the final results nor their mutual interaction is still completely clear. In addition, it is worth to point out that the final result is strongly dependant on the mechanical behavior of the substrate material, which adds to the problem an additional degree of freddom with a wide interval of variability. The choice of the best process is often referred to the empirical knowledge of the shot peener and the result can not be predicted with adequate precision. Moreover, not only RS measurement are always destructive (hole-drilling, x-ray diffraction, contour method), but they are also too expensive and time consuming to be used in extensive experimental campaigns having the aim of exploring the effects of all the process parameters. In addition, it is worth noting that SP is particularly effective in the case of components carrying geometrical details acting as stress raisers [47]–[50], such us grooves or notches. In this case, due to the thinnes of the layer in which RS are generated in the substrate (tens of µm to 1 mm) and to the geometry of the substrate itself, RS measurement in the vicinity of critical spots are, in many cases, not even feasible. On the other hand, a better understanding of the mechanisms whereby SP enhances the fatigue resistance, particularly for components having notches or grooves, is of paramount importance for designers, who would benefit gretly from a quantitative assessment of the effect of SP in the fatigue prognosis of machine parts. Until now, the effect of SP is generally neglected during the fatigue calculation (a choice in favor of component safety) or incorporated in the form of empirical coefficients. A quantitative and precise *a priori* knowledge of the RS state in a peened component would allow the designers to apply optimized design methods, capable of fully exploiting the enhanced fatigue resistance.

Attempts in this direction have been made by some authors in recent years. You et al. managed to devise numerical simulations to take

into account the RS state generated by SP in the computation of the crack growth both in samples [51] and in real components [52]. Eriksson et al. [53] experimentally studied the effect of shot peening on the fatigue life of a real component, while the work of Salvati et al. [54] showed the scientific interest in taking into account the RS coming from SP also in additively manufactured components.

Analytical or semianalytical approaches to relate the process parameters of SP to its results have been studied by some authors. Shen et al. [55] developed an analytical model to compute RS in peened parts, considering a single impacting shot, according to the Hertzian contact theory with simplified elasto-plastic material model. Guechichi et al. [56], and similarly Miao et al. [57], extended the same approach to the computation of the arc height in an Almen strip, to simulate an Almen test. Chaise et al. [58] used a combined analytical-FEM approach based on the FEM simulation of a single impinging shot to predict the interaction of closely impacting shots in an Almen test for the USP process. Korsunsky[59] aimed at creating a predictive model for RS due to SP based on eigenstrains. As a further development, Achintha et al. [60] developed a model to compute the RS in a finite component using eigenstrains obtained from a single impact finite element (FE) simulation. Zhang et al. [61] developed an analytical model to predict bending deformation in peen formed plates, based on experimental measurements of single impact indentations. Similarly, Faucheaux et al. [62] studied the RS and deformations in peen formed plates using eigenstrains obtained from FE analysis od the SP process. These methods, in spite of being (in some cases) very elegant solutions to the probelm, do have some limitations. Analytical methods require very simple material models or do have a strong dependance on numerical methods to take into account the nonlinear effects of plastic deformation. In pratice, however, substrate materials do present complex mechanical behavior which requires the material model to be capable of account for peculiar phenomena such as strain softening (*Bauschinger effect*) or strain rate sensitivity. Semianalytical methods usually require prior numerical analyses, which make the model not self-supporting. Moreover, on the RS field developing due to SP on easy geometries (flat surface) can be faced through an analytical approach; surface morphology modifications or more complex geometries require other tools or a semi-empirical approaches

which need to rely on experimental data whose criticality has already been hilighted. Introducing coverage as a variable in an analytical model is also a hard task, and none of the previously referred studies considered a condition other than full coverage. Last but not least, analytical methods require a precise knowledge of the *true* process parameters (not the nominal ones), to be related to the results. This is not an easy-to-fulfill requirement, especially when parts with complex geometrical features are treated.

In the light of these considerations, it appears evident how numerical simulation can be an effective and powerful tool to deal with the study of SP. In particular, FE method or analysis (FEM, FEA) can be used to simulate the SP process to predict the results on the substrate material, both in terms of RSs and surface layer modifications. Simulations can be extremely convenient with respect to the extensive experimental study of the many variables involved, in order to devise a time and cost saving approach. They are extremely flexible, and can be used to study the specific effect of *each* process parameter on *any* substrate, their mutual interaction, and the effect of coverage related to the mechanical behavior of the treated material. Simulations can be even more effectve than experimental measurements when it comes to study the true peening condition and effects in the vicinity of small or very small geometrical details, such us grooves or notches, where narrow spaces and geometrical discontinuities represent are sometimes insurmuntable obstacles to the measurement. Moreover, the data regarding the effects of SP obtained from FE simulations are easy to integrate in the design process, in order to optimize the design process even for fatigue dimensioning.

In recent years, many authors have focused on the study of the numerical simulation of SP, as will be discussed in detail in the next Chapter 2. The first attempts at simulating SP have been made in the early times of FEA on computers, with extremely simplified models and coarse (still disruptive) results. Simulations have become more and more complex and realistic in recent years, together with the increase in computational performances of computers. Clearly, in order to have trustworthy simulations it is necessary to devise an appropriate model of the SP process. Moreover, it is required a precise knowledge of the peening conditions of the component, and most of all, it is essential to validate the model by comparison with experi-

mental results, at least in the cases when experimental measurements are possible.

Modelling SP in not an easy task: the process involves a high number of variables and it needs to be simplified; at the same time it is essential to point out and preserve the significant parameters in order to avoid oversimplification of the problem. First of all, a high number of shots do impact on the target with in rapid dynamic conditions. Then, the mechanical behavior of the substrate material needs to be adequately represented in complex strain conditions, with repeated impacts and cyclic strain. Since it is inconceivable to exactly study and model the process in each detail, the simulation has also to deal with statistical variability of some parameters, due to the stochastic nature of this (as well as any other) process. As will be shown, the correct representation of coverage is challenging, also due to the disputable measurement method used in practice. The true peening conditions, i.e. mainly the true velocity of impacting shots, is not always known for sure, particularly when SP is performed in the vicinity of geometrical features and not on a flat surface. Last but not least, to correctly capture the RS generated in the target or, even worse, its surface morphology modification, a very fine mesh is required in the FE model, which make the computational cost a hard rival to deal with.

The aim of this study is to develop a model (or rather a procedure) to simulate SP using FEM. The model is aimed at being as most realistic as possible, still using only widespread computational tools (i.e. a powerful yet common workstation PC) in order to devise a procedure which the industrial practice can easily benefit from.

The chosen SP treatment is the B120 micro shot peening (μSP) with micrometric ceramic beads. As will be seen in detail in Chapter 3, the process is performed using ceramic beads (a mixture of zirconia and silica) having a nanometric diameter (50÷120 µm), on aeronautical grade Al-alloy samples (Al7075-T651) to full coverage (100%). This treatment has proved to be very effective in improving the fatigue resistance of aluminum alloys (with respect to stronger SP using conventional steel shots) as it gives a shallow and intense compressive RS peak without excessive surface roughening [35], [50], [63]–[65].

The first part of the work will be focused on the simulation of SP on a flat surface. The analysis will be carried out paying attention

to the correct representation of the statistical phenomena involved in the process. A FE model with be devised, consisting in a target prismatic body and a number of shots having variable dimension and velocity according to the experimental measurement provided by the shot peener. A MatLab script will be devised and used to compute the number of shots needed to achieve full coverage, with randomly arranged impact locations. The results will be used to compute the resulting in-depth RS profile and the final surface roughness of the peened target.

The second part of the work will be focused on the simulation of SP on an edge, as a first step towards the simulation of SP on complex geometrical features. As will be showed later in more detail, true SP condition are not known in the vicinity of geometrical features, and they can have a great influence on the final result of the process. A discrete element (DE) model will be used to simulate the air-blowing nozzle of the peening machine, and obtain the true process condition on an edge. FE models, based on the previous results, will be devised to compute RSs in the target for different scenarios. The role of the fillet of the tip of the edge will be analized as well, and its importance will become clear.

Finally, an attempt will be made to simulate SP in the root of a sharp notch, again using DE simulations to set up FEA.

The thesis will be organized as follows.

In Chapter 2, a review of the scientific literature on the topic of the simulation of SP will be presented, to show a brief history of the modelling strategies used to simulate SP and to update the reader about the state of the art in this field.

Chapter 3 will report the details of the shot peening analyzed, as well as the experimental measurements used to characterize its results on the substrate, wich will be later used as a reference for the resuls of the simulations to be compared to.

Chapter 4 will be focused on the simulation of SP and its results. In Chapter 5, the simulation of SP on a corner and its results will be displaied and discussed.

In Chapter 6 the simulation of SP on an edge will be completed by studying the effect of the fillet radius on the edge tip, and the study will progress with the simulation of SP on a sharp notch and its results.

In Chapter 7, the work will be ended by discussing some conclusions and future advancements of the research field.

Chapter 2

Definition of some process parameters and state of the art in SP simulation

To better understand SP and its simulation, it is useful to sottle some definitions used to characterize the process. The next Section is devoted to the presentation of these definitions, as well as the main process parameters and their basic effect. In Section 2.2 the progress towards the simulation of SP will be continued with a review of the scientific literature in the field of the simulation of SP, up to the current state of the art.

2.1 Intensity, process parameters and coverage

The standard method used to assess the "strength" of the applied treatment is the so-called *Almen intensity*. The intensity is determined through a standard test called "Almen strip test"[66], regulated by the SAE J442 standard anche schematically shown in Figure 2.1. Essentialy, the chosen SP process is performed on one face of a tool steel strip with standard thickness and dimensions, clamped in four points. Since only one face of the strip is peened, once the clamps are removed the RS are not self equilibrated in the undeformed configuration. The strip bends in an arch-shape configuration in order to restore the internal equilibrium of stresses[67]–[69]. The deflection of the strip is measured and is used to compute the intensity of the SP

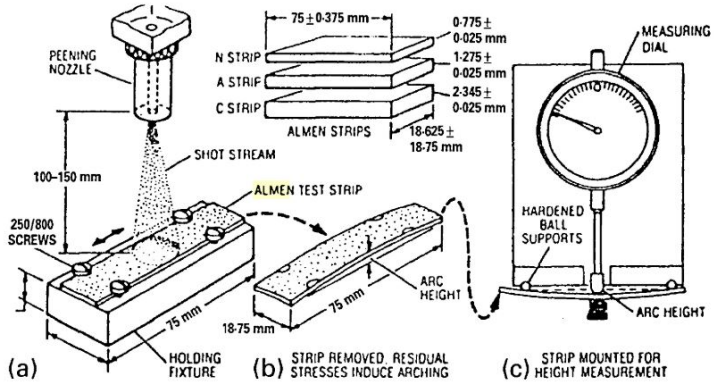

Figure 2.1: Example of increasing coverage on the surface of a peened component, picture from [67]

treatment. The intensity is eventually defined by a number (related to the deflection of the strip) and a letter N, A or C, according to the thickness of the strip (N for thin strips, C for thick strips) [70]. The Almen strip test is in the SP practice to compare different treatments, and its value is representative of the the real RS state in the Almen strip [57], [68]. Nonetheless, since the mechanical behaviour of most of the substrates is far from the one of the tool steel of the Almen strip, no further informations on the specific parameters and effects of SP can be retrieved from the intensity measure, so usually the parameters of the SP process need to be specified.

The process parameters involved in SP are many. Any SP treatment is characterized by the material of the peening media, its dimension (and shape) and velocity, its mass flow rate and a working distance and direction, i.e. te distance among the nozzle outlet of peening machine and the surface of the peened component and their mutual orientation.

The peening media has to be harder then the substrate, in order to plasticize the component surface without breaking or deforming, so that it can be collected and re-used for more than one treatment. Iron, steel, ceramic and glass are the materials used to produce peening media for most applications. Cylindrical steel particles are sometimes used due to the convenience of producing cut-wire peening media. Nevertheless, nowadays, spherical particles are widley more used

in all the SP treatments [71]. The dimension range for particles is extremely wide, with very thin particles (from 50 µm in diameter) for micro SP and way bigger particles (even some millimeters) for more intense treatments.

Also the blasting velocity is scattered over a relatively wide range between 30 m/s and 150 m/s according to the desired result and the compressed air system used to perform the treatment. Usually, treatments in the range 35 m/s ÷ 80 m/s are applied [57], [72].

Higher shot velocities or shot density do have similar effects, since they both end in insreasing the kinetic energy of the peening media. Increased peening energy do cause a higher resulting surface roughness [57], [73] and a deeper positioning of the compressive RS peak [69]

Some studies [74] suggest that mass flow rate may have a significant influence on the results of SP. A higher spatial density of shots could indeed increase the number of interaction among shots, and thus "disturbs" the flow of peening media; this causes the actual peening velocity to be far lower than the nominal one. A similar effect can be presumably ascribed to the working distance and direction. Nontheless, to the best knowledge of the autor, these parameters have not been thoroughly studied yet, and their choice is referred to the empirical knowldege of the shot peener.

Once the aforementioned treatment parameters are fixed, the process is performed on the component up to a preordered coverage level. Coverage is one of the most important parameters to characterize the process, and is defined as the fraction of surface plastically deformed by indentations over the total treated surface, as a percentage [75], [76] (Figure 2.2).

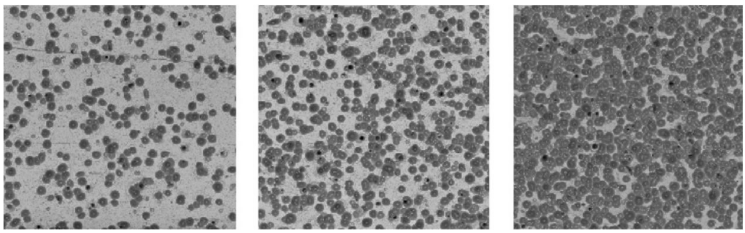

Figure 2.2: Example of increasing coverage on the surface of a peened component [77]

Coverage is a fundamental parameter in the SP process, since it is extremely influencing and is the way through which a specific treatment is modulated to achieve different results. The coverage level is measured by visual inspection or image analysis, in order to set up the process and adjust the massflow of peening media needed to achieve the desired result. Since completely indenting the whole surface is a demanding task due to the aleatory arrangement of the impacts [78], 100% (full) coverage is coventionally achieved when 98% of the treated surface is indented. For higher coverage levels the treatment duration is measured, i.e. to have 200% coverage the component is peened for double of the time required to achieve full coverage, keeping constant the process parameters [4], [79].

The most relatable effect of coverage is the resulting surface roughness on the substrate. According to experimental and simulation studies, when coverage increases the surface roughness also increases with a trend showing two (or three) main stages. In the first stage coverage is far lower than 100% and most of the surface is not indented; each impacting shot creates a new impact dimple and the surface roughness sharply increases with coverage. In the second stage, coverage approaches 100% and most of the surface is already indented. Thus, indentation of new impacts do partially or entirle superimpose to existing ones [71] and the surface roughness keeps increasing but with lesser slope [73], [78], [80]. Some authors refer a third stage, where roughness stops increasing and shows a plateau [57], or even a decrease[81]. Anyways, the third stage occurs when coverage is well over 100% and is easier to achieve if faster or bigger shots (i.e. having more impact energy) are used [57], [73]. Moreover, the trend of the resulting surface roughness also depends on the parameter used to characterize roughness (e.g. R_t, R_a or S_a) [73]. A similare trend is shown at increasing coverage for both intensity and RSs. Deflection of Almen strips shows a sharp increase with coverage up to 100% and a clear saturation for higher coverage level [58], [71], [82], [83]. Since RSs are related to the Almen intensity, as aforementioned, also the RS field gets to the saturation for coverage over 100%[67], [69], [84], [85]. Some slight variations on the depth of the maximum compressive RS and the thickness of the plastically deformed layer can be expected for higher coverage levels [68], [86], [87].

Analytically predict the number of impact (i.e. the treatment time)

to achieve the desired coverage level is a hard task. The simplest and most known one is directly derived from the Avrami equation [88], [89] by Kirk and Abyaneh [75]:

$$C = 100 \quad [1 - e^{-A_r}] \tag{2.1}$$

where C is the coverage level as a percentage, and A_r is the ratio of the indented surface over the total surface, thus $A_r = \frac{nA_i}{A_t}$ with A_i is the indentation area of a single impingement, A_t is the total to-be-peened area and n is the number of impacting shots from which the treatment time can be computed through the mass flow of peening media (Figure 2.3).

The Holdgate model [90] is more complex and extends the compu-

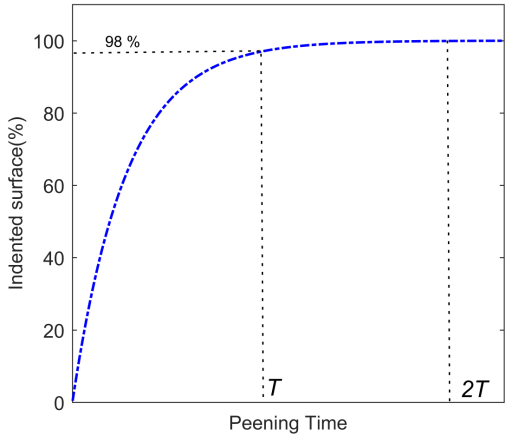

Figure 2.3: Indented surface vs peening time according to the Kirk and Abyaneh equation. T is the peening time to achieve nominal full coverage, $2T$ is the peening time for 200% coverage.

tation of coverage to a general peening sytem with multiple peening media sources:

$$C(t + \delta t) = 1 - [1 - C(t)] \prod_{j=1}^{N_s} (1 - \frac{A_j}{S})^{\delta N_j} \tag{2.2}$$

where $C(t)$ is the coverage elvel at a certain time t, δt a treatment time interval, N_s is the number of peening sources, A_j is the indented

area ascribable to the j-th peening source and δN_j is the number of impacts due to the j-th peening source in the δt time interval.
The two models are valid only for coverage within 100%. Experimental and simulation studies proved the Kirk and Abyaneh equation is accurate for vast surfaces (with respect to the indentation area), while it underestimates the coverage level in case of a low coverage level or total area over indent area ratio less than 10 [57], [76], [91]. To set up the Kirk adn Abyaneh model, it is required to determinate two parameters: the indentation area and the area where the impacts are spread. Clearly, the indentation area depends on the substrate material and its mechanical properties, as well as the shot impacting velocity, its dimension and weigth. A_i can be assessed by direct measurement as well as using empirical or semi-empirical formulas. On the other hand, despite being more adaptable and accurate, the Holdgate model requires the assessment of the coverage level at a certain peening time t. The main limitation of the Kirk and Abyaneh model lies in the fixed indentation area. Therefore, no variability in the shot dimension or impact velocity are considered, as well as work hardening in the substrate is neglected. Since overlapping indents are frequent in the SP process [81], [91], [92], work hardening may affect significantly the indent dimension when overlapping occurs. At the same time, shot dimension may be variable on a relatively wide range in some processes, and peening velocity is usually a nominal value (measured in the proximity of the nozzle outlet), whose relationship with the actual impacting velocity is still not precisely known.

2.2 Review of scientific literature on the simulation of SP

Simulation of SP has been an interesting research topic since when FE codes became a relatively widespread tool in research in the 80's. Very simplified models were devised at the time, due to the scarceness of available computational resources. Studies in this field became more and more popular with the increasing in the computational performances of computers in the late 90's, with a firm expansion in the last 15 years.
Simulating SP is a computationally-demanding task, since it requires

to take into account rapidly moving bodies which impact on a target involving strongly non-linear phenomena like plastic deformation, friction, huge deformations and others. For this reason, computational cost has been the main obstacle to the development of realistic models, and the reduction in the size of models has been the main concern of researchers in the early years of this research field. A robust increase in the computer performance even in widespread Pcs moved the focus of the simulation more on the correct and *coherent* representation of the process. Hereafter, a review of the main studies in the scientific literature is presented. Some words will be spent to present the earlier works in literature, for a better overview of the problem of simulating SP and a better depiction of the development of the solution found to address the problem until now. Later on, more recent works will be analyzed up to the depiction of the state of the art in this field.

The first known application of FE to simulating SP was made by Meguid et al. [93]. The study is aimed at exploring the effect of incomplete coverage, as frequently happens in the case of hard metals due to the diffuclty in exactly moniroting coverage. The analysis is based on the 2D model of two flat rigid punches indenting the flat surface of an elasto-plastic target, in quasi static regime. The resulting in-depth RS state, extracted from a single line of nodes in the middle of the target is presented as a function of the distance of the two punches and the indenting pressure. Despite its extreme semplification, the study highlights the eminent role played by work hardening in generating RSs, and the importance of the correct representation of the hardening behavior of the material.

Khabou et al. [94] studied the RS due to the impact of a rigid shot impacting on a target, using quasi-static 2D simulations. The contact pressure is assessed using analytical considerations based on the Hertzian theory. The in-depth RS is computed under the impact point in the simulation, and good accordance is found with the experimental measurements of RS generated by SP, at least in a qualitative way. A step forward was made by Al-Obaid [95], who simulated the impact of a single shot devising a 3D model both in quasi-static and in dynamic regime.

A sudden advancement in the simulations was introduced starting from the late 90's, due to the increase in computing power. Guagliano et al. [96] devised a 3D dynamic model of two rigid shots impacting on

an plane target body. Elastic behavior of the target is used to compare the impact pressures computed with FEM to the theroetical result of Hertz's thery, with a very matching result. A bilinear elasto-plastic model for the target is used to compute the RS generated by the impacts of two shots with partially superimposing indentations. Three substrate materials (with different yield stress and tangent modulus) are analyzed, for 4 shot dimension between 0.3 mm and 1 mm and 4 shot velocitie between 20 m/s and 120 m/s. RSs are computed by considering the row of nodes under the impact point of the first shot, and comapred to the experimental measurements. A similar model, with some improvements, was used by Guagliano et al. [68]. An increased number of shots (5) impacting in predetermined close locations is considered (Figure 2.4), and the target body is modelled as 1/4th of a circular plate with symmetry constaints. symmetry considerations. As in the previous study, different cases are considered

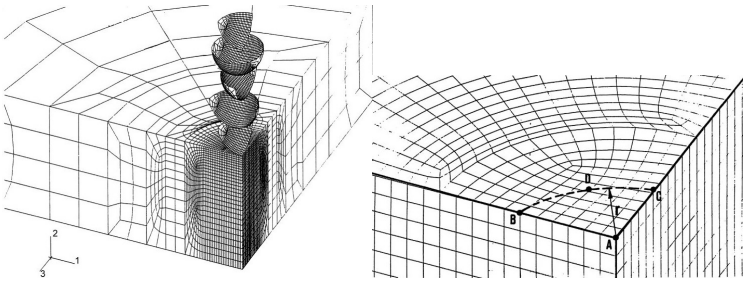

(a) (b)

Figure 2.4: Model used in [68]

for different shot velocity and dimension. RSs are computed in the center of the plate and clearly display the saturation effect of superimposed impacts, as weel as the influence exerted by close impacts on the resulting RS. The comparison of the effects due to different shot velocity or dimension is in good accordance with the trend already known and brefly mentioned in the previous chapter. Resulting RS are used in the study as an inout for the theretical model used to compute Almen intensity from the known RS state.

Meguid et al. [97] studied the impact of a spherical shot on a prismatic target body using a 3D. Exploiting symmetry, only 1/4th of the entire model is simulated. A rigid shot with 50 m/s, 75 m/s or 100 m/s

velocity is simulated to impact on the bilinear elasto-plastic target. The time evolution of contact force, contact point displacement and plastic strain is studied, as well as the effect of the shot radius and velocity, and the tangent modulus, on the depth of the compressed layer. An improved model, with two identical impacting shot is used by Meguid et al. [98] to simulate the effect of two shots impacting in a short distance. In this case, symmetry is used only on one face, so one half of the bodies is modeled. Two distances for the impact point are considered, i.e. equal to the shot radius of one half of the radius. The resultng RS field is computed in the nodes under the middle point between the two impact points; despite the coarseness of the analysis, the influence of closely impacting shots is clear and indisputable.
A milestone in the study of SP simulation was set by Meguid et al [99] with the introduction of the *symmetry cell* (Figure 2.5). To achieve a more realistic representation of the real process, the simulation consists in 4 rows of 4 identical shots (modeled a 1/8th of a sphere each, 16 impacts), impacting on the corners of a prismatic target using symmetry considerations.

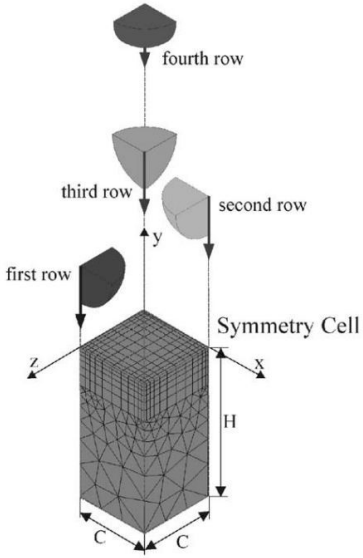

Figure 2.5: Scheme of the symmetry cell approach, picture from [99]

To simulate the effect of coverage the dimension of the cell side

C varies, and the ratio between the cell side and the shot radius is $C/R = 1, 1.5, 2$. No further considerations are made on the indent dimension of actual coverage of the surface. Simulations are carried out using isotropic strain hardening with or without strain rate sensitivity, with rigid and elastic shots having velocity in the range $25\,\mathrm{m/s} \div 100\,\mathrm{m/s}$. Resulting RS is computed considering vertical line of nodes in the cell vertex or on its side. Despite the approximated assessment of coverage, the results remark the influence of either strain rate sensitivity and deformability of shots. Saturation of RS (magnitude and depth) is found for increasing SP intensity (shot velocity). The most important result is the evident dishomogeneity in the RS field when impact locations of shots are far from each other, which becomes less evident when impact get closer.

An approach completely different from the symmetry cell was used by Dai et al. [81] to simualte SNH. A 3D model of 3 rigid shots impacting in close sites on a disc-shaped target is used to study the indent morphology and surface roughness after 1, 2 or 3 impacts. Interaction among the subsequent indents results in having a major role in the final surface morphology. A FEM simulation with a huge number (714) of rigid shots impacting on the same target in random impact locations is performed, but no considerations on the true coverage are made. The results are displaied to assess the final surface roughness of the processed target.

The study of Schwarzer et al. [100] highlights some interesting questionf in the modelization of SP. 38 rigid shots, with fixed velocity and equal dimension, impact on the surface of a target body, having their 19 impact locations in a hcp-like arrangement (Figure 2.6).

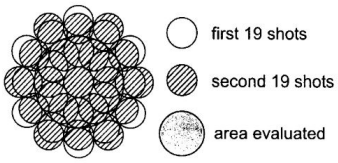

Figure 2.6: Scheme of the symmetry cell approach, picture from [100]

The impact order is varied in the simulations. The resulting RS field is shown to be strongly influenced by the impacting order of the shots. This highlights the stochastic nature of the SP process, and

the difficulty found in simplifying the model still mantaining a realistic representation of the phenomena. Moreover, in-depth RS profile in computed considering the average RS on an evaluation area, which is consistent with the area-averaged RS usually measured by XRD due to the dimension on measurement spot.

Majzoobi et al. [101] aimed at having the best representation of the material behavior considering strain rate sensitivity. The peened material (AISI4340 steel) is characterized at high strain rate using a the Hopkinson bar test, and the results are verified by comparing single shot experiments and 2D FEM simulations, with a very good match. The same approach devised in [99] is used for the FEM model, and simulations are carried out with an increasing number of impacts (4 to 25) in deterministic positions of the symmetry cell. All the shots have the same dimension and velocity. The importance of the material model used in the simulations is strongly asserted by the authors; simulations are run in LS-Dyna. RS are computed in various locations, considering in-depth node under chosen points on the symmetry cell surface. Results are displayed with the aim of clarify the effect of the increasing number of impacts, and the influence of the location used when the nodel RS is computed. RS are shown to saturate in the whole model, when an increasing number of shots impacts. At the same time, RS are strongly non-uniform in the model when few impacts are considered (low coverage) and get to a more uniform distribution at higher coverage. The RS in-depth profile matches with the "ideal" one only if the impact point of one shot is used to extract the results. It is worth noting that these results do stress the importance of a correct modeling of coverage, in order to have a uniform RS state, as well as a consistent method for computing the results in the whole model.

The study of Frija et al. [102] despite its basicness has some interesting aspects which will be analyzed also in the work presented in this thesis. A single shot simulation is used to represent SP, by supposing that the RS under the indent is representative of a 100% coverage condition: this neglects the interactions which have been proved to arise among the RSs generated by successively impacting shot. Nontheless, the material model used for the target is the Lemaitre-Chaboche model which is suitable to represent the material behavior in cyclic deformation. Moreover, the problem of variable dimension of the shots

in a nominal interval is raised, even if the nominal dimension is used. At last, a first analysis of the effect of shot-target friction on the final RS is presented.

Meguid et al. [103] based their work on a improved version of the symmetry cell, with a larger size; simulations are carried out in LS-Dyna. Elastic shots with fixed and equal dimension and velocity orthogonally impact in 13 deterministic positions of the symmetry cell. Simulations with 25, 50 or 100 shots are carried out in order to account for coverage. Isotropic hardening is considered for the steel target, as well as strain rate sensitivity. As in [99], RS are computed in 3 point of the symmetry cell, considering vertical lines of nodes. It is worth noting that saturation of RSs happens at increasing number of impacts, nut not in the case of strain rate sensitivity. RS show a significant dishomogeneity in the target according to the detection location. Deterministic arrangement of the impacts is recognized as a source of error, and the disuniformity in RS suggests the need for a more accurate assessment of the true coverage level of the surface.

Dai et al. [22] interestingly introduced randomly distributed impacts in simulating SNH of a Hastelloy target using WC spheres. Single shot 3D simualtions are used to study the evolution contact pressures and deformations in time, as well as the indent profile. A noticeable concept in the study is the devisement of a multi impact model, with 714 shot impacting on a disc-shape target in random locations. No assessment is made on the final true coverage level of the process; the final in-depth RS state is not validated as well. Nevertheless, this is the first DP simulation using randomly impacting shots as a realistic modelization of the process.

The first study of Hong et al. [104] is focused on the 3D simulation of a single impacting shot, with a parametric analysis of the effect of shot radius and velocity on the RS and deformation of the target. The effect of the yield stress and tangent modulus of the target is studied as well. Interestingly, the RS in-depth profile and the depth of the plastically deformed layer appear to remain steady if normalized over the dimension of the shot. The effect of the other parameters is confirmed to be pretty close to the expected results. The study of the RS and surface deformation caused by an inclined impact (60°), leads to important observation. The tangential velocity of the shots does not perturb significantly the final morphology of the indent, which

is only slightly asymmetryc. Difference in the indent and RS appears to be more ascribable to the decrease of normal velocity than to the presence of tangential velocity. A disruptive improvement in SP simulation is devised by the same authors with the introduction of DEM in the simulation of SP. An enhanced FEM model is created, with six shots impacting in the same location on a disc-shape target. The development of the RS field and the increasing thickness of the plastically deformed layer makes clear the importance of considering superimposing indents when simulating SP. For this purpose, a 3D simplified DEM model of the SP process, including the peening nozzle and the flat target surface, is devised (Figure 2.7). The core of

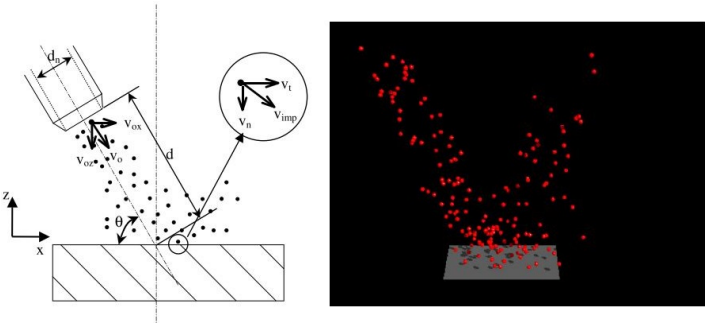

Figure 2.7: Scheme of the symmetry cell approach, picture from [104]

the model is a "particle factory", which generates shots having all the same dimension and only slight arbirtary deviation from the nominal velocity. The shots are supposed to flow through the nozzle outlet and impact on the target surface with only elastic interactions. Simulations are carried out for 3 different initial velocity, 3 mass flow rates and 5 tilting angles of the nozzle between 35° and 90° at fixed working distance. Results are extracted mainly in terms of impact velocity. The impact velocity distribution seems to be independant on the number of detected impacts (i.e. the system reaches steady state immediately), and strongly dependant on the mass flow rate which causes higher dispersion in velocity. Similar observations are made on the effect of the shot dimension and the nozzle tilting angle.

Majzoobi et al. [80] worked on an improved version of the model created in [101], with up to 22 shots impacting in deterministic positions. Shots are rigid and ave the same dimension and velocity, and

impact on a prismatic target body whose mechanical behavior is simulated using the Johnson-Cook model. RS is detected in the center of the target surface. RS profile and surface roughness (as PV value) is displayed as functions of the number if subsequent impacts, with interesting results that confirm the empirically known trends. Nontheless, this work presents a novel and disruptive advancement in the assessment of coverage in SP simulation. A single shot simulation is used to evaluate the plastic equivalent strain (PEEQ) at the boundary of the indentation. Coverage is assessed in the FEM model as the percentage of nodes of the target surface having PEEQ greater than the threshold value. This method is the first one used in FEM to quantitatively evaluate coverage, and is coheret with the visual inspection method commonly used in SP practice.

The question of neglected evaluation of coverage in simulation is studied also by Miao et al. [78] in their work. With an accurate study of the state of the art in SP simulation at that time, the authors highligth the two main criticalities in the field: the neglection of the stochastic nature of the process, with deterministic arrangement of the impact location of shots, and the lack in evaluating coverage in the simulations. To deal with this problem, the model devised by the authors consists in a stack of spherical rigid shots impacting on a 2x2x2 mm^3 prismatic aluminum target body, having bilinear isotropic hardening rule. The shots have equal dimension and velocity (50 mm,50 m/s) and their impact location is randomly arranged inside a $1.5\,mm^2 \times 1.5\,mm^2$ impact area. Simulations with 6, 12, 24, 48 and 96 shots are carried out, both with orthognally impacting shots, and with 60° inclination. Coverage is assessed using the method seen in [74] and compared to the prediction of the Kirk and Abyaneh equation 2.1, which is set up using single shot 3D FEM simulations to evaluate the indent dimension. RS stress are obtained by averaging the values measured in different point of the target body. Interesting results are displaied for the saturation of RS at increasing number of impacts, as well as for the validation of the Kirk and Abyaneh equation. The analysis of the single shot inclined impact gives some interesting results. The perturbation due to the tangential velocity is slight and involves only the most surface layer of the target body. Most part of the effects of the inclined impact seems to be ascribable to the reduction of normal velocity of the impacting body.

Klemenz et al. [105] showed the importance of considering a consistent number of nodes laying on the same layer when computing the in-depth RS profile in order to emulate the XRD measurement, by comparing the results of experimental measurements and single shot simulations. To simulate SP on AISI4340 steel, 121 rigid shots with fixed velocity and dimension are made impact on a target body, in deterministic position. Full coverage is claimed, but no evidence of this results are shown. An elaborate viscoplastic model with a combined isotropic-kinematic behaviour is used to simulate the behavior of the target, tuned on the experimentally measured cyclic behavior of the material.

The work of Kim et al. [106] follows the approach of the symmetry cell, with shots impacting on the corner of the cell. No evalutation of the true coverage is presented, but a novelty element is introduced in the computation of the in-depth RS profile, which is indeed computed considering the average stress of all the nodes of symmetry cell at each depth, in order to have a more realistic evaluation of stresses.

Zimmermann et al. [107] directed their study towards the comparison of deterministic and random arrangement fo impact in FEM simulations regarding the development of coverage, residual stresses and surface topography. The number of impacting shot is estimated from the mass flow rate of the treatment, assuming a uniform dimension of the shots. No variability in the shot dimension or velocity is assumed, and nominal values are used. Random impact locations or deterministically arranged patterns are compared on a prismatic target body, using a strain rate sensitive isotropic-kinematic hardening law for nickel-based alloy IN718. Good predictions of residual stress profiles are achieved, but significant differences in the final surface topography are highlighted, as well as a great underestimation of the surface cold work in the case of deterministic patterns.

Bhuvaraghan et al. [108], [109] studied, for the first time, the coupling of the DEM and the FEM in simulating SP. Single shot FEM analysis are used to tune the DEM analysis, in particular the coefficient of restitution, and to study the pressure field generated by a single impacting shot. Based on the DEM simulation of SP on a flat surface, a procedure to couple DEM and FEM is devised, with the aim of reducing the computing cost of the entire simulation. Interesting observations are made on the use of the couple DEM-FEM method for

simulating SP on a finite domain are made, even if no reliable results are provided on the subject. Nonetheless, the potentiality of using DEM and FEM in a synergistic approach is introduced in the field.
Bhuvaraghan et al. [109] simulated the Almen strip test on SAE1070 steel an Inco718 superalloy. The simulation in performed using rigid shots having all the same velocity and radius; S110 and S170 peening media are simulated to impact on a target bosy modeled using the Johnson-Cook material law. Interestingly, the number of shots required to achieve full coverage is evaluated using a "fictitious" mesh grid, where impact locations are randomly arranged with a dent dimension evaluated from a single shot analysis. A big model with a relatively coarse mesh (0.0125 mm elements) is subject to a number of impacts (up to ∼1950). No statistical variability is considered in the simulations. Interesting results are presented in terms of RSs and surface roughness, but with no comparison to experimental data.
A great step forward in the realistic simulation of SP is provided by the work of Bagherifard et al. [86], where SSP is simulated. The model consists in a stack of hemispherical shots, impacting on a prismatic target body. Since high coverage levels are simulated (i.e. high strain level on the target surface) a mixed isotropic-kinematic hardening model is used for the target, tuned of the cyclic stress-strain behavior of the 39NiCrMo3 studied. The number of elastic, orthogonally impacting shots is predicted using the Kirk and Abyaneh equation; the shots are assumed to have homogeneous velocity and dimension, and the dent dimension is computed usign PEEQ in a single shot simulation. Impacts are randomly arranged and 134 shot impact on a 1 mm^2 impact area (Figure 2.8). The actual coverage is not checked in the simulation, but 200% coverage simulations are carried out. RSs state show and interesting trend towards saturation in the 100% and 200% simulations, and PEEQ in the surface elements is used to predict surface nanocrystallization, with fair accordance with the experimental results.
Mylonas et al. [110] suggested another joined use of DEM and FEM in a simulations. A "kinematic simulation" (i.e. a DEM simulation) is used in a 2D simplified approach, to compute the number of impacting shots per unit area, given the mass flow rate and the translational velocity of the nozzle, for S110, S230, S330 and S550 type shots. The impact velocity distribution is computed as well, and the number of

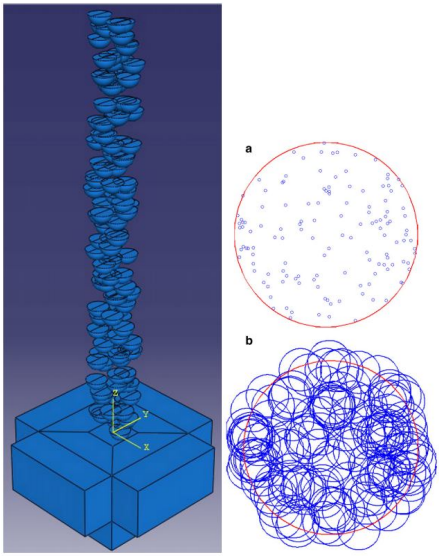

(a) (b)

Figure 2.8: Model used in [86] and impact arrangement with dent prediction

impact having effective velocity (i.e., velocity $\geq$ the 60% of the nominal velocity). The following FEM simulation is aimed at simulating SP on AA7449-T7651 alloy using a 1x1mm^2 target body and rigid shots having fixed dimension and velocity. Shots are randomly arranged, and their number is obtained from DEM simulations according to some assumptions. First of all, 50% visual coverage is considered as 100% plastic coverage, since the plastically deformed volume is bigger than the impact dent. Then, impacts il close sites are assumed not to contribut significantly to the RS field, and are neglected, contrarily to what stated in [100]. In this way, the number of impacting shots is greatly reduced in the simulation ($\frac{1}{20} \div \frac{1}{100}$ according to the shot type). Shots are spaced in their distance from the surface in order to avoid simulateous impacts. The mechanical behavior of the target material is simulated using the Cowper-Symonds model, since the strain rate sensitivity is considered to be more influencing than the strain softening of the material. The in-depth RS profile is computed and compared to the experimental one, with good accordance. It is worth noting that the approach devised in the study, despite making the simulation much faster by reducing the number of impacting

shots, shows two main problems. First of all, visual comparison of the surfaces in the peened specimen and in the FEM model highlights the great difference in coverage (Figure 2.9), and further studies should be provided to support the negligibility of the additional impacts in order to consider full coverage achieved in the FEM. Furthermore, the accordance in the RS field may be ascribable to the used model, relying on isotropic hardening, which may could help in increase the overall Rs magnitude even in partial coverage conditions.

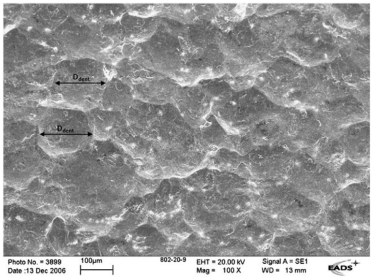

(a)

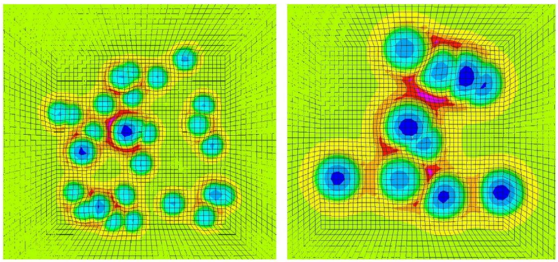

(b)

Figure 2.9: Comparison of the real specimen peened surface and the FEM model surface, picture from [110]

Gariepy et al. [111] furtherly improved the work seen in [78], by introducing a random variability of the shots dimension around the nominal diameter. Shots are assumed to impact in random location on a prismatic target body. Some uncertainties remain in the true final coverage achieved, since the number of shots is computed using the Kirk and Abyaneh equation. In this study, an interesting method to compute the final distortion due to RSs in shot peened formed is proposed. Nodal loads are applied instead of simulating impacts, thus

to reproduce the RS state generated by impacting shots; the to-be-applied RS field is computed by single shot simulations. This method can be promising when the macroscopic deformation of the target is studied, but does not take into account small deformations due to impacts (dents), thus can not truly be considered as simulation of SP.
Hassani-Gangaraj et al. [87] aimed at devising a more realistic version of the symmetry cell approach. A careful analysis of previous works based on the symmetry cell is carried out to evaluate the actual coverage level using the PEEQ approach (seen in [80]). Defectiveness is found in the evaluation of coverage and very low coverage levels (even $\sim$16%) are often mistaken for full coverage. In view of these observations, an evolution of the raw symmetry cell is proposed, having variable size dimension: the cell side dimension is tuned according to the PEEQ approach in order to achieve the desired coverage level. This approach is shown to be effective in capturing the cold work in the case of very high coverage levels. Still, some uncertainties do remain on the validity of this approach to realistically simulate the process.
Also in the work of Kim et al. [112] the topic of coverage in symmetry cells is addressed. Two different simulation approaches are considered: a 3D multi-impact model, with spherical shots impacting on a disc-shaped target, and the symmetry cell approach; identical shots with the same velocity are used. In both cases, shots are arranged in deterministic position, and the problem of coverage is solved by simply reducing the distance between impact loactions or by increasing the number of shots (by repeating impacts in fixed positions) until the desired coverage level is achieved. Clearly, this approach does not contribute to move towards a more realistic simulation approach of the process. Nonetheless, some interesting observations are made. First of all, it is highlighted once more the importance of computing the in-depth RS profile by considering a significant amount of nodes at each depth, to have an homogeneous result. Then, the RS field is showed to be strogly influenced by the impact order of shots and the true coverage level, especially if low coverage level are considered. Lastly, significant difference is shown in the resulting RS field if elstoplastic shots are used, in comparison to elastic or rigid shots, at least in the case studied (steel shots on AISI4340 steel substrate).
Interestingly, the study Bagherifard et al. [73] is focused on the ex-

ploration of the surface topology modifications caused by the treatment. Hemispherical elastic shots are simulated to impact on a very finely-meshed target body, whose mechanical behaviour is ruled by the Chaboche model, in order to correctly simulate the material behaviour in the case of repeated loads. Impacts are randomly arranged in a 1 mm diameter circular area, and the number of shots is chosen according to the Kirk and Abyaneh equation. 3 shot dimensions (namely 0.3 mm, 0.45 mm and 0.6 mm) and 3 shot velocities (namely 30 m/s, 60 m/s and 90 m/s) are considered; in each simulation shots are assumed to have identical velocity and dimension. The impact dimple dimension to be considered in the Kirk and Abyaneh is experimentally measured for the 0.3 mm and the 0.6 mm shots, and infered through a bilinear function of the shot velocity and diameter for the 0.45 mm shots. This approach proved to be agreeably precise and will be used in the following work (Section 4.1.2). 3 coverage level (namely 100%, 200% and 300%) are simulated for each combination of shot dimension and velocity. As a result, the 2D roughness parameters R_a, R_c and R_z are computed. The finely meshed model (Figure 2.10) requires a tremendous computational cost; nonetheless good results are obtained in the comparison between the experimental and the numerical results.

The next work of Bagherifard et al. [91], at last, clearly raises the

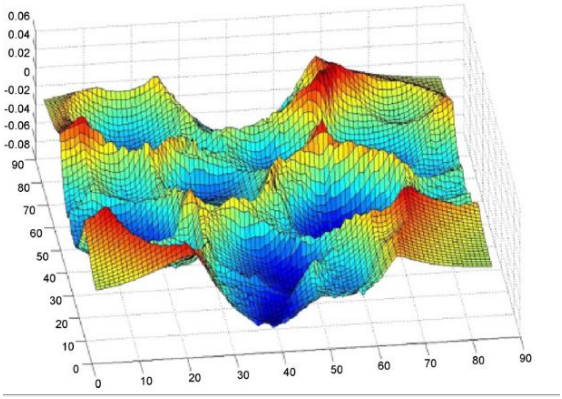

Figure 2.10: Detail of the finely meshed target and the topology modifications in [73]

problem of correctly considering coverage in the simulations. Once

again, the true coverage level achieved in some previous work is put under investigation, and the representativity of the symmetry cell approach is questioned, due to the intrinsic stochastic attributes of the SP process. At the same time, the use of "plastic coverage" is discussed, since the commonly used (and sandard defined) coverage measurement method is true visual inspection. In view of these observations, a lightened simulation method is proposed as an alternative to the approach presented in [86]. A semi-random approach is proposed for the impact location arrangement, where shots are randomly arranged but no superimposing shots are permitted until a certain coverage is achieved; some additional shots are then randomly arranged. This lowers significantly the number of shots required to achieve full coverage, despite being professedly a stretched intepretation of the randomness of the process. The approach is proved to give satisfactory result for what concerns the RS field, but doubts on the realism of the simulation are not dissolved.

Gariepy et al. [113] applied the FEM simulation to the study of the effect of the peening trajectory in shot peen forming. An extensive experimental characterization of the shot stream is carried out, with the analysis of the shot velocity distribution and the impact location distribution. This is applied to the study of the developed RS field using the method proposed in [111]. Interesting results are obtained in the application of this method to the simulation of an Almen test, with increasing arc height due to subsequent peening passes. Nonetheless, surface topology modifications are completely neglected, as well as the microscopic aspects of the RS field which is studied only in its macroscopic trend.

The studies of Nouguier et al. [114] and Badreddine et al. [17] focused on the extensive study of the dynamics of the peenind media in USP. Both are based on the DEM simulation of the process, with interesting results on the actual peening conditions in the real treatment. Depsite being specifically restricted to the field of USP, theese studies highlighted the importance of studying the *actual* peening conditions, which can be relatively far from the nominal.

A further development in this field can be find in the study of Nguyen et al. [115], who devised an extremely detailed multiphysics CFD-mechanical model for the prediction of coverage on peened parts. The model is aimed at simulating the peening nozzle during the process,

and particularly the interaction between the popellent gas and the peens (Figure 2.11). The dependency of dent dimension on shot ve-

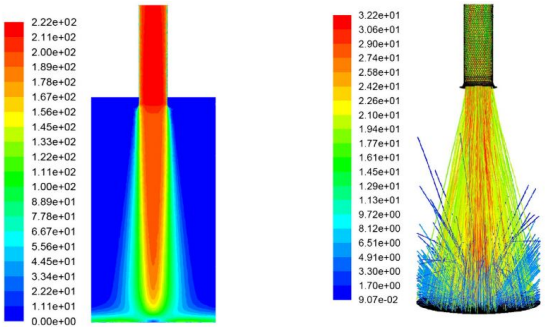

Figure 2.11: CFD model of the peening nozzle and the peens, picture from [115]

locity (for fixed dimension shots) is computed using side single shot FEM simulations, and is used to predict the actual coverage both on a flat surface and on an realistic component, according to the nozzle velocity, the air pressure and the mass flow rate. Some interesting observations are made, in particular on the alleged acceleration of peens after exiting the nozzle outlet, which would be worth to be further explored; moreover, the simualtions showed good agreement with the Kirk and Abyaneh equation. Nonetheless, this approach appears somehow too complex and time costly to be advantageously used in the industrial practice.

Yang et al. [116] devised a developed version of the symmetry cell in order to study the effect of inclined impacts. The work clearly states the obsolescence of any simulation method based on deterministically arranged impact; nonetheless some interesting results are obtained. Above all, it is observed how the effect of inclined impact is mainly limited to the shape of the impact dent, while the effects on plastic strain and RSs is only due to the difference in the velocity components, with very little effect of the tangential velocity.

In the study of Hassani-Gangaraj et al. [117] the problem of lack in coverage in the symmetry cell models is observed again and a solution is finally proposed a truly realistic approach to address the problem of simulating coverage in SP simulation. Shots having fixed dimension and velocity are assumed to randomly impact on a disk-shape target,

and are continuously generated in the model until 98% of the surface is plastically deformed according to the PEEQ. No experimental validation of the results is showed, and no statistical analysis of the number of shots is reported. Nonetheless, by comparing the model results with the Kirk and Abyaneh equation in relating coverage to the number of shots, the expected overestimation of the Avrami law on a finite area is verified. It is noting that, if the PEEQ threshold to evaluate coverage is carefully tuned, this approach could realistically reproduced the actual visual check used in the SP pratice.

The work of Bagherifard et al. [118] is aimed at studying the influence of the mesh size in the simualtion of SP. Single shot simulations are used, with different mesh sizes in equivalent models. Interestingly, the mesh shows to be relatively uninfluencing in a relatively wide range, even for the target body, in RSs are studied. Some more care is required to precisely cath strain in target elements, in particular if nanocrystallization is studied; nonetheless, simulations seem to achieve full convergence even for relatively coarse meshes.

The study of Sanjurjo et al. [92] put an important remark on the influence exerted by the material model used for the peened substrate in the FEM simulation. Rigid shots with fixed velocity and dimension are randomly arranged to impact on an AISI 2205 prismatic target body. The number of shots is computed by assessing the average number of shots to achieve full coverage in a side routine, based on a mesh grid, knwon the dent dimension from single shot simulations. No great effort is put in making the most realistic simulation, since the focus is mainly on the comparison of material models. Three material models are used for the target body namely: an isotropic hardening model with strain rate effect (Johnson-Cook), an isotropic–kinematic hardening model (Chaboche) and a purposely devised new isotropic-kinematic contistitive model, based on the Chaboche model, where strain rate effects are included in the isotropic component of the law. Little amount of experimental data is proposed for the comparison with the numerical results, nonetheless remarkable differences are shown among the various material model, with a substantial preeminence of the Chaboche and , even better, the modified Chaboche model.

Murugaratnam et al. [119] aimed at pushing the combined use to DEM and FEM simulation to the complete simulation of the SP pro-

cess directly on a realistic component. A purposely devised script in the DEM model is used to take into account the work hardening in the substrate. The DEM model is also based on a particle factory (the peen source) which emulates the in a simplified form, using the nominal velocity and mass flow rate of peens. The results of the DEM simulations with a dynamic nozzle insisting on a flat surface are used to analyze the velocity distribution of impacts in various conditions for the mass flow rate and angle of attack, with results similar to the ones referred in [81]. The resulting impact locations and velocity are used to set up the FEM simulation of the SP process with 66 shots on a 2.4 mm diameter disk-shaped target. The resulting in-depth RS profile appers to be reasonable, but no comparison is made with experimental data. In a further development, a complete routine for the full integration of the DEM and FEM simulations for the study of SP on a realistic component (a gas turbine) is proposed (Figure 2.12). Despite the interesting perspectives of this approach, it appears to

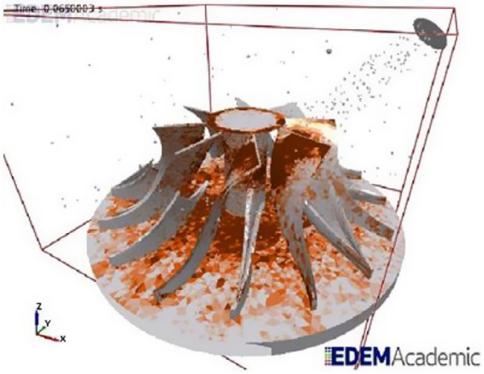

Figure 2.12: DEM simulation of a real component in [119]

be a bit green. The models, indeed, needs to be carefully tuned to be fully realistic, which is not verified in the study, and an extremely high computational cost is required for the whole simulation.
Jebahi et al. [120] devised an extremely interesting procedure to facilitate the practical used of the DEM/FEM simulation on real-like target components. Basically, the authors assert the RS field in the substrate being characterizable by studying the RSs in small volumes having peculiar geometrical characteristics, called Representative El-

ementary Volumes (Figure 2.13). The knowledge of the RS in these specific small volumes (flat surfaces, edges, geometrical features) is, according to the authors, enough to infer the overall RS state in the component. This approach seems to be indeed reasonable and attractive for a ready-to-use approach to reduce the computational cost of simulations. Nonetheless the effectiveness of this approach is still

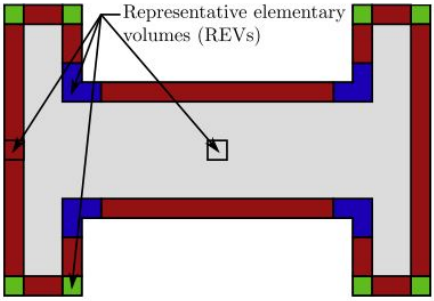

Figure 2.13: Schematic representation of REVs , image from [120]

to be proved. The authors proposed the application to the coupled DEM/FEM approach to the simualtion fo the Almen test. Results of a simplified DEM simulation, similar to what seen in [119] are used to set up the FEM model on a flat surface. Edges and border effects are assumed to be neglectable, so the REV approach needs to be further studied.

The study of Gallitelli et al. [121] may be, at least partially, a solution for this problem. In this case, the overall RS field in a finite component (a gear) subject to USP is obtained from the RS field resulting in a single shot simulation. The RS field is applied to all the free surfaces of the component via a fictitious thermal load (Figure 2.14), tuned as to generate eigenstrains matching with the actual RS field obtained by SP under a flat surface. It is worth noting that this approach could ease the practical application of the DEM/FEM simulation of SP to models having large dimension. Nonetheless, further studies are needed to clarify the RS state in the vicinity of geometrical details, in accordance with the REVs approach. MNoreover, it has to be taken into accoutn that this method is only applicable to the study of RSs, while surface topology modification are not considered.

Similarly to [92], Ghasemi et al. [85] used a side routine in Python to

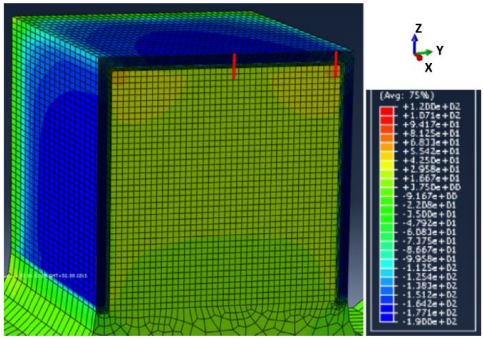

Figure 2.14: RS field generated using thermal loads on a gear tooth, picture from [121]

assess the number of randomply arranged impacts required to achieve full coverage. Fixed dimension and velocity shots are used, in order to have a relatively stable dent dimension, and very high coverage level (1000%) is simulated on a prismatic AISI4340 target, whose mechanical behavior is accounted with a kinematic hardening model. Very good results are obtained, in particular for the resulting surface roughness, when compared to the experimental data.

Chapter 3

Process characterization and experimental measurements

In this Chapter all the experimental measurement used to characterize the SP process, to set up the simulation and to validate the results are displayed. First, the characteristics of the peening media and the parameters of the peening treatment are presented in Section 3.1, as well as the mechanical characterization of the base material. The effects of the treatment are displayed in Section 3.2 in terms of RS field and resulting surface roughness. RS measurement on the edge and the root of the notch are impossible to measure. Therefore, the RS measurement is performed in the vicinity of the geometrical features and the RS field will be reconstructed through a FEM simulation; these data will be presented in Section 3.3. Part of the data displayed in this Chapter has been published in [34], [35], [50], [63]–[65], [122]–[124].

3.1 The SP process

3.1.1 Peening media and peening parameters

The process chosen for this work is the micro SP treatment named CE-B120. Spherical fused ceramic shots are used as peening media. The composition and the physical-mechanical characteristics of the peening media material is displayed in Table 3.1

The particle-size distribution of the peening media is studied via a granulometric analysis performed on a 100±0.5 g sample using a

Table 3.1: Physical-mechanical characteristics of the peening media material

Composition	Young modulus (GPa)	Poisson ratio	Hardness (HV)	Density (g/cm^3)
$Zr0_2$ 67% $Si0_2$ 31%	300	0.3	700	2.3

Rotap Sieve Shaker machine. As prescribed by the standard ASTM-C-136 the measurement is performed using 6 sieves with decreasing size between 150 µm and 53 µm. After 600 s shaking time, the beads retained by each sieve are weighted. The weight fraction of retained beads for each sieve size is reported in detail in Table 3.2.

Table 3.2: Size-particle distribution of the peening media

Sieve dimension (µm)	Over sieve mass (g)	Cumulated mass (g)
ASTM 150	1,8	1,8
ASTM 125	0,9	2,7
ASTM 106	21,2	23,9
ASTM 90	36,6	60,5
ASTM 63	35,0	95,5
ASTM 53	3,0	98,5
Bottom 0	1,5	100,0

The velocity of the shots at the nozzle outlet is provided by the shot peener. Measurement is performed using a DSLR camera and flash unit are focused on the shots stream at the outlet of the nozzle. A patterned screen is used as a background, and the flash is synchronized with the camera shutter. A scheme of the equipment used is shown in Figure 3.1. Pictures of the shots are taken, and the velocity is assessed by measuring the contour of the shots in the pictures, known the exposure time. The mean value of the shot velocity is estimated in ~ 57 m/s.

The SP treatment is performed at 100 mm working distance (the distance between the nozzle outlet and the treated surface), with a 12 mm diameter Tetra nozzle. The nozzle is oriented normally to the treated surface. As will be seen in more detail later, the nozzle turns arounf the edge tip keeping constant its peripheral velocity when turning around an edge.

The SP process is carried out at a 5 kg/min mass flow rate. Full (100%) coverage is achieved on the studied specimens, which corre-

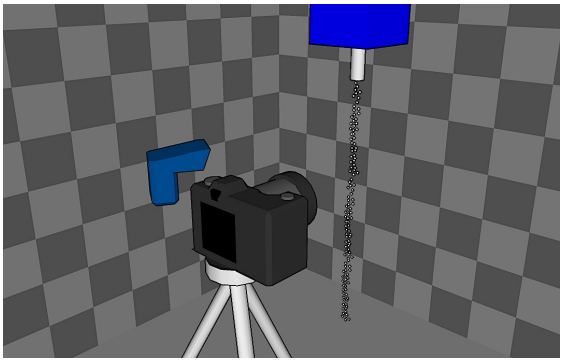

Figure 3.1: Scheme of the photographic equipment used to measure the shot velocity.

sponds to a grade 4.5 N Almen intensity. A short recap of the SP process parameters is reported in Table 3.3

Table 3.3: Peening process parameters.

Almen intensity	Nozzle	Mass flow rate (kg/min)	Angle of impingement	Coverage	Average shot velocity (m/s)	Shot diameter range (µm)
4.5 N	Tetra 12 mm	5	90°	100%	57	63 ÷ 125

3.1.2 Characterization of the base material

The SP process is performed on aeronautical grade aluminum alloy Al-7075-T651, commercially known as Ergal. The main alloyant elements are Zinc (5.1÷6.1%), Magnesium (2.1÷2.9%) and Copper (1.2÷2.0%). The T651 thermo-mechanical tratment is applied to the alloy, which mean the the solubilization treatment at 748 K for 30 min is followed by water quenching and stretching to a 2.5% permanent set to release some RSs. A 6 h artificial ageing concludes the thermomechanical treatment. As a result, a relatively fine-grain microstructure is obtained (Figure 3.2), with very fine $Cr_2Mg_3Al_{18}$ and $(Fe,Mn)Al_6$ precipitates.

The specimens are extracted from 4 mm thick rolled plates. In Figure 3.3 the geometry of the used specimen is displayed.

The mechanical properties of the base material are reported in 3.4

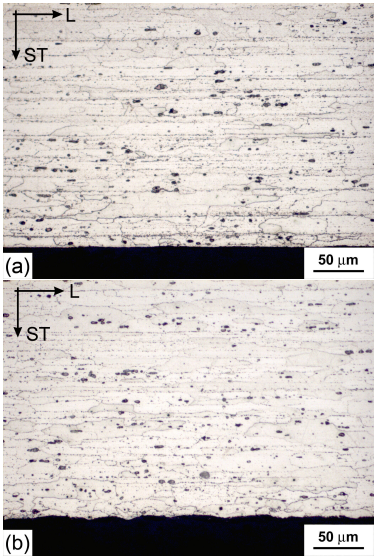

Figure 3.2: Longitudinal section of the non-peened (a) and peened (b) specimen. The longitudinal L direction shows the rolling direction.

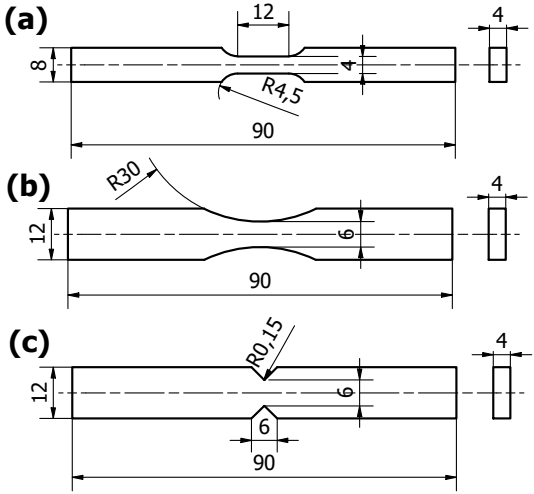

Figure 3.3: Geometry of the specimens for tensile and cyclic strain test (a), SP on a flat surface and on an edge (b), SP on a sharp notch (c).

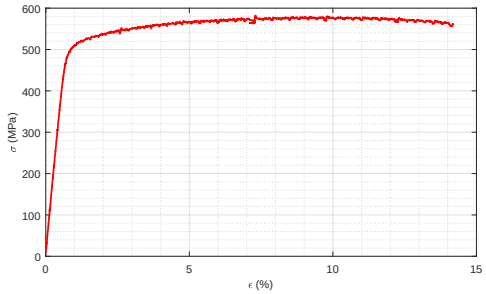

Figure 3.4: Stress strain curve from tensile test of the Al7075-T651 alloy.

and obtained from quasi-static tensile testing (initial strain rate $10^{-3}\,\mathrm{s}^{-1}$. The stress-strain curve is shown in Figure 3.4.

Table 3.4: Mechanical properties of the Al7075-T651 alloy.

E (GPa)	$\sigma_{Y0,2}$ (MPa)	UTS (MPa)	σ_F (MPa)	TE (%)	RA (%)
72 ($\pm$ 1)	515 ($\pm$ 5)	565 ($\pm$ 5)	760 ($\pm$ 10)	18 ($\pm$ 2)	24 ($\pm$ 2)

The cyclic strain behavior of the alloy is characterized through fully reverses axial strain tests. Single step tests are carried out at $10^{-4}\,\mathrm{s}^{-1}$ initial strain rate, with strain amplitudes in the range $0.006 \div 0.014$. Stabilization of the hysteresis loop occurs after $10 \div 15$ cycles. The stabilized stress-strain curves are shown in Figure 3.5. A slight anisotropy is found in the mechanical behavior of the material under cyclic strain [34], depending on the initial strain used applied in the test (compression or tension). This aspect is ascribed to the complex microstructure of this alloy, but will not be considered in this work.

3.2 Peening effects on flat surface

The effects of SP on a flat surface are devised through surfaces roughness measurements and RS measurements.

Surface roughness 2D surface roughness measurements on the peened surface are acquired through a contact profilometer, on a 5 mm measuring length. Results are reported in Table 3.5.

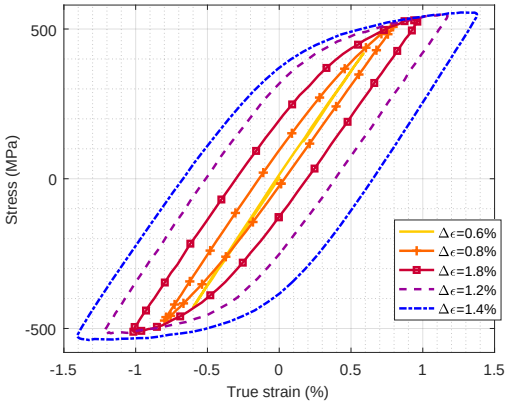

Figure 3.5: Stabylized cyclic stress strain curve for the Al7075-T651 alloy.

Table 3.5: 2D surface roughness parameters of the peened surface.

Condition	R_a (µm)	R_q (µm)	R_t (µm)	D_p (µm)
As received	0,25	0,3	0,9	
Peened B120	1,35	1,67	7.12	110

3D surface roughness measurements are acquired with a Sensofar Plu Neox confocal optical profilometer, having a plane surface spatial sampling resolution of 0.83 µm and a z-axial measurement resolution of 0.83 µm. The 3D surface morphology and roughness were evaluated on a 636x477 µm^2 measuring area, both on the surface of the peened specimens and on the surface of the as-received ones (Figure 3.6). The results of the surface characterization are displayed in Table 3.6.

Table 3.6: 3D surface roughness parameters of the peened surface.

Condition	S_a (µm)	S_q (µm)	S_{sk}	S_{ku}	S_{pk} (µm)	S_k (µm)	S_{vk} (µm)
As received	0.29	0.38	0.19	5.98	0.59	0.81	0.41
Peened B120	1.24	1.54	0.14	3.03	1.75	3.96	1.42

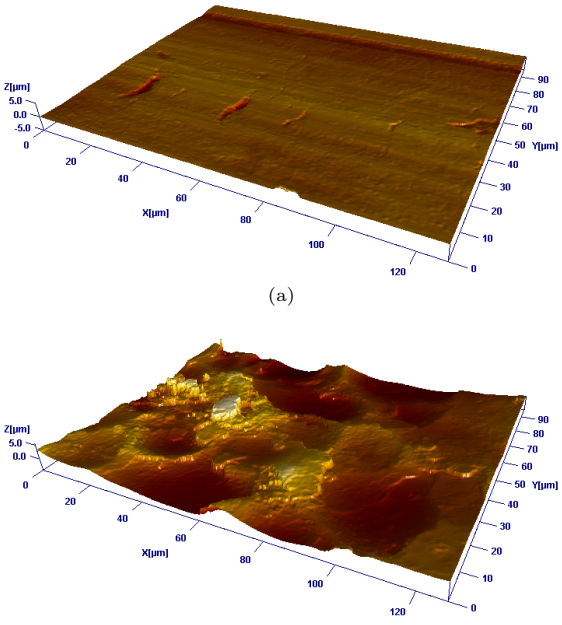

Figure 3.6: Rendering of the confocal optical profilometry of the as received (a) and peened (b) surface.

The stress concentration factor exerted by indentations caused by SP is computed according to the formula proposed by [125]:

$$K_t = 1 + 4\left(\frac{R_t}{D_p}\right)^{\frac{1}{3}} \tag{3.1}$$

wich returns $K_t = 1.11$ according to the experimental measurements.

RS field In-depth RSs generated by SP are measured by X-ray diffraction (XRD) using an AST X-Stress 3000 X-ray diffractometer. The measurements are performed in the center of the front surface of the specimen, detailes are reported in [34]. Cr Kα radiation is used, with a 1 mm^{2}collimator. 9 tilt angles (ψ) in the range [$-45°$,45°] are used to compute RS using the $\sin^2(\psi)$ method, with a 2Θ =139° diffraction angle. The Neerfeld-Hill method is used to account for the elastic properties of the material. Electro polishing technique is used to incrementally remove material layers in the y direction to acquire in-depth measurements. Clearly, the RS component acting on the plane of the free surface (xz plane) is measured. The measurement is arrested when layers in tensile RS are exposed, i.e. about 50 µm under the surface. Since this depth is much lower than the specimen thickness, no correction of the RSs for removing the surface layer is prescribed, as stated in [126]. Three measurement are taken on different samples; the in-depth RS profile is displayed in Figure 3.7

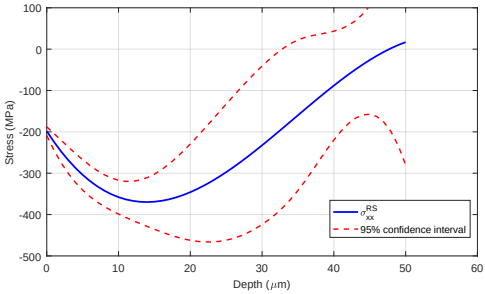

Figure 3.7: In depth residual stress profile as measured from XRD analysis.

Previous studies [34] showed that the magnitude of RSs in the samples caused by the manufacturing process are negligible. On the other hand, the thickness of the removed layer is comparable with the penetration depth of the chromium radiation into aluminum, i.e.

about 12 µm. To make possible to directly compare the RS profile from the experimental measurement and the one from the numerical simulation, the true in depth RS profile is computed. For this purpose, the deconvolution technique devised in [65] is used. At each depth (y coordinate), the in-plane true RS ($\bar{\sigma}_{xz}$) is considered as a weighted average of the RS value in deeper layers, in the form:

$$\bar{\sigma}_{xz}^{RS}(y) = \frac{\int_0^\infty \sigma_{xz}^{RS}(y+y')e^{-\frac{y'}{\xi}}dy'}{\int_0^\infty e^{-\frac{y'}{\xi}}dy'} \tag{3.2}$$

The parameter ξ is the information depth [127], which has been estimated in [65] equal to 5 µm for chroumium radiation. The true in depth RS profile is displayed in Figure 3.8.

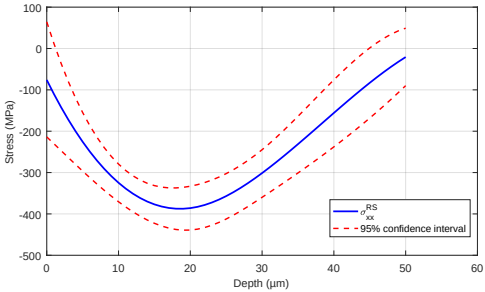

Figure 3.8: True in depth residual stress profile computed from experimental measurements.

3.3 Peening effects on an edge and a notch

In order to study the effects of SP on a sharp edge or a sharp notch, the treatment is performed on the specimen showed in Figure 3.3. Specimens depicted in Figure 3.3 (b) are supposed to be representative of the condition of an edge, since, the radius of the carving in the specimen is much greater than the characteristic dimension of the studied phenomena. Specimens depicted in Figure 3.3 (c) are provided with a notch and two notch root radii are considered, namely 0.5 mm for the standard notch and 0.15 mm for the sharp notch. RS in correspondence of an edge or a notch are extremely difficult to mea-

sure due to the technical complexity of performing XRD analysis in a very narrow space. Moreover, the characteristic dimension of these geometrical features is short and requires very narrow collimation of the X-ray beam in order to reduce the measuring spot and detect RS in precise locations. To study the RS field in these locations, a two step procedure was used: first, a micro XRD analysis (μXRD) was carried out in order to measure RSs as close as possible to the edge/notch. Then, the experimental data were used in a FEM model, where a thermal field was fitted to the measured data to compute a complete reconstruction of the RS field.

μXRD measurements μXRD measurements are performed using a Bruker's D8 Discover XRD2 micro-diffractometer, having a collimator with a 50 µm diameter. Details on the XRD analysis of these specimens are reported in [123]. Cu Kα radiation with high penetration depth ($\sim$40 µm) is used and tilt angles (ψ) in the range [$-20°$,50°] are explored to apply the $\sin^2(\psi)$ method. Measurement point are located on the front surface of the specimen, in the vicinity of the edge or the notch root along the bisector y axis, as shown in Figure 3.9.

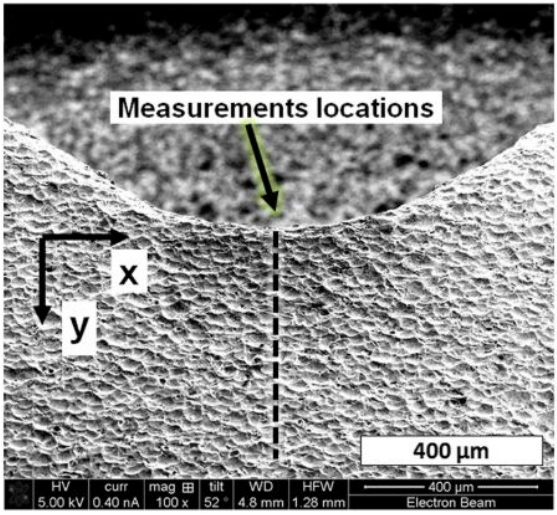

Figure 3.9: FEGSEM image showing the measurements locations. Picture taken from [123].

The RSs in the x-direction (with reference to Figure 3.9) are

mapped on the surface and at 30 µm depth under the surface ($\sigma_x(y)$). The RS profile is detected with measurements in 11 locations spaced 50 µm apart starting from the edge or notch tip. True RS profile is obtained by removing the radiation penetration component through the 3.2 with an information depth equal to 16 µm [65]. The measured surface RS field is shown in Figure 3.12 both for the case of the edge and for the case of the sharp notch. The confidence interval in both cases is quite large, due to the surface morfology which affects the measurement.

RS reconstruction The measured RSs are used in [65] to reconstruct the RS field on the symmetry plane of the notch and the edge using the Eigenstrain method. First of all, a reference system is established as depicted in Figure 3.11.

It is worth highlighting that thermal fields do generate Eigenstrains, being the strains induced by thermal fields self-equilibrated in themselves. Thus, a FEM model is used to simulate the stress stat generated by the superposition of the misfit strains produced by two fictitious temperature distributions. The intensity and spatial distribution of the thermal fields are deduced by fitting the experimental data after being corrected for the radiation penetration depth. More specifically, the first temperature field is a function of the depth below the treated surface and takes the following expression for the Front (FS) and Lateral Surface (LS), respectively:

$$\begin{aligned} T_1^{FS}(z) &= A\, f(z) \\ T_1^{LS}(r) &= A\, F(r-R) \end{aligned} \tag{3.3}$$

Where f is a dimensionless temperature distribution, function of the distance from the treated surface, which can be found in [123]. The perturbation of the RS field in the vicinity of the edge is accounted by a second temperature field, which is assumed to decay with increasing distance from the edge and to be a function of the circumferential coordinate θ:

$$T_2(r,\theta,z) = \sum_{j=1}^{2} B_j \cos[2\,(j-1)\theta] e^{-\frac{(r-R)+z}{\tau}} \tag{3.4}$$

The unknowns A, B_j and τ were determined in [65] and their

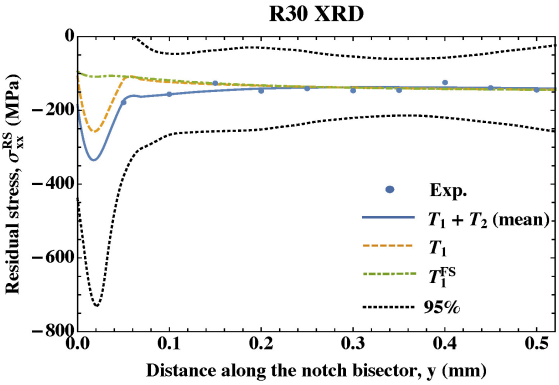

(a)

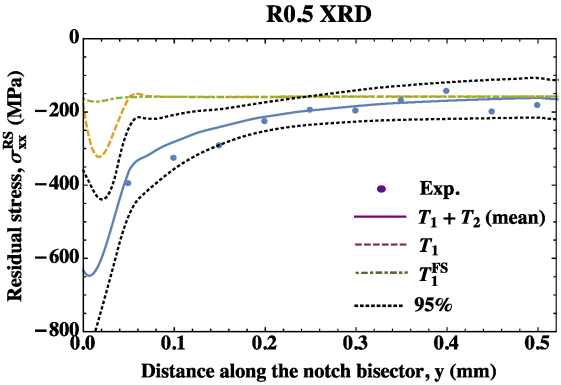

(b)

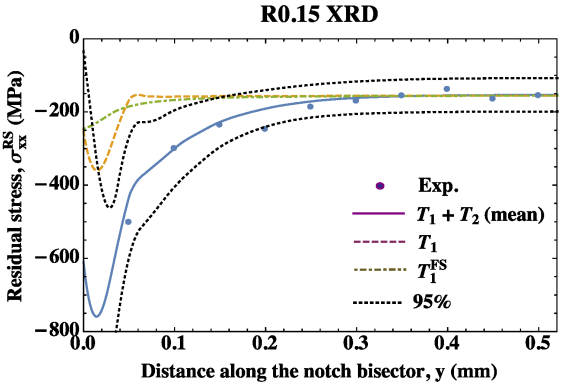

(c)

Figure 3.10: Surface RS profile from the XRD analysis, measured on the notch bisector, at increasing distances from the edge (a), 0.5 mm notch (b) and 0.15 mm notch (c) tip.

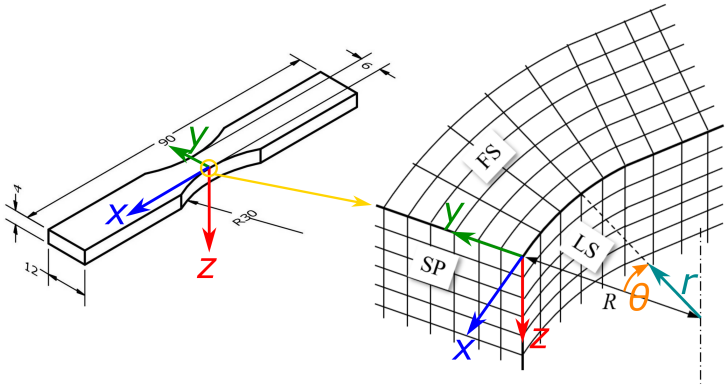

Figure 3.11: Reference system used in the reconstruction of the RS field.

values are listed in Table 3.7 both for the edge and the sharp notch.

Table 3.7: Coefficients for the fitting functions 3.3, 3.4, coomputed in [65]

Case	A	B_1	B_2	τ
Edge	46.7	-230280	230723	0.4
Notch 0.5 mm	48.5	-7344	-10484	0.14
Notch 0.15 mm	47.6	7642	-11604	0.05

The reconstructed RS fields are plotted in Figure 3.12. In the case of the notch, the reconstructed RS field exceeds the elastic limit of the aluminum alloy. This simplified modelization of the notch and the thermal field in its vicinity generates an eigenstrain distribution not compatible with the elastic properties of the substrate at the root of the notch. In order to deal with this issue without increasing the number of terms in the definition of the thermal field and preserve the robustness of the fit, the elasto-plastic behavior of the substrate were considered in the FEM model. A bilinear kinematic hardening is used to model the elasto-plastic properties of the alloy. Since the peening treatment causes intense work hardening of the surface layer, the yield stress value of the subsequent layers under the surface is inferred from the microhardness in-depth profile and implemented into the FEM model as a function of the depth under the surface. This causes the equation system expressed in 3.4 to become non-linear; the solution is achieved an iterative algorithm searching for the value of the parameters A and B_j that minimizes the mean square deviation

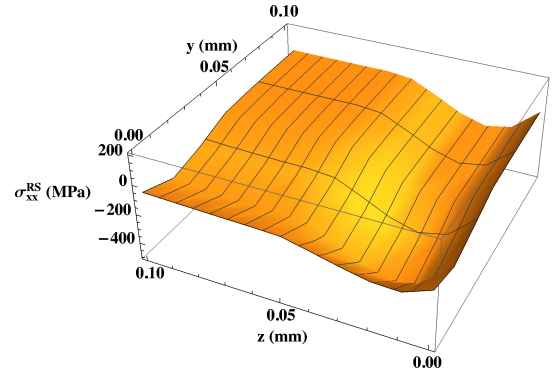

(a)

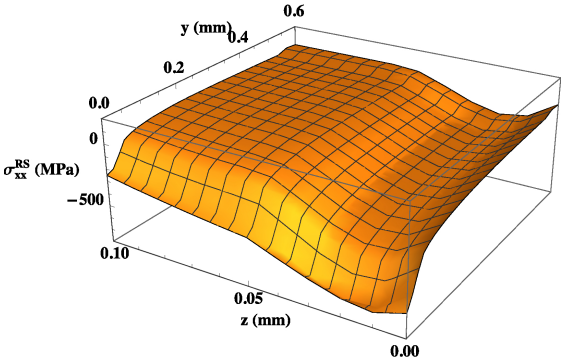

(b)

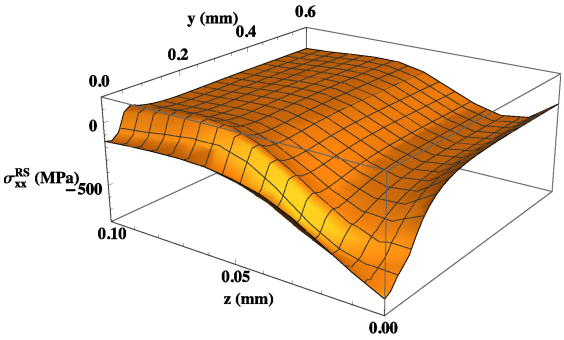

(c)

Figure 3.12: RS field reconstructed on the symmetry plane of the notch for the edge (a), 0.5 mm notch (b) and 0.15 mm notch (c) specimen.

from the experimental measurements. The intense compressive RS peak at the notch root is attenuated by the plastic flow, and returns a much more satisfactory reconstruction result.
Both in the measured RS profile and consequently in the reconstructed the RS field, the confidence interval is relatively wide, in particular in the vicinity of the edge or notch tip. This is caused by the intense deformation of the surface layer and the high penetration of the X-radiation, which interferes in the RS measurement. The compressive RS layer, for this kind of substrate and SP, is indeed extremely thin ($\sim$50 µm). Moreover, the technological limit of XRD does not permit to have measurement a at distance closer than $\sim$50 µm from the edge tip.

Note to the simulations

This Section is devoted to the presentation of the simulations of SP, as mentioned in Chapter 1 and schematized in Figure 3.13, the core of this study, which will be seen in detail in the next Sections.

In the first place, it can be appropriate to specify that the canonical partition into methods and results will not be observed. Methods and results, instead, will be alternatively presented step by step, following the developement of the work. Simulating SP requires a complex sequence of hypoteses in order to move towards realistic simulation of SP on finite domains. Since experimental measurements are expensive and time costly, or even impossible in some cases, the results of each simulations are used to devise or tune following models. Thus, partial results will be shown in the course of the dissertation to help a better inderstanding of the work and its flow. The organization in the following Sections will be explained in detail hereafter and is schematized in Figure 3.14.

At first, the simulation of SP on a flat, infinite surface will be addressed in Chapter 5. The average shot velocity and particle distribution of the peening media is obtained from experimental measurements, as well as the mechanical behaviour under monotonic tensile and cyclic strain conditions. These data are used to calibrate a bilinear function to predict the indent dimension from the shot velocity and diameter. The function is used in a MatLab script to compute the number of shots required to achieve full coverage on a 100 µm diameter circular impact area, where random impact locations are assumed. The shot radii, velocity and impact location are used to generate the explicit dynamic FEM model of SP on a flat surface, with orthogonal impacts. Particular care is put in modeling the cyclic strain behavior of the target material. Results are obtained in terms of in depth RS

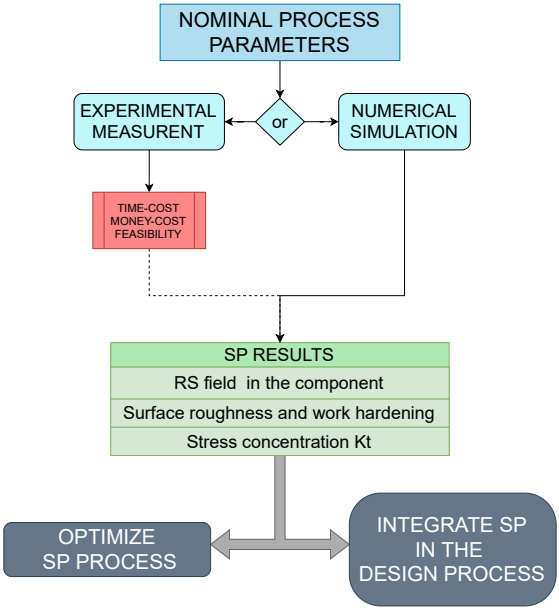

Figure 3.13: Framework of the SP simulation and main focus of this work.

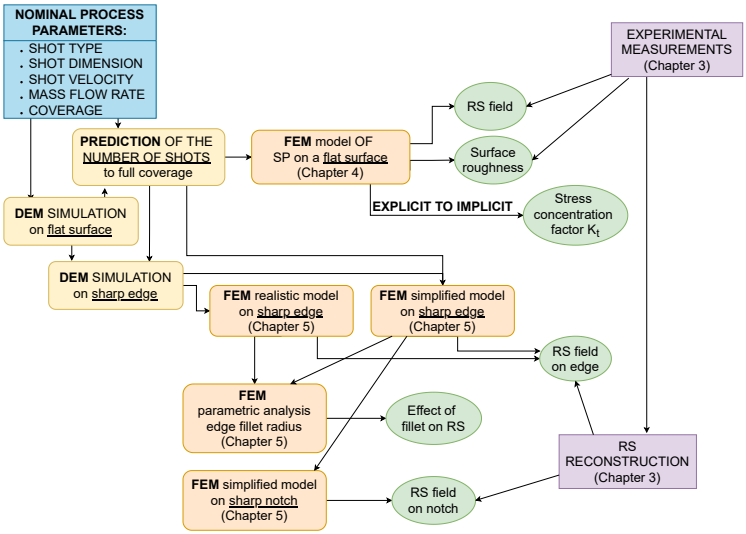

Figure 3.14: Organization of the study in the next Sections.

profile surface roughness and final morphology of the peened surface. The nodal displacement and radiation penetration is considered in computing the RS field generated by SP, which is compared to the experimentally measured one. 2D and 3D surface roughness parameters are computed as well and compared to experimental results. The target body deformed by the impacts is used in a static model, without RS field, to compute the stress concentration effect exerted by the deformed morphology when an external load is applied.

Then, Chapter 5 is devoted at simulating SP on an edge, in order to move towards the prediction of RSs in finite domain, i.e. geometrical features acting as stress raisers. Since exact peening conditions in this location are not known, and their influence on the generated RS field is not clear in advance, a DEM model is devised to study the process in all its aspects. Only the nominal peening parameters are known, so a quite a complex process is required to get to the FEM simulation. First of all, the DEM model of the peening machine nozzle is devised, to tune its parameters in order to have mass flow rate and average velocity of the shots equal to the nominal one. This model is extended to the DEM simulation of SP on a flat surface, in order to study the spatial density of impacts which is used to estimate the translational velocity of the nozzle. This latter, is used for the DEM simulation of the process on an edge. Realistic and simplified FEM simulation approaches are devised, and the resulting RS fields are compared to the reconstructed RS field retreived from experimental measurements.

In Chapter 6 the simulation of SP on an edge is used to study the effect of the radius of the fillet on the edge tip. Indications on the real dimension of the fillet radius are used to enhance the model. No recostructed RS field to compare the result is available, but some interesting observations are raised.

Eventually, the model of SP on a notch is devised. A simplified simulation approach is used, with orthogonally impacting shots, and two notch root radii are considered for the model. Resulting RS field are compared to the reconstructed ones. Extremely promising results are obtained, and some more observations on the technological aspects of SP on a notch, and its simulation are discussed.

Lastly, it is of the greatest importance to highlight how this work is *not* aimed at perfectly simulating the micro SP process. The main focus is indeed on the study of the procedure to be used to achieve a

reliable prediction of the effects of SP, without overlooking the technological usability of this approach. For this reason, attention will be paid to the identification of the most influencing parameters and, in particular in the last part of the work, to the devising of simplified approaches for a practical use of the simulation.

Chapter 4

Simulation of SP on a flat surface

In this Chapter the problem of simulating SP on a flat surface is addressed. This work aims at achieving a realistic simulation of the process, and to this purpose the stochastic phenomena affecting the treatment are taken into account, as will be explained in detail later. FEM is the tools chosen to accomplish the task of simulating and is assumed to be capable of being representative of the treatment as long as the model is properly devised. Explicit dynamic FEM simulations are carried out using the commercial software Ansys/LS-Dyna.
In order to devise a realistic model of the process, some set up is required prior to carry out the simulations. First of all, an appropriate material model is chosen and calibrated to realistically reproduce the mechanical behavior of the substrate. Then, considerations are made on damping and friction in the simulations. A MatLab procedure is devised in order to achieve full coverage in the simulation while accounting for stochastic variability of phenomena involved in the process. Statistical distribution of impact velocity and shot dimension are considered, as well as randomly arranged impact locations. Set of shots to be simulated are generated through a predictive model. The FEM model is described in Section 4.1. The results of the numerical simulations are validated by comparison with 2D and 3D surface roughness and in-depth XRD residual stress measurements shown in Chapter 3. To consistently compare experimental and numerical estimations of the residual stress field, the effect of radiation penetration and surface roughness is taken into account according to an approach specifically devised in this work. Finally, the nodal locations esti-

mated at the end of the dynamic analyses are imported into a static FE model to evaluate the effect of surface roughness on the external stress field. In this way, it is possible to estimate the stress concentration factor and notch fatigue factor induced by the surface treatment.

Part of the data displayed in this Chapter has been published in [124].

4.1 FEM model of SP on a flat surface

4.1.1 Material model of the substrate and the shots

Particular care is taken in modelling the elastic-plastic behavior of the target material, since it has great influence on the correct representation of the substrate material and on the final result, in particulr for the RS field, as proved by many studies [86], [92], [99], [101], [103]. Nontheless, none of the available material models is capable of realistically represent all the phenomena occurring in the elasto-plastic deformation of a metallic material, i.e. strain rate sensitivity, strain hardening even in cyclic strain cases, anisotropy, failure. Since experiments did not reveal pronounced anisotropy [50], as usual for metallic materials, this effect is neglected. As regards the strain rate sensitivity, neglecting it tout court is not as straightforward as anisotropy is. Most of the SP simulations in literature do take into account strain rate sensitivity, which plays an important role in steels and superalloys. The Johnson-Cook model [80], [86], [117] or the Cowper-Symonds model [99], [101], [110] are used by many authors, since they make possible to easily take into account strain rate by shifting the stress-strain curve of the material according to the deformation velocity. However, both models rely on a purely isotropic hardening law, which can be an oversimplification of the material behavior in the case of interest. In fact, all the aforementioned works focus on the simulation of SP on steels and superalloys, for which strain rate sensitivity plays a major role in the representation of the material behavior. The Johnson-Cook model is often used to simulate the mechanical behavior of aluminum alloys at very high strain rate, such as in the case of balistic simulations [128]–[134]. The material characterization in these studies provide enough evidence to assert that strain rate sensitivity

has not an overwhelming effect at deformation velocities involved in the SP process for aluminum alloys. Moreover, peened parts are subject to repeated elasto-plastic deformation, due to overlapping indents and subsequent impacts necessary to achieve full coverage [81], [91], [92], experiencing complex non monotonic load histories. Under these conditions, the strain-hardening of most metallic materials displays a significant kinematic component, responsible for the Bauschinger effect, which is completely neglected by the aforementioned material models. For this reason, in recent studies [86], [111], [135]–[137] a mixed isotropic-kinematic hardening model is preferred, in particular for aluminum alloys. Looking at Figure 4.1, where the experimental stress-strain curves are compared with the ones obtained from a FE model applying the Johnson-Cook model, the excessive material hardening is evident, resulting in a large discrepancy between the curves, increasing with rising accumulated strain. The same consideration applies to the Cowper-Symonds model. While the first branch of the stress strain curve is well reproduced, viz. the one based on the monotonic axial strain test, the cyclic strain behavior of the material is not equally well simulated. The isotropic hardening model does not reproduce the stabilization of the hysteresis loop, and the accumulated strain makes the hardening model lose all its nonlinear components. This leads to a wrong representation of the true material behavior.

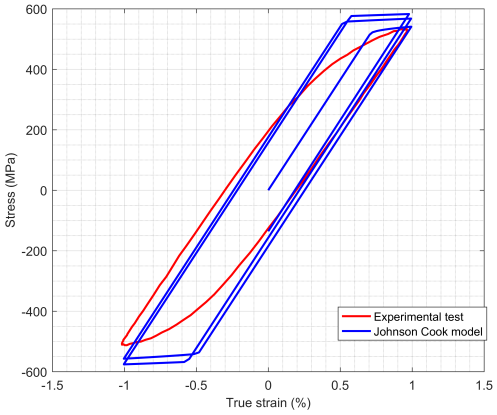

Figure 4.1: Comparison between the experimental mechanical behavior under cyclic strain and the numerical simulation of the Johnson-Cook model.

In view of these observations, we decided to adopt the Lemaitre-Chaboche mixed hardening model [138]–[140] in order to incorporate both kinematic and isotropic hardening components. The Lemaitre-Chaboche model appears in the form:

$$\sqrt{\frac{2}{3}(\bar{s}-\beta)\cdot(\bar{s}-\beta)}-\sigma_Y=0 \tag{4.1}$$

where σ_Y is the yield stress, $\bar{s}$ is the deviatoric stress tensor and β is the backstress tensor, determined as:

$$\dot{\beta}=C\,\dot{\epsilon}_{pl}-\gamma\beta\lambda \tag{4.2}$$

where C is the hardening parameter,γ is the rate of decrease of hardening modulus that rules the non-linearity of the model ϵ_{pl} is the plastic strain and γ is the accumulated plastic deformation. σ_Y depends on the plastic deformation as:

$$\sigma_Y=\sigma_{Y0}+H\epsilon_{pl} \tag{4.3}$$

where H represents the isotropic strain hardening modulus, not used in this study. This material model does not account for strain rate sensitivity, but this aspect is of minor importance in the present study, given the aforementioned low strain rate sensitivity of Al7075-T651 and the bead impact velocities, which are far lower than the ballistic velocities used to characterize the strain rate sensitivity. The FE software Ansys allows to use as a material model the superimposition of up to 5 nonlinear Chaboch models. A good tuning of the model parameters makes possible to exactly represent both the monotonic stress strain curve and the stabilized cyclic strain behavior of the material, if both kinematic and isotropic hardening are calibrated. Since the explicit solver LS-Dyna does not admit this option, no isotropic hardening is considered; this would, indeed, prevent the model from getting to the stabilization of the hysteresis loop. A trial and error procedure is used to tune the material model and fit the stabilized hysteresis loop curves mentioned in Section 3.1.2, using a simple FEM simulation. The resulting parameters are reported in Table 4.1. Figure 4.2 shows the resulting cyclic strain curves compared to the experimental ones. Figure 4.3 shows the monotonic tensile stress strain curve of the model, compared to the exprimental one.

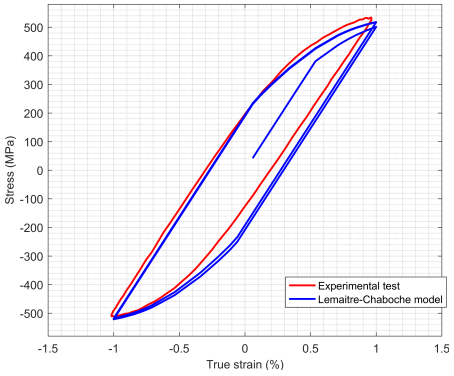

(a)

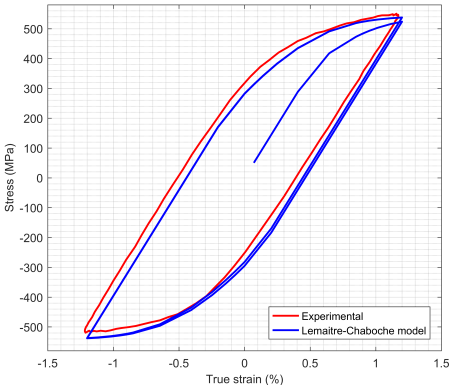

(b)

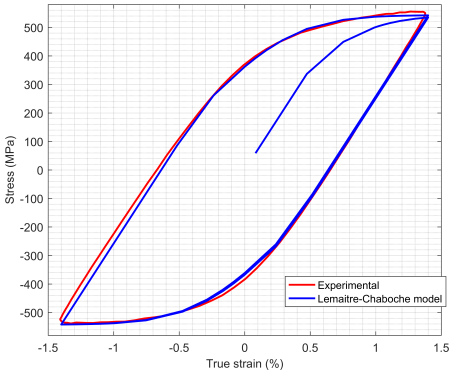

(c)

Figure 4.2: Comparison between the experimental mechanical behavior under cyclic strain and the numerical simulation of the Lemaitre-Chaboche model.

Table 4.1: Parameters for the Lemaitre-Chaboche material model for the target substrate.

σ_Y (MPa)	C (GPa)	γ
370	75	460

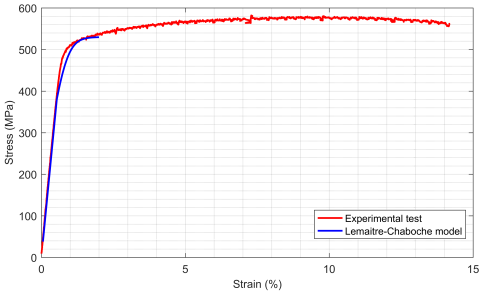

Figure 4.3: Comparison between the experimental mechanical behavior under monotonic tensile strain and the numerical simulation of the Lemaitre-Chaboche model.

As regards the shots, since the beads are made of ceramic material, a linear elastic model should be the most obvious choice, but some experience suggests that solver stability increases if an artificial elasto-plastic behavior of the shots is implemented. For this purpose, a bilinear elastoplastic model is assumed, wherein very high yield strengthand tangent modulus are taken to make the plastic deformation negligible (Table 4.2).

Table 4.2: Parameters for the bilinear model for the shots.

Yield stress (GPa)	Tangent modulus (GPa)
3	300

4.1.2 Impacts arrangement and coverage assessment

The most challenging problem in simulating SP is to correctly assess the true coverage level. Since in this simulation statistical variability of shot velocity and dimension is considered, non of the commonly used formulas is capable of predicting *a priori* the number of impacts required ro achieve full coverage. To this purpose, a MatLab routine is devised in order to generate, prior to the FEM simulation,

a set of shots capable of achieving the 100% nominal coverage on the circular area of 100 µm of radius, in the center of the upper surface ofthe target body, denoted as the control area (see Section 4.1.3 for details). In practice, each generated set is a bunch of data, containing the impact point coordinates, as well as the dimension and velocity of each shot. The logic flow of the procedure is shown in Figure 4.4.

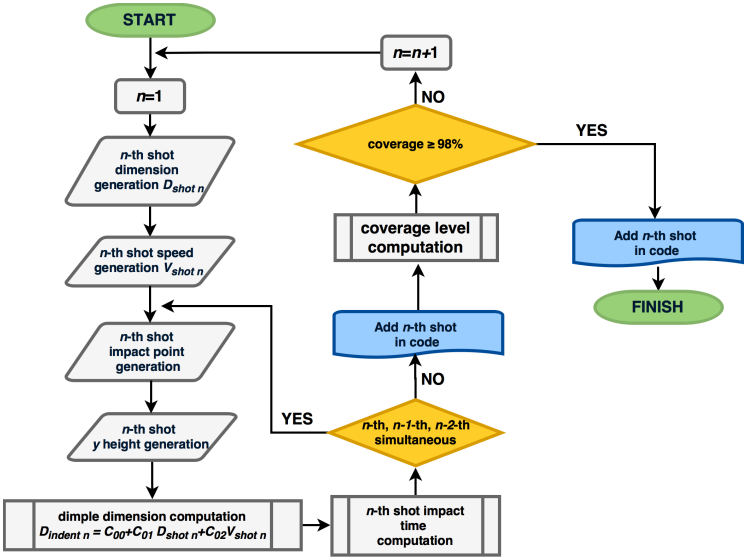

Figure 4.4: Schematic representation of the MatLab algorithm that generates the FEMmodel.

The script at first randomly assigns the dimension value to the first bead on the base of the stochastic size distribution. The sieve analysis results mentioned in Section 3.1 are converted in terms of number of beads by simply assuming an average radius for the shots in each size interval. A Weibull cumulative distribution function is fitted to the shot size distribution as shown in Figure 4.5: the shot dimensions in the FEM model are chosen between 53 µm and 125 µm, in order to avoid the generation of unrealistically large or ineffective small beads.

Since no specific data are available, the shot velocity is assumed to be normally distributed, with an average value of 57 m/s and standard deviation 2.5 m/s as suggested by the experimental measurements. In order to avoid unrealistic values of the shot speed generated by the

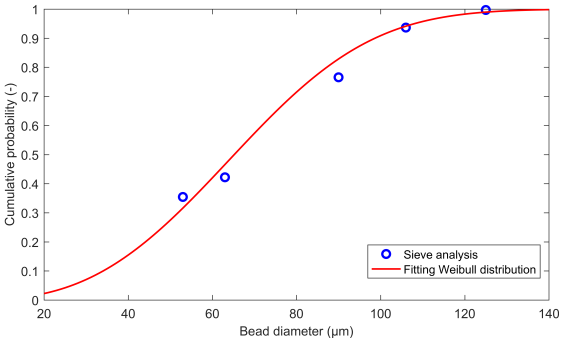

Figure 4.5: Comparison between the results of the sieve analysis on the dimension of the beads and the fitting Weibull distribution used in the simulation.

theoretical distribution, the velocity values are chopped below 52 m/s and above 62 m/s.

A specific simulation campaign is carried out to estimate the dimple dimension on the base of the shot dynamics. Using three levels for both shot size and velocity, 9 single impact 2D axisymmetric simulations are carried out (Figure 4.6) to perform a DOE, as reported in Table 4.3. Indent dimension are measured on the external part of the annulus, in agreement with the visual inspection method used to assess coverage in pratice. The resultant impact dimple dimensions fill a factorial plane having the beads velocity and radius as variables.

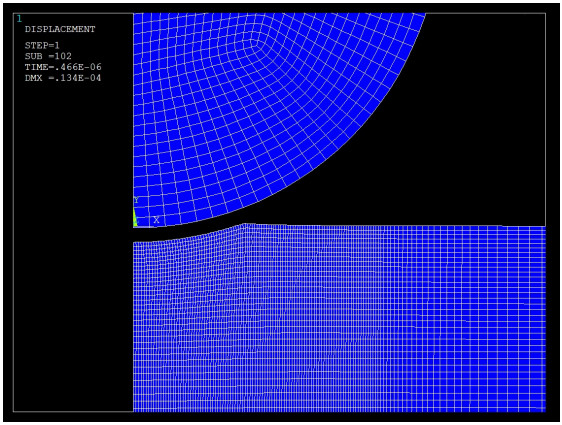

Figure 4.6: 2D axisymmetric simulation used to estimate the indent dimension.

Table 4.3: Impact parameters for DOE.

Impact velocity	52 m/s; 57 m/s; 62 m/s
Shot dimension	53 µm; 89 µm; 125 µm

Through a linear regression it is possible to compute the coefficients of the bilinear relation, originally proposed by [73] and corroborated by the observations of [114], [141], having the form:

$$D_{indent} = c_{00} + c_{01} D_{shot} + c_{10} V_{shot} \tag{4.4}$$

where D_{indent} is the dimple diameter, D_{shot} is the bead diameter and V_{shot} is the impact velocity; the best fit parameters are reported in Table 4.4.

Table 4.4: Best fitting parameters for Equation 4.4.

c_{00}	c_{01}	c_{10} (s)
-7341	0.1657	$0.1347\ 10^{-6}$

Equation 4.4 is used is used by the MatLab routine to compute the dimension of the indent caused by the impact of each shot randomly located inside the control area. The shots are stacked up over the target, equally spaced out along the height direction, similarly to the approach used in [110]. From the speed and the distance from the surface, it is possible to evaluate quite precisely the impact time of each shot, except for some uncertainty due to the deformation of the surface caused by previous impacts.
Previous studies [99], [101], [103] showed that it is not indispensable to consider the interaction among shots, as long as the shots do not interfere in the impact stage [86]. Therefore, the shots interpenetrate when stacked, and no interaction is considered among them; however, a check is performed in order to prevent two or more shots from imping at the same time in close locations.
The number of shots generated in each simulation is the minimum number to achieve full coverage (when at least 98% of the target surface is affected by dimples). Figure 4.7 shows an example of arrangement of the impact locations in the control area.

It is worth noting that the applied method does not consider at all the effect of material strain hardening, even if it is not rare to

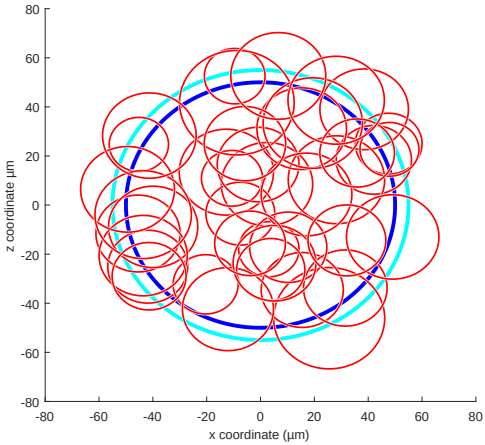

Figure 4.7: Example of random arrangement of impacts. The impacts are gathered in the 110 µm diameter impact area (cyan), results are collected in the 100 µm control area (blue). Red circles represent the theoretical dimension of indents.

observe overlapping dimples (both in the simulation and in the experimental practice). However, only the not-overlapping part of every dimple really affects the coverage evaluation, being the overlapping part already considered in the previous impingement. As regards the overlapping part of the indentations, the strain hardening of the alloy is not very marked, and is supposed not to change significantly the overall dimension of the indents. Therefore, it is assumed to be reasonable not to consider the strain hardening of the substrate in the predictive evaluation of coverage. This method is valid as long as the coverage is less than 100%; for higher coverage level, not only the impact dimples must be considered but also the mass flow rate and the treatment time. When the MatLab routine reaches the desired coverage level, the Ansys commands file is created, and the FEM simulation is started.

4.1.3 Model geometry and mesh

The dynamic FE simulations are carried out with the explicit Ansys/LS-Dyna™17 commercial software. The FE model consists in

a target body, representing a part of the peened component, and in a certain number of beads impinging on it, as shown in Figure 4.8.

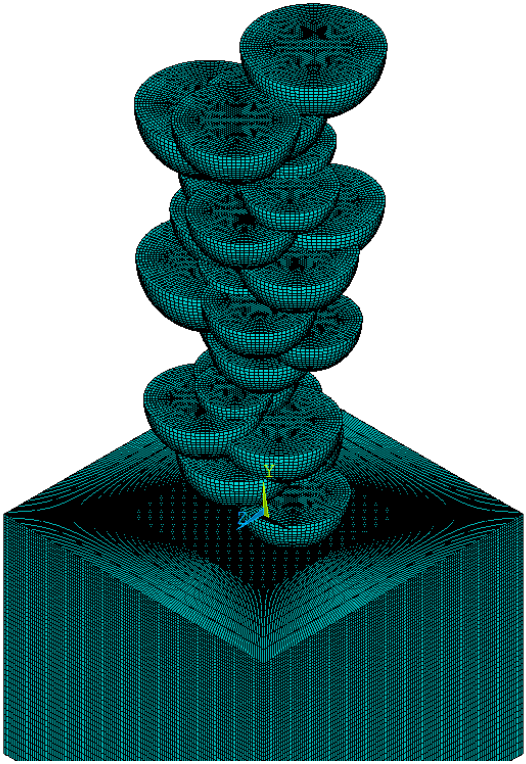

Figure 4.8: The FEMmodel with the stack ofbeads standing above the target body.

Symmetry considerations would suggest adopting the cylindrical shape for the target, also in view of the spherical shape of the beads. Unfortunately, Ansys/LS-Dyna does not permit to define a cylindrical coordinate system. Thus, the target is modelled as a square-based prism, with 300 µm side and 240 µm height; this solution ensures perfectly homogeneous and regularly distributed elements. The thickness ofthe target body is chosen according to the indications provided in [103] with the intent of not perturbing the development of residual stresses; similarly, the target size is chosen according to [117]. The impacts are confined in a circular area of 110 µm diameter in the center of the target upper face, hereinafter denoted as impact area.

The beads are modelled as hemispheres with the aim of discretizing them with sufficiently small elements without penalizing the computational efficiency of the simulation. The shot density is doubled in order to preserve their original kinetic energy. All the bodies are meshed with 4 nodes brick elements SOLID164 with reduced integration and hourglassing control.
The prismatic volume encompassing the impact area, with 156 µm side and 120 µm height, is finely meshed with 1.3 µm size elements, while the surrounding volume of the target body, subject to low-gradients of elastic strains, is discretized with elongated elements to reduce the node number (Figure 4.9).

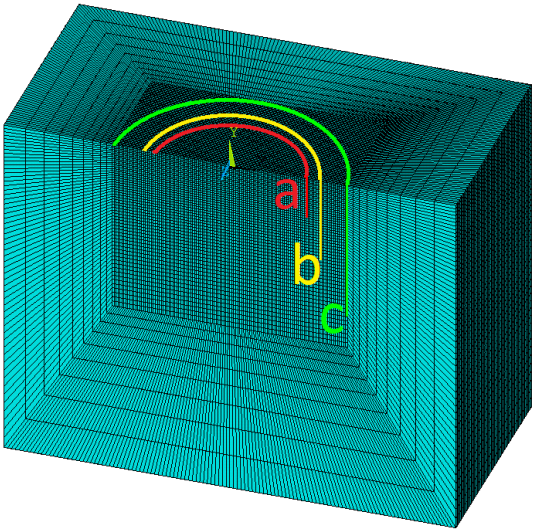

Figure 4.9: Mesh of the target body, section. a: full coverage area; b: impact point area;c: impinged area.

The fine-mesh element size is about $\frac{1}{20}$ of the average impact dimple diameter, smaller than the maximum dimension suggested in [86] for a reliable simulation; this allows an adequate resolution ofthe residual stress state, without an excessive computational cost. Moreover, a convergence analysis is performed starting from 5 µm sized elements, to verify the accuracy of the solution. The boundary of the target volume is constrained to prevent normal nodal displacements in order to take into account the constraint exerted by the surrounding

material, and silent boundaries are applied on all the constrained surfaces to prevent the reflection ofthe shockwaves. A surface-to-surface automatic contact couple is established between the target surface and each bead surface, where the beads represent the master surface, which rules the penalty stiffness necessary to minimize the contact interference.

4.1.4 Damping

No damping is required for a realistic modelization of the process; nevertheless, some damping helps the stability of the nuemrical solver since it contains the obscillation induced in the target body by the impacts.
Two types of damping exist in FEM, α and β, respectively acting on the mass matrix or the stiffness matrix:

$$\mathbf{C} = \alpha\mathbf{M} + \beta\mathbf{K} \tag{4.5}$$

where $\mathbf{C}$, $\mathbf{M}$ and $\mathbf{K}$ are the damping, mass and stiffness matrix. α damping is more commonly used, since it is more effective on the lower harmonics (the closest to the fundamental frequency) and easier to tune. Two approaches are found in the literature [99], [117] to compute the α coefficient, both based on the formula:

$$\alpha = 2\zeta\omega_0 \tag{4.6}$$

where ω_0 is the fundamental frequency ofthe target body and a suitable value for the modal damping coefficient is $\zeta = 0.5$. The first one, used in [99], suggests computing α as:

$$\alpha = \omega_0 = \frac{1}{h}\sqrt{\frac{2E}{\rho}} \tag{4.7}$$

where h is the height of the target body, E is its Young's modulus and ρ its density; resulting in $\omega_0 \simeq 30\,10^6$ /s. A second method, used in [117] for a disk-shaped target, computes α as:

$$\alpha = \omega_0 = \frac{2\pi}{h}\sqrt{\frac{2E}{\rho}} \tag{4.8}$$

resulting in $\omega_0 \simeq 180\,10^6$ /s. The latter method widely overestimates

the damping factor, setting the system in overdamping, so the former approach is chosen.
A small set of simulations, developed to check the local vibration of the impact point after the shot impingement, is used to adjust the damping parameter and to reduce it slightly, in order to obtain an effective damping ratio having a subcritical oscillation regime, as shown if Figure 4.10. The final value is set to $\alpha = 24\,10^6$ /s.

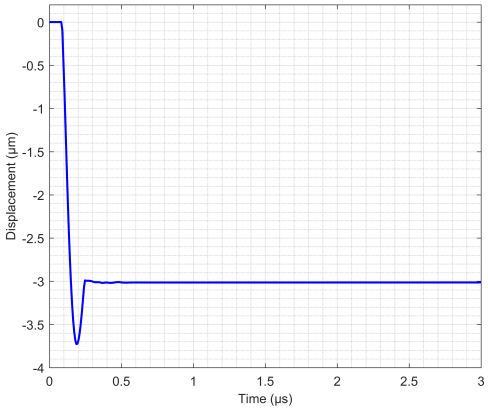

Figure 4.10: Obscillation of the impact point in a single impact simulation for $\alpha = 24\,10^6$ /s. The system is slightly underdamped.

4.1.5 Shot target friction

Very little information is available about the tribological conditions occurring at the contact between ceramic materials and aluminium, even less in the specific case of alumina or zirconia and Al-7075. Moreover, the few data available in the scientific literature refer to tests in vacuum, where higher friction coefficients are measured than under ambient conditions [142], [143].
For this reason, the way chosen to adjust the friction coefficient follows a top-down approach: a small set of 4 simulations having different number of impacting shots is generated. It is verified in the single impact simulation that even a big change in the friction coefficient does not modify considerably the impact dimple dimension. Hence, the simulations set can be carried out with different friction coefficients

without altering the coverage level. This simulation set, therefore, is computed with 6 different values of the friction coefficient, namely [0,0.05,0.1,0.2,0.3,0.4].

The average value of surface roughness and a residual stress profile is computed for every friction coefficient value (Table4.5 and Figure 4.11). The frictionless simulation gave the best results in terms of surface roughness but showed an irregular trend of the residual stress profile; on the other hand, higher fiction coefficients showed a marked tendency to saturation, so that the three highest value gave approximately the same results.

In the real process, the metal components are subject to a degreasing treatment, but no other surface treatment is done; during the shot peening no lubrication is provided. For these reasons, neither a zero nor a high friction coefficient seems to be realistic. The simulations and the previous considerations indicate a friction coefficient value of 0.05 as the best choice; this value of the friction coefficient is applied to all the simulations.

Table 4.5: Estimated surface roughness for different friction coefficient in the simulation.

Friction coefficient	0	0.05	0.1	0.2	0.3	0.4
Surface roughness S_a (µm	0.1122	0.1085	0.1079	0.1061	0.1057	0.1057

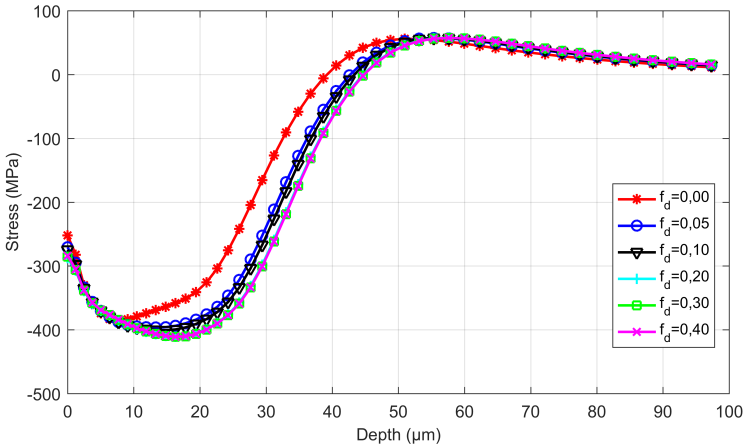

Figure 4.11: Residual stress profile for different friction coefficient (f_d). Notice the saturation trend in the stress profile.

4.1.6 Number of simulations

Given all the statistical aspects involved in the process and the importance of their correct representation, it is clear that many simulations are needed to obtain reliable results. The parameters chosen to monitor the correct distribution are both the overall kinetic energy of the entire bead stack and the number of impacts in each simulation. Quite unexpectedly, the two parameters showed to be roughly equivalent. 30 simulations are randomly generated by the MatLab routine, and they are processed without any selection in order not to alter the stochastic representativeness of the sample. The cumulative probability distribution is computed for the entire population, both in terms of kinetic energy (Figure 4.12) and and number of shots, through a MatLab code that generates over three thousand shot arrangements. The results in term of surface roughness and residual stress seem to be very close to the convergence value at the end ofthe simulation campaign, if the average value is plotted as a function of the increasing number of simulations. Moreover, the kinetic energy and number of shots reproduced by the set of simulations are in satisfactory conformity with the expected cumulative probability distribution, thus the experimental campaign is considered to be statistically representative. In conclusion, it is possible to assert that the study accounts for the statistical variability of the phenome involved in the real process.

4.2 Data processing, discussion and results

4.2.1 Control volume

The nodal solutions are extracted in terms of nodal displacements and stresses after a short relaxing/springback period (0.5 µs) when the damping coefficient is raised to $\alpha = 60\,10^6$; in this way, the nodal velocities and acceleration are very low and the dynamical effects are negligible.
Transverse displacements of the nodes lying in the control area (see Section 4.1.3) are extracted to compute the surface roughness.
The RS field is computed from nodal stresses contained in the cylindrical volume having base equal to the control area and height of 120 µm in depth; in this way, all the nodes on the control volume are well inside the projection of the 100% coverage area, and the nodal

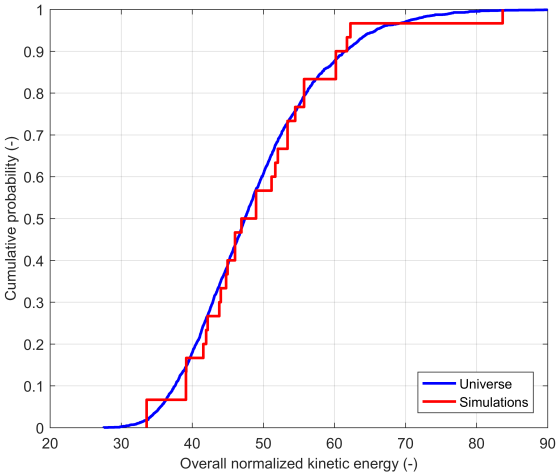

Figure 4.12: Comparison between the distribution of the kinetic energy of the bead stream in the simulations and in the entire population.

results are not affected by undesired border effects.

4.2.2 Surface roughness

The surface roughness is calculated from simulations reproducing the measurements done by the 2D contact and 3D scan profilometers. 2D and 3D roughness parameters are evaluated considering out-of-plane displacements of nodes lying on two orthogonal diameters and on the whole control area, respectively. Specifically, R_a and R_q line-integral as well as S_a and S_q area-integral roughness parameters are numerically evaluated using the same domain discretization scheme of the FE model.

The only controversial issue in this phase concerns the choice of the reference plane to be used to compute the surface roughness. According to the common definition of roughness, the average out-of-plane displacement of the nodes should be used. However, as shot impacts have been concentrated only in the central portion of the target surface, the drop in the average height of the impacted area is accompanied by a rise of the surrounding areas because of the material incompressibility. In this way, the overall surface average height does not change signifiantly. In the realistic case, however, the whole target surface would be peened, and no great change in the average

surface height is expected; for this reason, the reference plane chosen for the roughness computing is the original plane where the nodes lie in the undeformed model.

The results are shown in Table 4.6. It can be seen that the numerical simulation slightly underestimates the actual surface roughness, both in the 2D and (even if to a lower extent) in the 3Dmeasurement. Specifically, the underestimation is 17.7% considering the S_a parameter and 27.4% considering the R_a parameter. It is also worth highlighting that the experimental values are well estimated by the maximum recorded surface roughness obtained in the simulations, and they also lie inside the 96% confidence interval around the average numerical value. The systematic underestimation of the surface roughness can be, at least partly, imputed to the FEM discretization of the target surface. Even if the impact area is finely meshed, the size of the elements may not be able to entirely capture the sharp peaks of the impinged surface. In other words, the FE mesh might low-pass filter the surface topology, thus eliminating the contribution ofdisplacement with high spatial frequency on the surface roughness.

In addition, Figure 4.13 indicates an increasing trend in surface roughness Sa with rising kinetic energy of the bead stream (in the figure normalized with respect to a reference kinetic energy value of a 90 µm diameter shot at 57 m/s velocity). Assuming constant, with a certain approximation, the portion of kinetic energy transferred to the target body in the form of strain energy, the kinetic energy of the stream scales with the treatment intensity. This confirms the intuitive feeling that more intense peening treatments tend to produce higher roughness values.

Table 4.6: Surface roughness resulting from the simulations.

Roughness parameter	R_a	R_q	S_a	S_q	R_t
FEM average value (µm)	0.98	1.16	1.02	1.23	6.12
FEM standard deviation value (µm)	0.22	0.25	0.11	0.13	0.7
FEM max value (µm)	1.48	1.67	1.29	1.54	8.43
Experimental value (µm)	1.35	1.67	1.24	0.54	7.12
Experimental standard deviation (µm)	0.14	0.15	0.05	0.07	0.61
Error(%)	-27.4	-30.5	-17.7	-20.1	-14.0

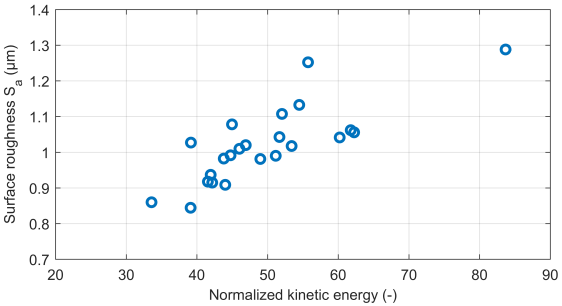

Figure 4.13: Surface roughness S_a vs. the normalized overall kinetic energy of the shot stream.

4.2.3 Residual stress field

The thickness of the surface layer where plasticization occurs is a significant estimator of the treatment intensity. EBSD analyses undertaken in [123] on the same peened material attested that this thickness is about 25 µm; this experimental value is in good agreement with thenumerical simulations, which indicate an average thickness of the plasticized surface layer of about 20 µm. This layer is subjected to intense compressive RSs. The comparison between numerically estimated and experimentally measured RSs is not straightforward and requires a data processing method specifically developed in the present study.

In many papers, the in-depth residual stress profile is evaluated from nodal stresses and nodal coordinates expressed in the undeformed reference system (e.g. [92], [103]). In a few papers (e.g. [81]), it is made clear that the nodal coordinates of the deformed model are considered with the aim of achieving a more realistic estimation of the spatial distribution of the RS values. This issue is marginal in conventional SP (i.e. steel shots on steel substrate), as the depth of the surface layer, where significant nodal displacement take place, is small with respect to that interested by compressive RS s. Conversely, in micro SP treatments, the depth of such layers is comparable; therefore, a realistic estimation of the RS profile requires the nodal displacements to be taken into account. In addition, the effect of X-ray penetration on the RS measurements must be considered for a consistent comparison of experimental and numerical data. The RS field in undeformed

configuration is use only to check the equibiaxiality of the RS on the xy plane and is shown in Figure 4.14.

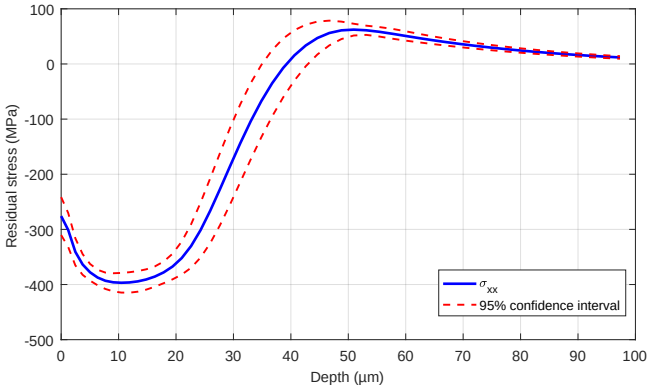

Figure 4.14: In-depth RS profile from the FEM simulations, in undeformed configuration.

In the present study, three main strategies are devised and applied to address the issue of substrate deformation.
The first one consists in ideally slicing the control volume in 2 µm thick layers starting from the highest peak on the surface and proceeding towards the specimen depth. An average of the nodal stress value for all the nodes in every slice is computed, and a residual stress profile is obtained as a function ofthe depth below the surface. This profile is comparedwith the profile obtained in Section 3.2 (see [65] for further detail) removing the radiation penetration effects from the XRD measures. Figure 4.15 shows experimental data corrected for penetration and the numerical estimates corrected for layer deformation. It can be noted that the 95% confidence interval ofthe numerical profile is almost completely comprised in that of the experimental measure. The depth of surface layers interested by compressive RSs (about 50 µm and the intensity of compressive RS peak (about −400 MPa) are well reproduced by the numerical simulations, while these latter tend to underestimate the peak location below the surface (12 µm vs 20 µm) and to overestimate the compressive RSs in the outer 10 µm thick

layer.

It is also interesting to observe that the numerical simulations indicate, below the surface layer interested by compressive RSs, a fairly low tensile RS peak (about 50 MPa) followed by a gradual extinction of them. This is in good agreement with neutron diffraction measurements done in [144] and contradicts the concerns that SP could induce an intense localized tensile RS peak thus jeopardizing the beneficial effect exerted by the surface compressive RSs.

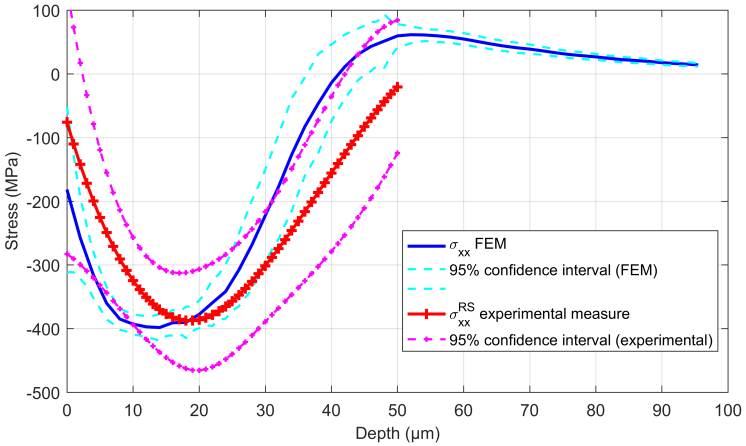

Figure 4.15: Comparison between true RS profile from the FEM in deformed configuration and the true RS profile from experimental measurements.

The second strategy is based on a completely different approach. Considering the known X-ray penetration depth, the nodal stresses are treated in order to obtain a RS profile comparable with the experimental RS profile directly obtained from the XRD measure. At each depth below the surface, the residual stress value is computed by numerical integration of Equation 3.2, whereby the integral is replaced by the following weighted average of discrete RS estimations:

$$\bar{\sigma}_{xx}(z) = \frac{\sum_{k=1}^{n} \sigma_i e^{-\frac{z-z'}{\xi}}}{\sum_{k=1}^{n} e^{-\frac{z-z'}{\xi}}} \tag{4.9}$$

where n is the number of nodes laying deeper than the chosen z value, z_i and σ_i are respectively the depth and the RS value for

each of the selected nodes and ξ is the information depth discussed in Section 3.2. Figure 4.16 compares raw experimental RS data (not corrected for radiation penetration) with the numerical estimations done according to this second strategy, namely corrected for layer deformation and X-ray penetration.

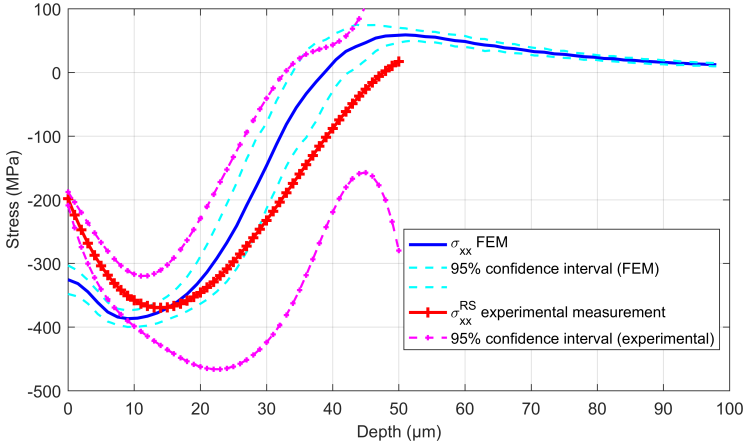

Figure 4.16: Comparison between RS profile fromthe FEM, considering the penetration effect of the X-ray, and the RS profile detected with the XRD analysis.

Also in this case the agreement is very good, especially in terms of overlapping between the confidence intervals, apart from a very superficial layer (8 µmthickness), where the simulations overestimate the compressive RSs. This could be related to the fact that the structure of this layer is greatly affected by the surface roughness, as its thickness is comparable with the maximum peak-to-valley distance.
The last approach attempts to take into account the effect of both surface roughness and radiation penetration on the XRD measurement of the residual stress profile. Specifically, the outer surface layers are not continuous owing to the irregular surface morphology composed of peaks and valleys. Surface layers can then be referred to as a continuum of pseudo-density lower than that of the bulk. For this reason, they are expected to contribute less to the residual stress information collected by the XRD technique. Therefore, in a first approximate attempt to estimate the true residual stress profile, the contribution of each material layer to the XRD measure is scaled proportionally to

its pseudo-density. To evaluate this parameter, the control volume is divided into thin "slices" (1 µm thickness) and the material continuity is estimated as the ratio of the number of nodes in every slice to the number of nodes on the undeformed surface. The stress value of each material layers is scaled as follows:

1. the penetration coefficient ξ is supposed to be related to the actual material density, being the material a filter to the radiation penetration, so for each material layer a different ξ_l coefficient is computed as:
$$\xi_l = \xi \frac{N_{surf}}{N_l} \tag{4.10}$$
where ξ_l is the penetration coefficient for the l-th layer, N_l is the number of nodes in the l-th layer and N_{surf} is the number of nodes on the undeformed material surface;

2. The RS is thus computed from the following expression:
$$\bar{\sigma}_{xx}(z) = \frac{N_{pv}}{N_u} \frac{\sum_{k=1}^{n} \sigma_i e^{-\frac{z-z'}{\xi_l}}}{\sum_{k=1}^{n} e^{-\frac{z-z'}{\xi_l}}} \tag{4.11}$$
where N_{pv} is the number of nodes having y coordinate lower than the highest peak and higher than the deepest valley, and N_u is the number of nodes enclosed in the same volume in the undeformed configuration.

As a first attempt to take into account this effect, the third strategy based on a pseudo-density of the surface layers is adopted in the comparison shown in Figure 4.17. In this case, the stress profile ap pears somehow artificial, indicating the need of a more sophisticated algorithm in the pseudo-density computation. Anyway, it is clear that the stress profile correction moves in the right direction, reducing the surface stress value; a better algorithm could make the stress curve smoother and presumably closer to the experimental curve.
In conclusion, these comparisons demonstrate how difficult it is to interpret the experimental surface RS values, as they are greatly affected by the actual penetration depth of the radiation into the roughness asperities. The irregular surface morphology makes also complicate establishing the origin of the depth coordinate used to map the residual stress profile.

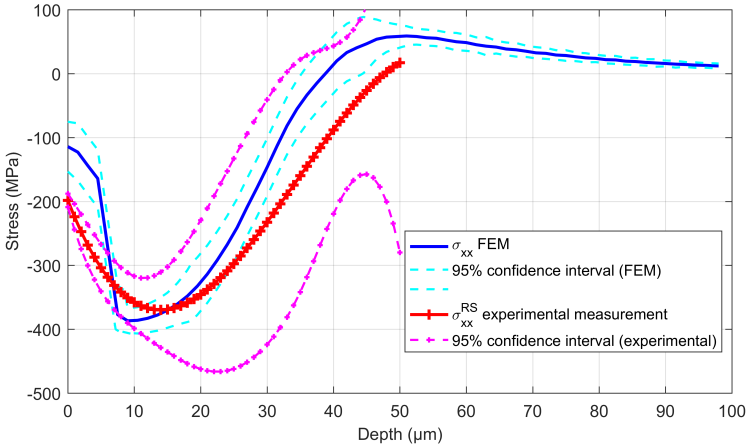

Figure 4.17: Comparison between RS profile from the FEM, considering the penetration effect of the X-ray and the pseudo-density of the peened surface, and the RS profile detected with the XRD analysis.

4.2.4 Stress concentration factor

The stress concentration exerted by the surface roughness is a key parameter to evaluate the capability ofthe surface treatment to improve the fatigue behavior of the peened part. In order to compute the stress concentration factor, an implicit procedure is performed after the ex- plicit dynamic simulation. The finely meshed central volume of the target body, where all the shots are already impinged, is exported into the static implicit simulation environment (Figure 4.18). The new model has roughly the shape of a square based parallelepiped with side 156 µm and height 120 µm, and preserves the deformed shape of the previous model but not the RS state. The model undergoes two static simulations, consisting in the application of a uniform tensile stress of 1 MPa on two opposite side faces, first in the x then in the y direction. The results are analysed in terms of von Mises equivalent stress to estimate the stress concentration factor K_t

The simplest method for the estimation of the K_t factor consists in computing the ratio between the nominal stress applied to the model and the maximum stress in the model. This method leads to a large overestimation of the stress concentration factor, since it considers the stress state that develops in very small volumes (virtually, in a single

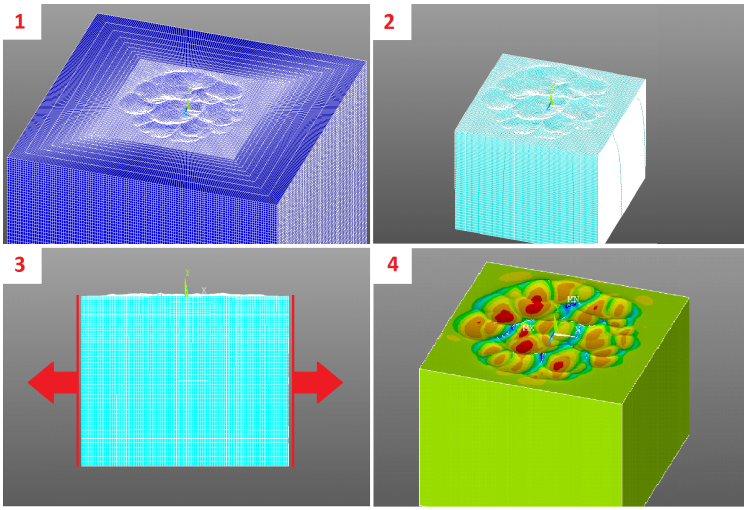

Figure 4.18: Representation of the procedure developed for the explicit-to-implicit simulation used to compute the K_t factor.

node) without taking into account the stress state in the surrounding material.

Indeed, in the shallowest points of the impingement dimples an intense stress state develops during the simulation of the tensile test, and the stress peak is higher if the dimple is deeper; anyway, its value decreases rapidly moving away from the bottom of the dimple. sIn the case of these FEM models, also the case of a singularity generated by the previous impacts has to be considered.

The concept of material notch sensitivity was introduced to account for this effect; more recently, the theory of critical distance has been developed and formalized to predict the fatigue resistance of parts carrying stress raisers [145], [146]. To predict the fatigue strength of notched shot peened parts, in [65] is proposed a critical distance theory in which the stress averaging domain is a circular area lying on the plane normal to the direction of load application and centred in the crack initiation site. The size of this circular area depends on the material and the number of cycles to failure and was estimated equal to 54 µm for predicting the high-cycle fatigue strength of Al-7075-T651. In the present study, the same approach is adopted to estimate the notch fatigue factor, where by the equivalent von Mises

stress is averaged over a half-circular area centred in the bottomof the crater characterized by the highest stress value and therefore in the most likely crack initiation site (Figure 4.19).

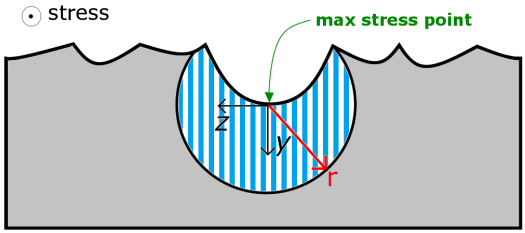

Figure 4.19: Schematic section representation of the model used to compute K_t. The striped area highlight the area used to compute the average stress value.

The plot representing K_t parameter versus the radius of the hemi-circular area is shown in Figure 4.20. The results obtained from the FE simulation show good accordance with the experimental/empirical results, also considering a critical distance of 54 µm, which gives a K_t value of 1.05. The semi-analytical approach devised in [125] and used in [123] predicts a value of 1.11 when the roughness parameters listed in Table 4.6 are used, while the 2D FEM model developed in [65] using the experimental surface profiles estimates a Kt value of 1.09. Also in this case the slight discrepancy of FE predictions from experimental measures can be ascribed to the numerical underestimation of the surface roughness, which is supposed to play the most important role on the stress concentration effect.

Some observations on stress concentration factor The population of SP experiments created in the present work has been analysed to search for possible relationships between the peening process parameters and the effects on the target material in terms of roughness and residual stresses. No evident relationship has been found between the stress concentration factor and the average shots energy in the simulation (Figure 4.21a), the maximum energy of a single shot in the simulation (Figure 4.21b), the standard deviation of the kinetic energy in the shots stream (Figure 4.21c).
Moreover, no clear correlation has been found between maximum compressive RS and the overall kinetic energy of the shot stream

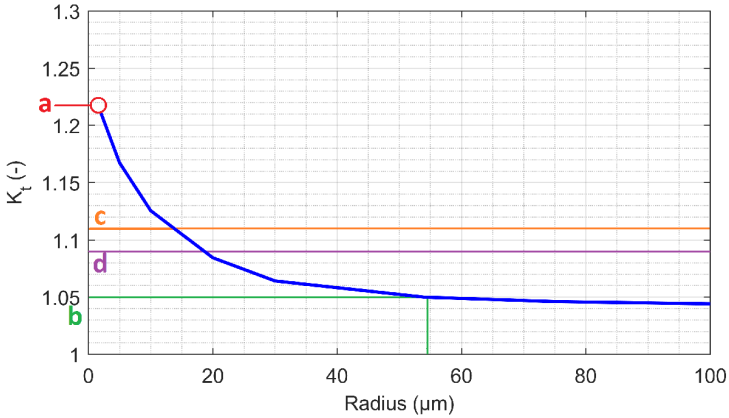

Figure 4.20: Stress intensity factor vs. radius of the hemi circular area used for its computation. a: maximum stress concentration near a single node; b: K_t computed using a 54 µm critical distance; c: K_t computed using the semi-analytical formula in [123]; d:K_t computed with a 2D FEMmodel in [65].

(Fig 4.21d). Even if the link between the surface roughness and the stress concentration is a matter of fact, the K_t value (computed using a 54 µm radius) does not show a clear correlation to the overall kinetic energy of the shot stream (Figure 4.22) while the resulting value of the surface roughness does (Figure 4.13). We must remind, however, that the surface roughness is a distributed phenomenon, which depends on the dynamics of a high number of beads impinging on a surface, while K_t is a strictly local phenomenon, depending on the morphology of a limited portion of the surface.

4.2.5 Conclusions

The present Chapter describes one of the first attempts to simulate a micro SP treatment. Special care is taken in reproducing the statistical variability that affects the process parameters: coverage, shot size distribution, shot velocity distribution, random impacts point. The Lemaitre-Chaboche material model is used to take into account the correct material behavior under repeated strain. A number of 30 explicit dynamic simulations in Ansys/LS-Dyna are carried out to produce a population of numerical results that is statistically significant. The simulations are validated through surface roughness

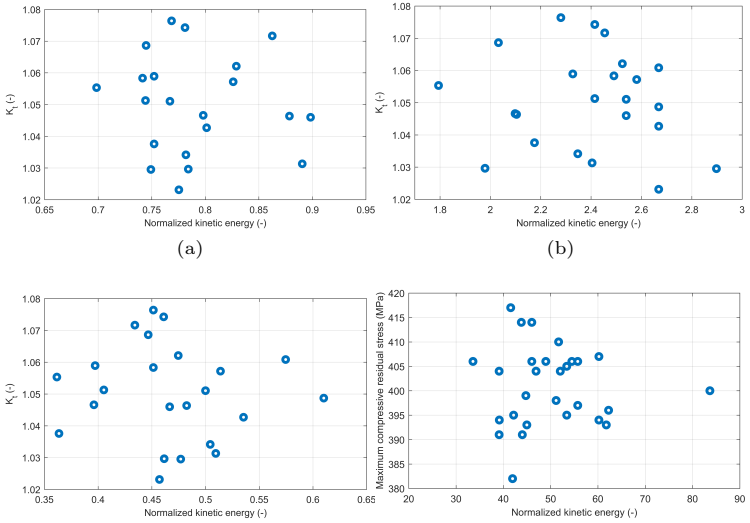

Figure 4.21: (a) K_t factor vs. normalized average kinetic energy of the beads in the simulation; (b) K_t factor vs. normalized maximum kinetic energy of a single bead in the simulation; (c) K_t factor vs. normalized standard deviation of the kinetic energy of the beads in the simulation; (d) Maximum compressive RS in the target vs. normalized overall kinetic energy of the bead stream.

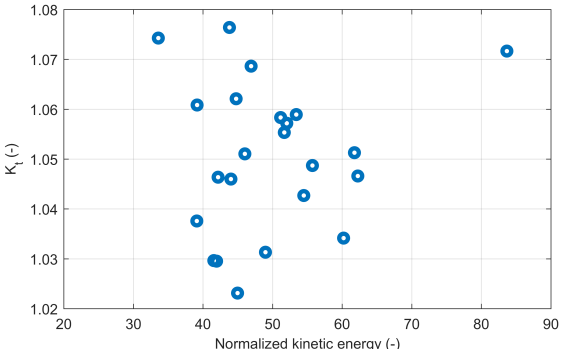

Figure 4.22: K_t factor vs. normalized overall kinetic energy of the bead stream.

and RS measurements. For this purpose, several procedures have been specifically developed in the present paper to permit a consistent comparison between experimentally measured and numerically estimated residual stresses. The following conclusions can be drawn:

1. The numerical simulations are in good agreement with both 2D and 3D roughness measurements. Nevertheless, the discretization of the target surface produce a systematic underestimation of the surface roughening effect.

2. If the numerically estimated residual stresses are corrected for layer deformation and experimentally measured values are corrected for X-ray penetration, a good agreement is obtained both in terms of stress magnitude and depth of the residual stress peak, even if the deep deformation of the surface layers in the target generates some uncertainties in the estimation of the stress profile.

3. If the numerically estimated RSs are corrected for both effects (radiation penetration and layers deformation), again a good agreement is obtained with the experimental data, especially in the stress peak region.

4. The discrepancy between numerically simulated and experimentally predicted residual stress in the outer layer can be reduced by considering the effect of surface roughness on the pseudo-density of the material.

5. The numerical simulations permit to estimate the stress concentration effect exerted by the surface roughness, in good agreement with analytical and numerical values taken from the literature.

6. It is very hard to identify clear correlations between the parameters governing the dynamics of the bead stream and the treatment effects. Only the surface roughness seems to be correlated with the overall kinetic energy of the bead stream.

Chapter 5

Simulation of SP on an edge

In this Chapter the problem of simulating SP on an edge is addressed, as an attempt to move towards the simulation of the process on geometrical details acting as stress raisers.
As mentioned in Section 1.2, simulation of SP is aimed at a better knowledge of the process, mainly in perspective of integrating the beneficial and detrimental effects of peening in the design process, in order to achieve a better optimization of components even when fatigue life dimensioning is involved. In this regard, the importance of geometrical discontinuities (edges, grooves, notches) in undercutting the fatigue resistance of components can not be neglected. The approach through which the knowledge of the peening effects (mainly the RS state) in specific point of the studied component can lead to a consistent integration of these in the design process is well stated by Jebahi et al. in [120].
Unquestionably, the geometrical features on the surface of the treated component do exert some kind of perturbation on the flowing of the peening media. Since the realistic simulation of the coverage is strictly related to the knowledge of the dynamic conditions of the stream of shots impacting on the surface, as also shown by Gariepy et al. [113], some more care is required in devising the correct model to simulate the peening process.
A first approximated model is devised on the basis of the experience gained in the simulation on a flat surface. Similarly to what seen in the previous Chapter, the model consists in a prismatic target body and a stack of hemispherical impacting shots (Figure 5.1).

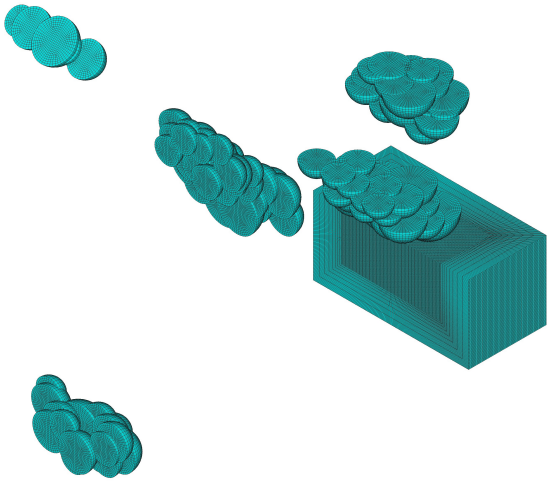

Figure 5.1: Simplified model of the SP process on an edge.

The impact area is still circular, having a 100 µm diameter; in this case it is "folded" on the ideally sharp edge where the process is simulated. In other words, impacts are gathered inside two hemicircular areas on the two concurring faces that form the edge. A number of shots is randomly arranged on the two impact areas, according to the MatLab routine seen in Section 4.1.2, in order to achieve full coverage. Since the peening nozzle turns around the tip of the edge at constant velocity, some more shots are required to simulate the process. Since not many data are available, a predetermined number of shots (24 on each face of the corner) are generated to impact with a 45° inclination with respect to the impacting surface, in random locations. 5 more inclined shots are generated to impact directly on the tip of the edge. An illustrative arrangement of impacts is shown in Figure 5.2.

The resulting RS field obtained from this model is not satisfactory, and shows some discrepancies with the reconstructed RS field mentioned in Section 3.3. Beyond the results of the simulations, this model is useful to highlight the critical aspects of the model: in particular the instability due to the intense deformation of the elements on the tip of the edge, and the diffulty in arranging the impacts on the target, without introducing arbitrary and unsubstantiated approximations.

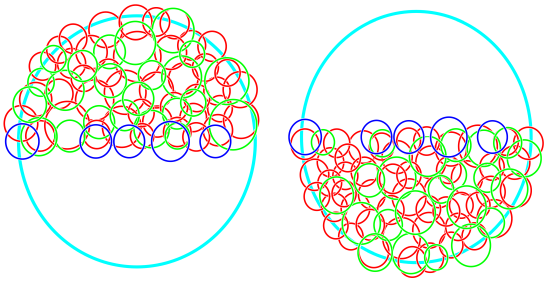

Figure 5.2: Illustrative arrangement of shots on the two impact areas on the two faces of the edge. In red, the indents of the shots randomly arranged by the MatLab routine. In green, 24 inclined shots. In blue, the shots impacting on the edge tip. The cyan circle represents the 100 µm diameter impact area.

To deal with the problem of instability, two features are introduced in the model: a fillet on the edge tip, and erosion of the target elements. No precise informations are available on the precise edge morphology, thus a 10 µm radius fillet is assumed on the tip. This helps the stability of the solution, since it avoids the excessive deformation of the elements on the sharp corner, without excessively modifying the target geometry. Moreover, bigger elements are used in the impact are (3 µm, in order to make elements capable of tolerating more intense deformation; on the other hand this makes the simulation not really suitable for the study of the morphology modification of the surface.
Arranging the impact in the surroundings of the edge is quite a more complex matter. For this purpose, a more accurate study is required, in order to evaluate the number of impacting shots and their dynamics. As seen in Chapter 2, discrete element method DEM is an eligible tool for simulating the interaction among shots and their dynamics.
The DEM is then used to simulate the shot stream dynamics, i.e. the velocity distribution of impacting particles in the edge region. This information is necessary to set up the FEM simulations of the SP process at the edge. Four different scenarios are modelled to investigate the contribution of the different process stages to the final RS distribution. In the first more complete simulation the nozzle approaching, turning around and finally receding from the edge is performed, then three simplified simulations were considered, i.e. respectively, only the shots blown by the nozzle when turning around the edge disregard-

ing the approaching and receding phase, or only the shots impacting orthogonally or with a 45° fixed inclination onto the two flat faces near the edge disregarding the turning phase of the nozzle. The effect of the fillet radius on the edge tip will be studied in a further parametric simulation campaign, for the two more promising approaches identified in the previous simulations. The RS fields resulting from the numerical simulations are compared with RS fields reconstructed using the results of Micro-X-ray diffraction taken in the vicinity of the edge of smooth samples, as seen in Section 3.3.

Part of the data displayed in this Chapter has been published in [147].

5.1 The DEM-FEM approach.

The FEM simulation of the entire SP process would require an excessive computational effort, given the high number of mutually interacting bodies involved. The cooperation between DEM and FEM is summarized in the logic flow shown in Figure 5.3; the cooperation is intended to give a realistic and detailed formulation of the SP treatment in all its aspects with an affordable computational cost. The DEM model assumes purely elastic shot-shot and shot-target interactions and simulates the dynamic conditions of the shot stream, i.e. the interactions between shots in the path between the outlet of the nozzle and the impact surface and the impact momentum of the impinging particles.

As well stated in [119], shot-shot interaction are supposed to play an important role especially in treatments with such fine peening media as the one being considered. DEM simulations are performed using the open-source software Yade-DEM. The model is set up according to the nominal parameters of the SP treatment mentioned in Section 3.1 and is used to compute the impact location and velocity of the shots on the target body. The subsequent FEM simulations focus on the complex elastoplastic phenomena produced by the multiple interactions between the impacting shots and the peening target and predict the surface deformation as well as the RS state generated in the aluminum alloy at the end of the treatment. To set the parameters up for the realistic DEM simulation, a preliminary calibration phase

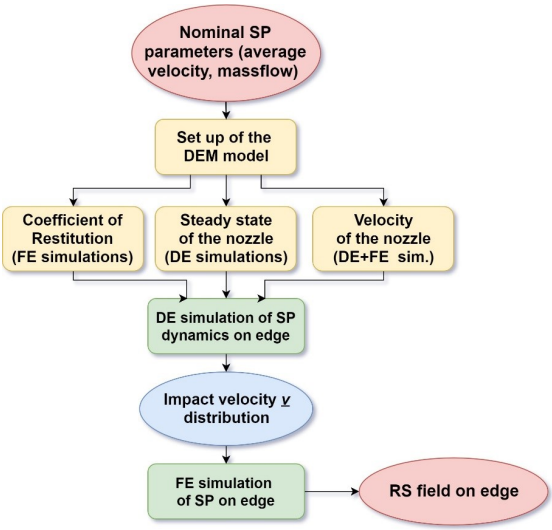

Figure 5.3: Schematic representation of the synergistic DEM-FEM approach.

based on specific FE analyses is needed. First, a coefficient of restitution CoR is computed, to take into account dissipative phenomena of the impacts; more details on the CoR can be found in [148]. Then, the correct parameters for the nozzle to achieve steady-state working are studied. Lastly, the translational speed of the nozzle to achieve full coverage in one single pass is computed.

5.1.1 Setup of the DEM simulation

Coefficient of Restitution CoR The first aspect to be solved for the simulation of the stream dynamics concerns the complex dissipative phenomena connected with the interaction among particles as well as between particles and target. The dissipation is due to friction between bodies, plastic deformation, and conversion of the translational kinetic energy into rotational kinetic energy. Shots in the DEM are indeed considered as punctiform bodies, having their own dimension, mass and inertia. The CoR is defined as the ratio between the relative velocity of two bodies, before and after an impact:

$$CoR = \frac{V_{in}}{V_{out}} \tag{5.1}$$

where V_{in} is the relative velocity of the shot before the impact and V_{out} is the relative velocity after the impact. For the sake of simplicity, it is assumed to be independent of the size and the velocity of the shots.
The CoR to be used in the simulations is computed using FEM simulations of a sphere impacting on the surface of a cubic body, which is constrained to prevent any motion; the ratio between the initial and final velocity of the impacting sphere gives the CoR. To compute the CoR for the shot-shot impact case, both the shot and the cubic body rely on a linear elastic material model having the mechanical properties of the ceramic beads. In the case of the shot-target interaction, the elasto-plastic material model used for the aluminum alloy is used for the target body.
The shot-shot interaction does not consider any plastic deformation, so the CoR is constant and has a value of 0.69. On the other hand, in the case of shot-target interaction, work hardening of the aluminum alloy causes the CoR to change slightly in case of multiple impacts. For the first impact the CoR value is 0.43 and it gradually increases to the asymptotic value of 0.6 reached just after the fourth impact.
Nevertheless, using a variable CoR would necessitate incorporating the strain hardening into the DEM simulation. Since neglecting the CoR variability does not affect the simulation significantly [119], the CoR is considered constant throughout the simulations and its value is 0.69 for shot-shot interaction and 0.43 for shot-target interaction, as well stated in [137].

Steady-state functioning of the nozzle The second step towards the DEM setup regards the study of the transient stage of the shots flow and the achievement of the steady state of the process. The DEM models used in the following consist basically of a nozzle, a stack of spherical bodies flowing through it and a prismatic target body.
The nozzle is a fundamental part of the DEM model, and the related parameters need to be adequately set in order to have a realistic representation of the process. The nozzle is modeled as a cylindrical rigid surface, having a diameter of 24 mm and an outlet diameter of 12 mm; the shape of the outlet is shown in Figure 5.4. The size of the shots in the stack is randomly generated according to the stochastic distribution obtained from the experimental measurements as seen in

Section 4.1.2.

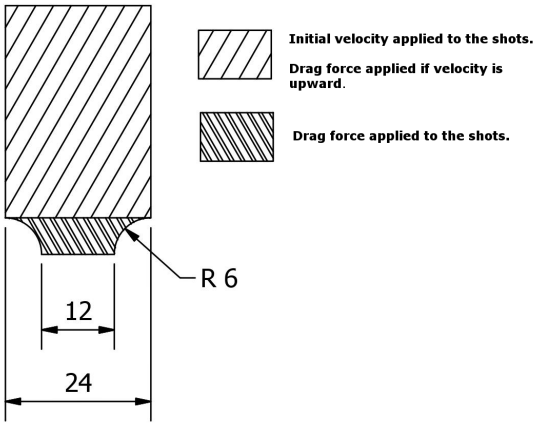

Figure 5.4: Schematic representation of the nozzle. The hatched areas show where initial velocity and drag force are applied to the shots.

The motion of the particles in the pipes and nozzle is expected to be chaotic, given the high number of impacts and interactions occurring among shots and shot and surfaces, and the turbulence of the air used to blow the beads. Nevertheless, the simulation of the entire path of the beads inside the peening machine is not feasible nor even necessary, since the nozzle plays the most significant role in determining the dynamic conditions (direction and velocity) of the shots; thus, the model is set up as follows. In the cylindrical part of the nozzle, the shots are randomly distributed in the volume by the software with a volume density (better said a "packing factor") chosen as a parameter of the DEM simulation. A constant and equal velocity is applied to all the shots, namely the average velocity of the shots which has been experimentally measured (57 m/s, see Section 3.1), and the direction is parallel to the axis of the nozzle. In the tapered part of the nozzle, a significant part of the shots impacts on the nozzle surface and their trajectory is deviated or backscattered, with the effect of generating also new impacts among shots. Most of the interactions among shots happen in this part of the nozzle causing flow congestion and decrease in the mean velocity. This is counteracted by the drag effect of the compressed air used to blow the shots and to preserve the mass flow

and average velocity of the stream. In the DEM model, a drag force (F_{drag}) is applied to the shots in this region whose magnitude is proportional to the square of the difference between the shot velocity and the nominal velocity:

$$F_{drag} = k \cdot (V_{shot} - V_{nominal})^2 \tag{5.2}$$

$V_{nominal}$ is the average velocity of the shot stream and V_{shot} is the actual velocity of each shot. The drag force is also applied in the upper part of the nozzle to the backscattered shots, i.e. to the shots which are moving in the opposite direction with respect to the bead flow because of previous impacts. A schematic representation of the nozzle is given in Figure 5.4.

The parameters to be set in the model are the packing factor of the shots in the stack (number of shots per unit volume) in the non-tapered part of the nozzle, and the coefficient k in Equation 5.2. Both these parameters are adjusted by trial-and-error in order to achieve the steady state functioning of the nozzle, with the mean velocity of the shots at the outlet of the nozzle and mass flow of the peening media matching the nominal parameters of the process.

Simulations (the nozzle is represented in Figure 5.5) are performed using an increasing number of shots, that means a progressively increasing simulation time. The evolution of the mass flow and average velocity of the shots is monitored to recognize the achievement of the steady state. The correct duration of the simulation is identified in 2.3 ms, with 130000 transiting shots. The final mass flow and average velocity of the shots are depicted in Figure 5.6 as a function of the simulation time. The steady state is achieved in $\sim$1 ms, after which the system is considered to be working in a stationary condition.

Translational velocity of the nozzle The last step for the setup of the DEM model is to adjust the translational speed of the nozzle to achieve the chosen coverage level. To do this, a DEM model of the SP process on a flat surface is devised, to get to know the spatial distribution of impacts.

The model consists in a cubic body, impacted by a stack of spheres coming from the nozzle as described in the previous section. The axis of the nozzle is orthogonal to the impact surface, as in the real

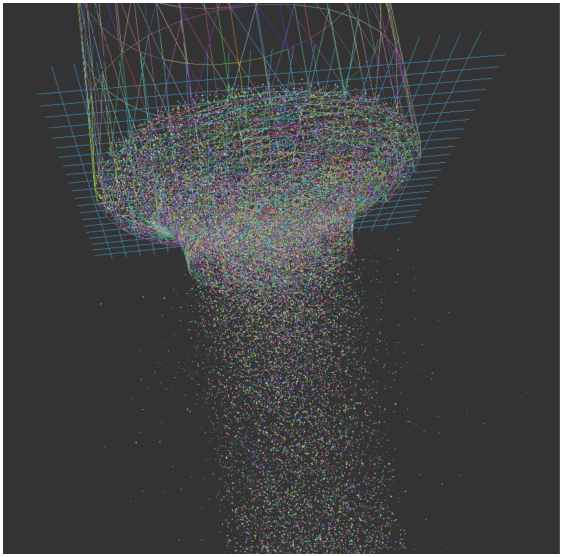

Figure 5.5: Nozzle in the DEM simulation.

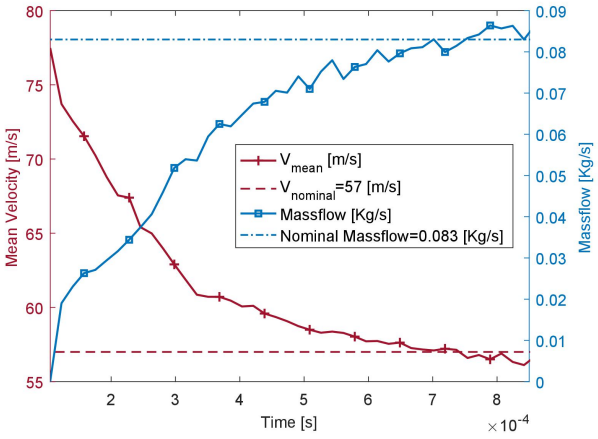

Figure 5.6: Mass flow and mean velocity at the outlet of the nozzle in the DEM simulation. The steady state can be noticed.

peening process and the distance between the nozzle outlet and the target body is 100 mm. 5 simulations with 130000 impacting shots and a simulation time of 2.3 ms are performed. Performing many shorter simulations is preferred to performing a single, longer one due to the memory required to record the data collected during the solution makes the simulation extremely space-costly and data storing in long simulation makes the solution slower.
The results are recorded in terms of impact velocity $\bar{v}$, and location of the shots, after the steady state functioning was achieved. When a shot has a positive velocity (i.e. it is approaching the target) and its center of mass is closer to the target surface than the shot radius +1 µm, its location and velocity are recorded as the impact ones. This causes a slight (though negligible) error in the detection of the impact location but prevents the recording from happening after the impact has already started, which would cause the detection of a mistaken impact velocity.
The distribution of the impact velocity intensity is computed considering all the impacts on the whole target surface and is shown in Figure 5.7 and is more broadly scattered than expected. For the sake of simplicity, the velocity distribution on the flat surface and the edge is assumed to be Gaussian as in [110], [149], despite the scattering due to shot-shot interaction shown in [74]. The spatial distribution of the impacts is useful for a visual check of the plausibility of the results and is shown in Figure 5.8. It is interesting to notice that no significant coorelation has been found between the shot radius and its impact velocity or its scattering angle. Bigger shots tend to impact wit a higher velocity and a lower scattering angle, but the difference is so weak (around 5% of the average velocity) that makes this correlation not worth to be taken into account.

The output data of the DEM simulation are used, in a first stage, to estimate the number of impacts getting full coverage un a chosen area. The number of impacts per unit area needed to achieve full coverage is computed using the MatLab routine devised in Section 4.1.2, based on the estimation of the indent diameter as a linear function of the dimension and velocity of the impacting shots. The routine simulates randomly arranged impacts on a circular area of 100 µm diameter. Random dimensions of the shots are assumed, using the

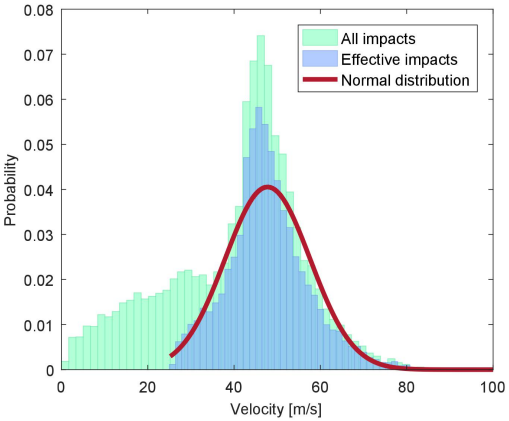

Figure 5.7: Fig. 7. Distribution of the magnitude of the impact velocities in the simulation on a flat surface. Comparison of the curves considering all the impacts or only the effective ones. In red the fitting normal distribution.

stochastic distribution obtained from the experimental measurements (Section 3.1). Random velocity of the shots is assumed, according to the stochastic distribution obtained from the aforementioned DEM simulation. The coefficients of the function used to estimate the dimple dimension are adjusted using a DOE of FEM simulations with single shots impacting on a flat surface, with different velocities and dimensions of the shots. The velocity distribution is highly scattered and the average impact velocity is slightly lower than the nominal velocity ($\sim$52 m/s vs. 57 m/s). This leads to estimate the average number of shots to achieve full coverage as 85, which is much higher than the average number of shots to achieve full coverage ($\sim$ 48) when nominal average velocity and less scatter in velocity is considered as in the previous Chapter 4.

It is worth noting that the results of these single shot simulations prove that shots having an orthogonal impact velocity V_{shot} <25 m/s do cause a negligible plasticization of the target. Moreover, it can be observed that impact dimple dimension and the generated RSs only depend on the component of velocity orthogonal to the impact surface, as also stated in [78], [116], [120]. This information will be usefully exploited in the following to increase the computational efficiency of

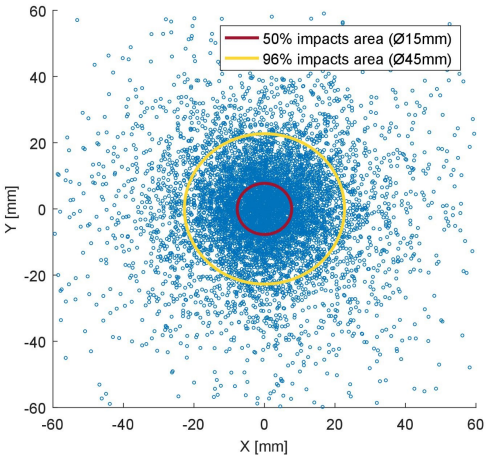

(a)

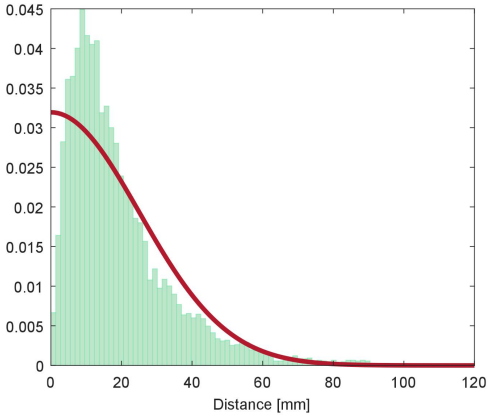

(b)

Figure 5.8: Example of scatter plot of the impacts in the simulation of the process on a flat surface and spatial distribution of the impacts as a function of the distance from projected center of the nozzle (polar symmetry is assumed).

the simulation on the specimen edge.
The spatial distribution of the impacts in an area directly under the nozzle is used to compute the number of impacts per unit time on a unit area. Given the number of impacts needed to achieve full coverage, the translational velocity of the nozzle to have full coverage in one single pass is estimated to be V_{nozzle} =9.1 mm/s. Importantly, we assume to achieve full coverage in a single pass of the nozzle; this assumption is furtherly supported by the observation made in [77] that the results do not significantly differ in the case of multiple passes with lower coverage.

5.2 DEM simulation of the SP process on the edge

The DEM simulation is now set up, and all the parameters relative to the process on a flat surface are known. The next step is about extending the simulation to the process occurring on the edge. The motion of the nozzle can be divided into three main stages. First, the approaching of the nozzle towards the edge on the front surface; then the turning of the nozzle around the edge tip; lastly the receding from the edge on the lateral surface. In the approaching, the nozzle translates remaining orthogonal to the Front Surface until its axis is on the edge tip; the receding stage is similar to the approaching stage, in a mirrored situation.
When the process is carried out on a flat surface, the impacts arrange on a quasi-circular pattern as seen in Figure 5.8. During the approaching stage, the pattern is gradually cut; namely, the peening media goes beyond the target without impacting. Moreover, at the end of this stage the impact pattern is semi-circular shaped. A small area directly under the nozzle, in the vicinity of the edge is considered. When the approaching stage ends, half a pass of the nozzle has been carried out on the considered area. Thus, the considered area has been hit by a number of shots which is, on average, one half of the impacts required to achieve full coverage. These shots have an impact velocity $\bar{v}$ distribution equal to the case of SP on a flat surface.
The same observations, in a symmetric condition, are also valid for receding stage. In this case, the Lateral Surface (see Figure 3.11) is hit, when the nozzle ends the circular trajectory around the edge tip. When rotating about the edge tip, the nozzle maintains its peripheral

velocity and working distance and bombards roughly the same spot. The angular velocity of the nozzle in the simulation is 0.091/s. Hence, the complete rotation of the nozzle about the edge would require 17.2 s and up to $\sim 10^9$ shots. The computational cost of such a simulation is terrific and for this reason an alternative approach to the problem is devised.
Considering the constant velocity of the nozzle while it turns about the edge tip, the behavior of the shot stream is assumed to be symmetric in the first and the second part of the arch, so only one half of the nozzle rotation about the edge is simulated. The dynamics of the particle recorded while the nozzle is tilting from 0° to 45° (with respect to the original position) can be mirrored to compute the dynamic behavior of the shot stream on the whole path.
A further assumption taken to make the computation faster is to discretize the nozzle motion in a sequence of 7 static simulations, as schematically represented in Figure 5.9. The nozzle points directly towards the edge tip and is tilted respectively by 0°, 7.5°, 15°, 22.5°, 30°, 37.5°,45° with respect to the normal vector to the Front Surface representing the initial direction (0°). This is assumed to be a reasonable simplifica-tion since the angular velocity of the nozzle is low enough, if compared to the average velocity of the shots, to consider the shot stream to be at steady state at any instant of its path around the edge. Accordingly, the discretization does not affect the behavior of the shot beam nor the interaction phenomena between shots.

Each simulation covers a time interval of 2.3 ms, with 130000 impacting shots. After achieving the steady state of the nozzle in each simulation, the impact conditions are recorded. Impacts between the backscattered and approaching shots often cause some shots to deviate from their initial trajectory. Monitoring these events in the DEM simulation is an onerous task, which requires the recording of a huge amount of data. Some of these collisions may also produce rupture of the involved shots, nevertheless this possibility is not taken into account to save time and computational cost.
To set up the FEM simulation of the SP in correspondence of the edge, it is required to know the process conditions in the close vicinity of the edge. Hence, only the impacts within 500 µm of distance from the nozzle axis and the edge tip are recorded. The impact velocity $\bar{v}$

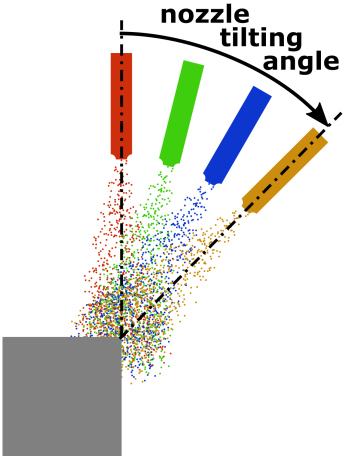

Figure 5.9: Schematic representation of the nozzle motion around the edge tip.

and location are recorded for each shot. The Gaussian distribution of impact velocity components are computed, the intensity and the orthogonal component of the velocity are plotted in Figure 5.10 respectively (a) and (b). Lower scattering is recorded for higher angles, due to the lower number of interactions between shots in this condition, differently from what found by Jebahi et al. [120] on a flat surface.

Figure 5.11 displays the fraction of shots whose orthogonal velocity is high enough to make them effective to the plasticization of the target surface (V_{ort} >25 m/s) as a function of the tilting angle of the nozzle, on both the Front (FS) and Lateral Surface (LS). Interestingly, the effective fraction of shots is quite high as long as the nozzle is slightly tilted with respect to the normal to the Front or Lateral Surface (tilting angle near to0° or 90°). The percentage is much lower when the nozzle moves in the central part of the arch and drops to zero when the relative angle between the surface and the nozzle exceeds 60°. The average fraction of effective shots is about 50%. This results in a number of impacts corresponding to a 200% coverage in the proximity of the edge. Such coverage level is deemed to be representative of high coverage processes, also considering the saturation phenomena occurring in the RS state in the peened component when

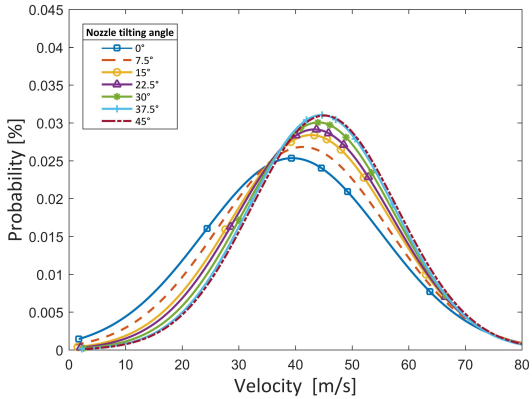

(a)

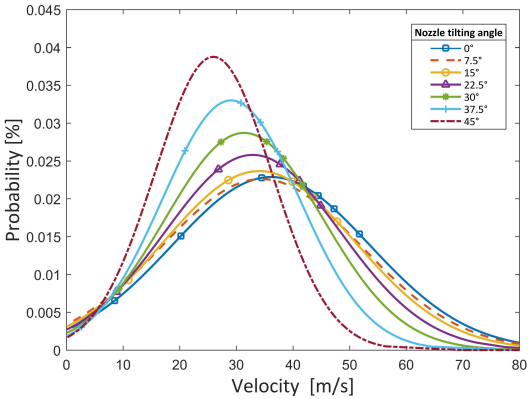

(b)

Figure 5.10: Impact velocity distributions at different tilting angles of the nozzle. (a) absolute impact velocity. (b) orthogonal impact velocity. Higher tilting angles result in higher impact velocity (a) due to fewer interactions between shots.

coverage exceeds 100% owing to to the work hardening of the target material [57], [68], [81], [85], [110]. We remind again that surface modifications induced by very high coverage level in shot peening are not being studied in this study, and only the RS state is under investigation.

To set up the FEM simulations the impact velocity $\bar{v}$ distribution in each angle interval is computed by combining the ones at the endpoints. E.g., the distribution for a tilting angle of the nozzle in the interval [0°,7.5°] is the combination of the distributions computed at 0° and 7.5°, by computing the arithmetic mean of the mean values and the geometric mean of the standard deviations.

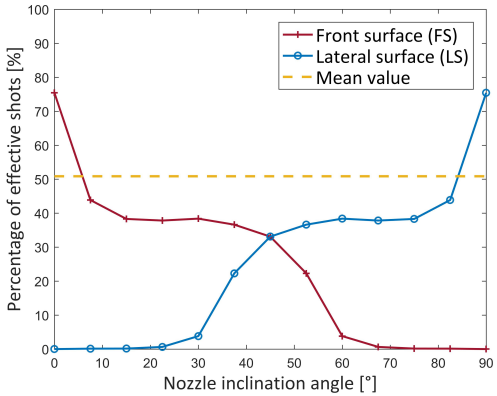

Figure 5.11: Percentage of effective shots (in terms of surface plasticization) on the two faces of the edge as a function of the tilting angle of the nozzle.

5.3 FEM simulation of the SP process on the edge

At first, one simulation approach is devised with the aim of have the most realistic representation of the process on the edge. The first approach in presented in Section 5.3.1. Three simplified modelling strategies are then studied, in order to better understand the phenomena involved in the development of the RS in the target, thus to devise an easier and businesslike approach. They are presented in Section 5.3.2.

5.3.1 FEM model for complete simulation

The FEM model consists in the target body and the stack of hemispherical shots impacting on two of its sides (Figure 5.12). The prismatic target body has a dimension of $240 \times 150 \times 300\,\mu m^3$, which is considered to be adequate for preventing the boundary conditions from perturbing the residual stress field, as also stated in [99].

Figure 5.12: The FEM model: target body and stack of impacting shots.

The target body is constrained on the four sides not exposed to impacts. The nodes on these faces are constrained in order to prevent any displacement normal to the surface, and silent constraints are used, in order to avoid reflection of the shock waves caused by impacting shots. To enhance the stability of the simulation by preventing the sharpening of the edge that would make the simulation unstable due to excessive deformation of some elements, the edge is provided with a very small fillet radius of 10 µm. This value is considered reasonable in view of the fact the samples were extracted from rolled plates by electro-discharge machining. Deeper attention will be devoted in the following to investigating the effect of such geometrical parameter on the shot peening process.
The whole model is meshed using 8 nodes brick elements (SOLID 164) with reduced integration; hourglassing control is active for all elements. No mass scaling is introduced, in order not to alter the

dynamics of the process, being the time step mostly dependent on the elements of the shots (small and rigid), which are also the ones whose kinetic energy is responsible for the development of the RS state in the target.
In order to prevent oscillations of the target surface, damping is applied to the target body. Being mass damping easier to set and more effective than stiffness damping, only α-damping is applied. The damping value is set on a sub-critic value of $\alpha = 24\,10^6/\mathrm{s}$ as previouslystated for the simulation of shot peening on a flat surface. Elements in the volume underlying the impact area are distributed on a regular mesh and have a characteristic dimension of 3 µm (Figure 5.13). In the surrounding volume, more elongated elements are used to fill the volume joining the impact volume to the constrained surfaces.

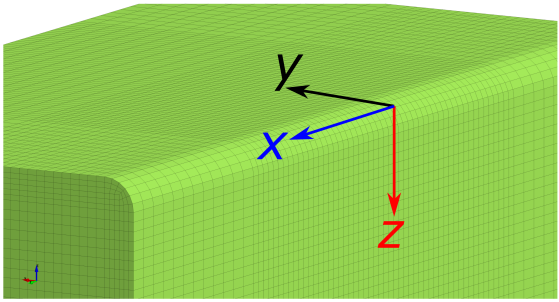

Figure 5.13: Detail of the mesh on the target and the reference system used.

As can be expected, the material model used for the target body has much importance in the development of the RSs. The shots are modeled using a bilinear elasto-plastic behavior with high yield strength (3 GPa), which is meant to represent the mechanical behavior of the ceramic material, where the plastic deformation is used only to get a more stable simulation, as seen in Chapter 4. On the other hand, as seen previously, the surface layer of the target body undergoes a strong deformation and due the stochastic character of the process, partially superimposing impacts happen frequently. This causes the complex non-monotonic deformation history of some volumes in the target. For these reasons, also in this case the Lemaitre-Chaboche

model is applied to the target body, and its parameters are adjusted using cyclic stress-strain curves after the stabilization of the hysteresis loop in order to have a realistic representation of the material behavior under cyclic load as seen in Section 4.1.1. The parameter of the Chaboche model are reported in Table 4.1.
An Erosion Surface-to-Surface algorithm is used to manage the contact phenomena between the shots and the target body. The friction coefficient between the target body and the shots has a value of $\mu = 0.05$, which is found to be suitable for the interaction between aluminum alloy and the ceramic beads [150]. Erosion is used to prevent unstable conditions for the simulation: elements are suppressed when they reach a deformation exceeding 200%.
Shots are arranged in order to impact over a circular impact area having 100 µm diameter, laying symmetrically on the two concurrent faces forming the edge. The MatLab routine mentioned in Section 4.1.2 identifies in 85 the average number of shots needed to achieve full coverage on a flat surface if a circular impact area having 100 µm diameter is considered. As mentioned in Section 5.1.1, the number of impacts required to achieve full coverage is higher than in the case of SP on a flat surfacem due to the wider scattering of shots velocity and the lower average impact velocity. As stated in Section 5.2, the average number of impacting shots is estimated in 170, which corresponds to a coverage of about 200% due to the shots blown when the nozzle is turning; moreover, the approaching and receding stage are to be kept into account.
Hence, 22 shots impact on the Front Surface of the impact are in the approaching stage. 170 shots hit on the whole impact area while the nozzle tilts. 22 more shots impact on the Lateral Surface due to the receding stage. The selection of the effective shots according to the impact velocity $\bar{v}$ is performed considering an ideal sharp edge; nevertheless, the selection is considered to be valid also when a fillet is added to the edge in the FEM simulation, due to the small dimension of the fillet.
The 22 + 22 shots on the Front and Lateral Surface are generated using the impact velocity $\bar{v}$ computed on a flat surface. The 170 shots are generated according to the percentage of effective shots at each tilting range. On the Front Surface, 18 shots are assumed to impact when the nozzle has a tilting angle between 0° and 7.5°, 16 when the

angle is in the range 7.5° to 15°, 13 in [15°, 22.5°], 12 in [22.5°, 30°], 11 in [30°, 37.5°], 8 in [37.5°, 45°]. On the Lateral Surface, no effective shots impact in the range [0°,30°], 2 shots impact when the nozzle has an angle in the range [30°, 37.5°] and 5 shots are generated for an angle in the range [37.5°, 45°]. On the second half of the nozzle path, the distribution of the shots is mirrored with respect to the bisector plane of the edge, considering the symmetry of the phenomena previously stated.
The so-determined number of shots in each range is provided with randomly sampled impact velocity $\bar{v}$, according to the value computed for its proper range from the results of the DEM simulation.
A MatLab script is used to arrange the 214 shots according to the criteria just explained (Figure 5.14). A visual inspection to assure a uniform coverage is performed after each simulation to check a reasonable uniformity of the impacts (Figure 5.15). The impact locations are arranged with a completely random approach, but the distance between each shot and the target is chosen in order to prevent simultaneous shot in close sites. For this reason, no interaction of the shots is considered, in order to make impacts as close in time as possible and reduce the simulation time. Nevertheless, the random arrangement of impacts makes possi- ble for shots to hit in close sites or even in the same point not at the same moment. Partial or complete superimposition of impact dimples happens, according to the statistical probability of this event.

The shots dimension is randomly generated, according to the distribution detected in the experimental measurements, as in Section 4.1.2.

5.3.2 Simplified modeling strategies

Three simplified modelling strategies are devised to develop a better knowledge of the peening process.
The first simplified model is aimed at studying the influence of the only shots blown during tilting stage disregarding the contribution of those impacting during the approaching and receding phases. Since 170 shots blown during the nozzle tilting stage are kept, this approach is regarded as the 170 impacts model. The model appears similar to the complete model, shown in Figure 5.12.

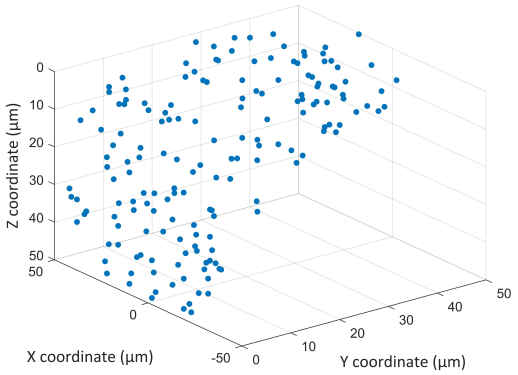

Figure 5.14: Illustrative arrangement of the impact locations using the MatLab routine.

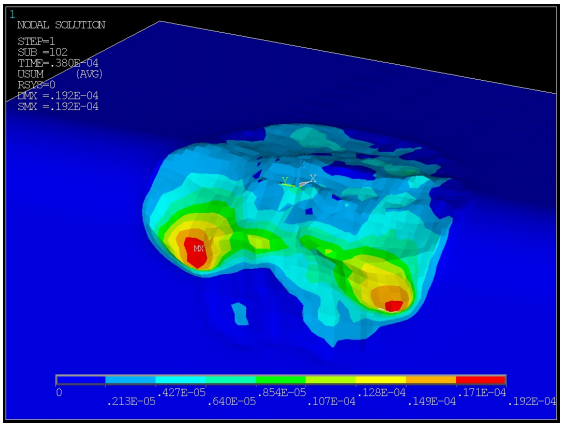

Figure 5.15: Deformed target body at the end of the simulation. Nodal displacement is plotted.

Moreover, the DEM-FEM synergistic approach is time-consuming and computationally heavy. A simplified and more manageable simulation would be preferable in the industrial practice. Hence, two more simplified models are devised, in order compare its results to the ones of the DEM-FEM approach. These simplified models are obtained straight-forwardly from the FEM model presented in detail in the previous section. The target body is kept the same, as well as the material model used, the constraints and the contact algorithm.
A coverage level of 100% is chosen, in order to perform an extremely simplified simulation, based mainly on the nominal parameters of the treatment. Hence, 85 shots are arranged to randomly impact on the front and lateral surfaces. The impact velocities are randomly generated according to the stochastic distribution computed from the DEM simulation in the case of the shot peening treatment on a flat surface. In the first model all the shots impact orthogonally to either face, as shown in Figure 5.17. In the second one, termed the 45° impacts model, all the shots have a direction corresponding to a 45° tilting angle of the nozzle.

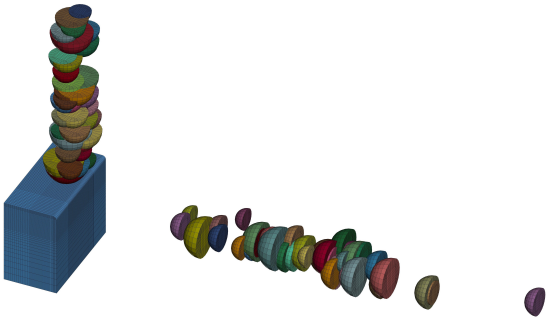

Figure 5.16: The model used in the second simplified approach, with orthogonal impacts.

5.4 Results and discussion

Given the stochastic character of the SP process, six simulations are performed for each model in order to have some statistical representativeness of the results. The final result is computed by averaging the results of each set of simulations. The FEM simulations are per-

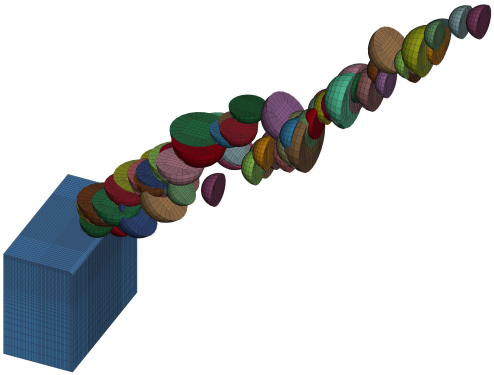

Figure 5.17: The model used in the third simplified approach, with 45° inclined impacts.

formed using the explicit dynamic solver Ansys/LS-Dyna.
The RS field is computed using the nodal results of the nodes laying in the volume subtending the impact area, namely the volume having the shape of a quarter of a sphere (with the Font and Lateral surfaces of the impact area as semicircular faces) and a radius of 70 µm. Some surrounding material is considered, even if not full coverage is achieved on its surface, just in order to plot the RS field. The model is considered in the undeformed condition, namely the original location of the nodes was considered. The σ_{xx} component of the nodal stress was considered in order to be consistent with the reconstructed RSs. The RS field is computed as σ_{xx}, function of the depth from the surface, that is the distance from the front surface (FS) and lateral surface (LS) of the edge, as represented in Figure 3.11.

In Figure 5.18 and Figure 5.19 the RS fields are represented for the case of the complete model with 214 impacts (Figure 5.18a) and for the simplified model with 170 impacts (Figure 5.18b), 85 orthogonal impacts (Figure 5.19a) and 85 impact with 45° inclination (Figure 5.19b).
The four models yield fairly similar results. The subsurface compressive peak is evident in all the cases. The face corresponding to the y axis is the Frontal Surface, where in all the three model the compressive peaks appears to be closer to the surface, in particular in the case of the 214 impacts simulation. This is probably due to the

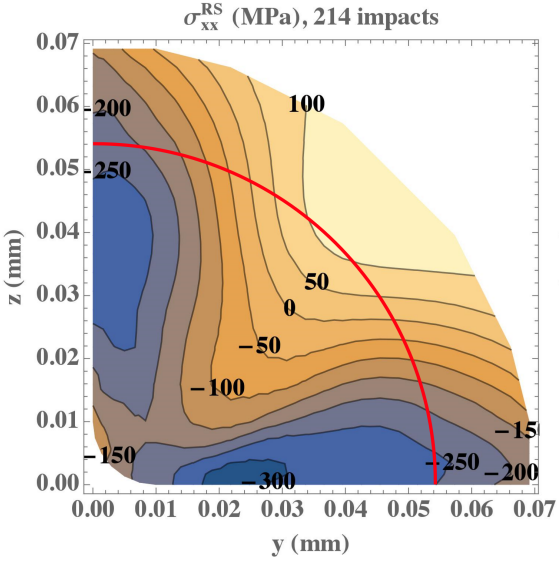

(a)

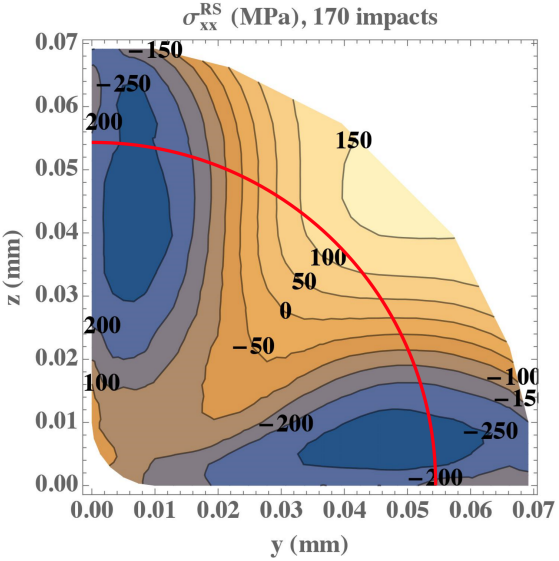

(b)

Figure 5.18: RS state computed from the simulations for (a) 170 impacts, (b) 214 impacts. The red arch encloses the area where the stresses are computed for the estimation of the fatigue life of the component according to the Critical Distance Theory [65].

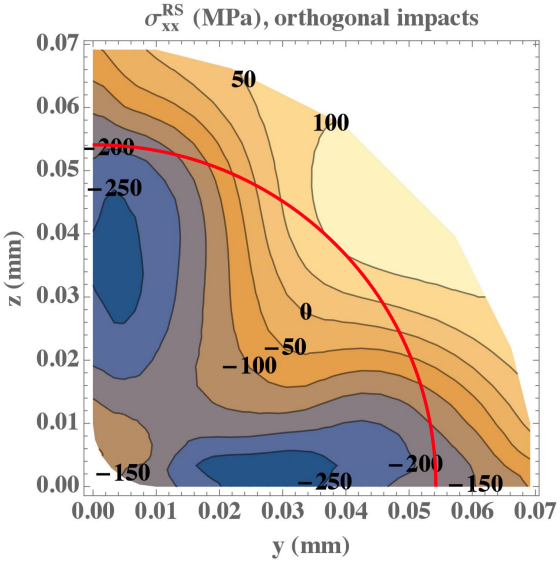

(a)

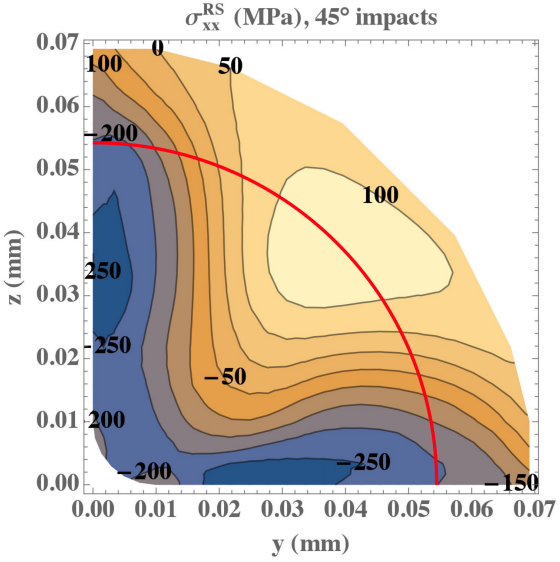

(b)

Figure 5.19: RS state computed from the simulations for (a) 85 orthogonal impacts and (b) 85 45° impacts. The red arch encloses the area where the stresses are computed for the estimation of the fatigue life of the component according to the Critical Distance Theory [65].

shots impacting on the lateral surface later in the simulation due to the motion of the nozzle. This causes a flow of material in the inner volume of the edge, which moves the compressive peak beneath the Front Surface towards the surface.
The shift towards positive RS values across the edge bisector, where the compressive peak is drastically attenuated, is due to the "squeezing" effect of the shots impacting on the Front and Lateral Surface, which is particularly severe in the case of a sharp edge.
Moreover, the orthogonal impacts as well as the 45° impacts simulations show a steep decrease of the magnitude of the RSs when moving away from the edge tip. This is probably caused by the reduced number of impacting shots. A higher number of impacts, indeed, extends the volume where the material is plastically deformed, as seen in [124] or the case of a flat surface. This helps to arrange the RSs and reduce the border effect.
The RS state from the simulations is also to be compared to the reconstructed RS field mentioned at Section 3.3. Figure 5.20 and Figure 5.21 show the relative deviation, as a percentage value, between the RS field computed in the numerical simulations and the reconstructed one. The values are normalized on the maximum absolute stress, in order to avoid the display of very high relative deviation where the magnitude of the RSs is low.

The comparison between the RSs field shows a slight deviation. Still, the difference is more evident as regards the qualitative distribution of the RS state in some areas, but is much lower in relative value, if the small magnitude of the RS state in a significant portion of the volume is considered. The best agreement of the RS fields is observed in the case of the 214 impacts simulation, which is supposed to be the most realistic model.
In Figures 5.20 and 5.21, the red arch encloses the area where the average stress is to be computed to estimate the fatigue life of the component according to the Critical Distance Theory [65], which in this case indicates a critical distance of about 54 µm. The average RS and the average normalized stress deviation in this area are reported in Table 5.1.

The importance of the shots impacting on the Front and Lateral

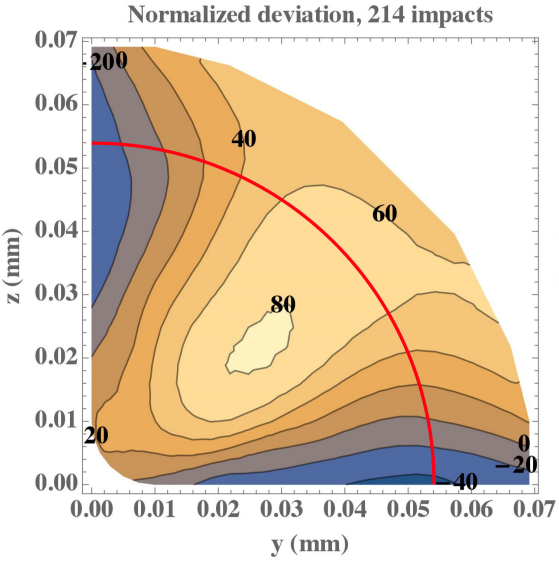

(a)

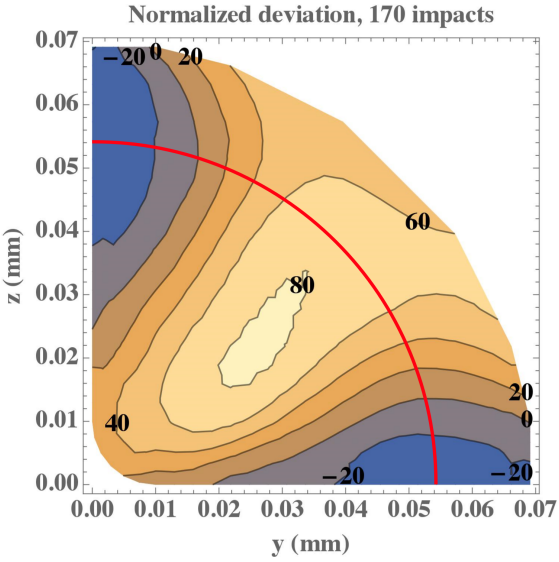

(b)

Figure 5.20: Normalized deviation of the RS field comparing the reconstructed map (Section 3.3) and the results of the simulations for (a) 170 impacts, (b) 214 impacts. The red arch encloses the area where the stresses are computed for the estimation of the fatigue life of the component according to the Critical Distance Theory [65].

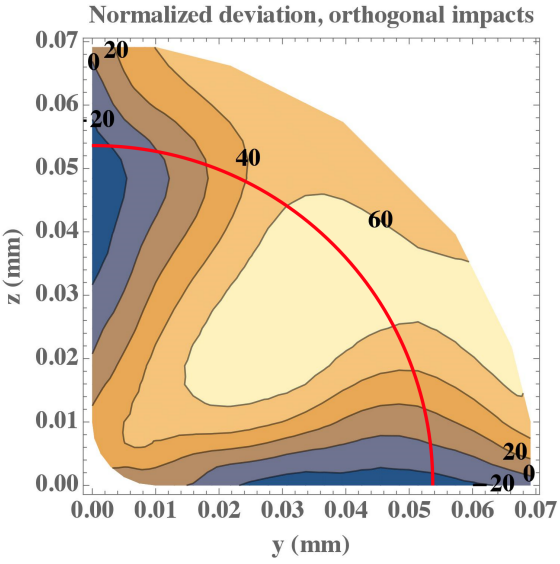

(a)

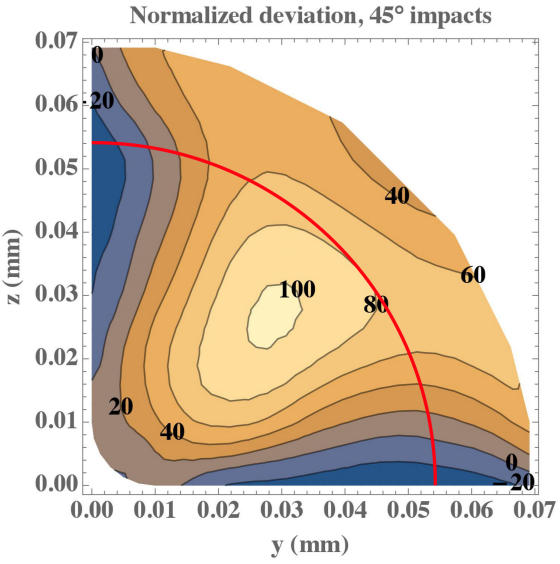

(b)

Figure 5.21: Normalized deviation of the RS field comparing the reconstructed map (Section 3.3) and the results of the simulations for (a) 85 orthogonal impacts and (b) 85 45° impacts. The red arch encloses the area where the stresses are computed for the estimation of the fatigue life of the component according to the Critical Distance Theory [65].

Table 5.1: Average RS and normalized stress deviation in the area indicated by the Critical Dis- tance Theory.

Model	Average RS (MPa)	Average deviation (%)
Reconstructed RS field	-243	-
14 shots	-190	22
170 shots	-166	32
Orthogonal shots	-175	28
45° shots	-156	36

Surface in the approaching and receding stage is clear; nonetheless the shots impacting in the turning stage of the nozzle have a not completely negligible effect.

The good accordance between the reconstructed RS field and the results of the simulations supports the reliability of both. Similar results are obtained using numerical simulations and an experimental based approach, thus having a mutual validation of the approaches and their outcome.

Moreover, in the comparison between the results of the simulation and the reconstructed RS state some aspects have to be considered. First of all, the undeformed configuration of the model was taken into account, even if an intense deformation state is developed on the peened surface. In addition, the reconstructed RS state is based on RS measurements performed at a minimum distance of 50 µm from the edge tip, themselves being affected by some measurement uncertainty, and this may cause some inaccuracy in the interpolation of the RS map. As seen in Fig. 3 , in fact, the confidence interval of the RS measurements is relatively wide, in particular in the vicinity of the edge tip.

It is worth noticing the very little deviation from the symmetrical distribution of the RSs, with respect to the bisector line of the edge, in all the three cases, except for the aforementioned change in the position of the compressive peak. This is probably ascribable to the micrometric dimension of the peening media, together with the scattering of the direction with which the shots impact on the faces of the edge. This generates a uniform effect of the peening treatment and suggests that the motion direction of the nozzle has almost no effect on the RS state development in this kind of peening treatment.

Interestingly, the RS field on the edge is related to very local phenomena and is almost not affected by RS in other parts of the component, i.e. at a distance much greater than the characteristic distance of the

compressive layer.

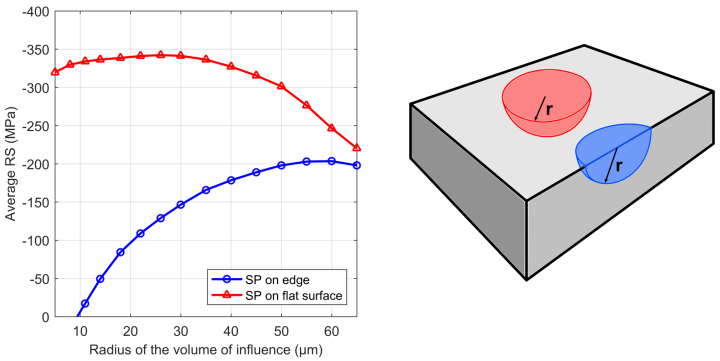

Figure 5.22: Average RS, as a function of the radius of the volume of influence r and sketchy rep- resentation of the volumes of influence, in the case of SP on an edge (blue), and in the case of SP on a flat surface (red). Data concerning the simulation of SP on a flat surface are computed in [124].

To this regard, Figure 5.22 shows the comparison between the average RSs in two volume of influence, in the case of the simulation of SP on a flat surface [124] and on an edge (for the aforementioned case (a)). The average RS computed in a volume of influence is used to estimate the fatigue resistance of components according to the Critical Distance theory applied in combination with a multiaxial fatigue criterion as explained in [64], [65]. In the case of SP on a flat surface, the volume of influence in a hemisphere having its center coincident with the center of the peening area and variable radius. In the case of SP on an edge, the volume of influence is a quarter of a sphere having its center on the tip of the edge, at the center of the peening area and variable radius. The graph shows the trend of the average RS in the volume, as a function of the radius of the volume of influence. For SP on flat surface, the averaged RS displays the characteristic subsurface peak of compressive RS. For the case of the edge, on the other hand, the averaged RS increases when the radius of the volume of influence increases. The difference between the two cases is clear and explains the interest in focusing on the simulation of the process on geometrical features. The lower intensity of RS in the vicinity of an edge, despite the higher coverage level of the treatment, is ascribable to the

morphology of the geometrical feature, where the discontinuity of the substrate material inhibits the development of the RSs introduced by SP. Therefore, fatigue calculations of plain prismatic specimens subjected to shot peening should be carried out near the edge because of compressive residual stresses of lower magnitude and hence less effective in suppressing fatigue crack initiation.

5.5 Conclusions

This work is, as the best of our knowledge, the first attempt to simulate the SP treatment on an edge. In order to realistically reproduce the process, a DEM simulation is used to set up the FEM simulation. A DEM simulation of the peening process is devised to adjust the simulation parameters and estimate the velocity of the nozzle, using the simulation software Yade-DEM.
Because of the extremely high computational cost, the sequential coupling of the DEM and FEM simulations is not feasible, as well as the DEM simulation of the movement of the nozzle on its entire path. Therefore, the DEM simulation of the peening treatment on the edge is linearized into 7 static-nozzle simulations, which are used to compute the impact velocity and direction of the shots in the proximity of the edge. The results of the DEM simulation are used to set up the FEM model, in which the shot dimension is stochastically distributed according to the experimental measurements performed in the peening media, and the impact direction and velocity are randomly generated according to the results of the previous DEM simulations.
4 FEM models are devised. The complete model accounts for 24 impacts. A 170 impacts simplified model focuses on the shots blown in the tilting stage of the nozzle, disregarding the approaching and exiting stages. Two 85-impacts models are developed, in order to study an easy-to-use approach for industrial application. The devised models have orthogonally impacting shots or 45° inclined shots and are intended to "extend " the simulation of SP on a flat surface to the case of the edge, without considering the turning of the nozzle. 6 explicit dynamic FEM simulations are carried out for each model, using the explicit dynamic solver Ansys/LS-Dyna, and the results are compared to the reconstruction of the RS field obtained by fitting experimental data, obtained through XRD analysis, using thermal fields in a FEM

simulation.
The following conclusions can be drawn:

- the RS state computed with the DEM-FEM and FEM simulations is in reasonable agreement with the reconstructed RS field based on experimental measurements. This corroborates the validity of both the approached, despite the absence of a direct measurement;

- the comparison between the simulation approaches shows the prevalent effect of the shots impacting in the vicinity of the edge with a quasi-orthogonal direction. The best results are obtained if all the shots are kept into account and the DEM-FEM approach is used. Nonetheless, an approximated approach could be based on the simplified model of orthogonally impacting shots with full coverage;

- the region encompassing edge and its immediate vicinity presents a highly perturbed RS state; this confirms that the consideration of the RSs generated by SP in the design process requires a careful study of the treatment in the vicinity of geometrical details, where the component is more prone to be subjected to fatigue failure;

- as well known in SP practice, the alteration of the RSs in the vicinity of the edge can be extremely dangerous for the fatigue resistance of the component: it is mandatory to keep into account these aspects in designing the component and is preferable to avoid sharp edges for the best success of the SP process.

This study is the basis for the development of the numerical simulation of the SP for studying the RS state near geometrical details. The developments of this work will be presented in the following, straightforwardly from the abovementioned results. the first step will be devoted to the analysis of the effect of the fillet radius on the edge tip. The alteration of the local geometrical conditions can strongly interfere with the results of the SP process, and the best conditions for peening edges will be studied. A further development for enforcing the technological value of this simulation approach, will be the study of the RS state generated by SP in the vicinity of a sharp notch.

Chapter 6

Applications for the simulations: effect of the edge fillet and simulation of SP on a notch

In this Chapter, the approaches devised in the former Chapter 5 will be extended to the analysis of two new scenarios, which can be addresses as particular cases of the SP on an edge. First, the effect of the fillet on the edge tip will be studied in view of some new data on the dimension of the real edge fillet radius. Then, the simplified approach to the SP simualtion will be applied to the study of the RS field on the root of a notch in the specimens.

As mentioned in the previous Chapter 5, the issue of sharp edges is a well known problem for operators dealing with SP. Very few data have been found by the author in scientific literature on this subject [151], nontheless the saying "always round the corner" is well known among shot peeners.[1].

Some additional experimental measurements, presented in Section 6.1 are aquired about the fillet radius on the tip of the peened edge of the specimens. These data are not sufficient for in-depth analysis, but still give clear indications on the real morphology of the edges. On the base of these indications, the model presented in the previous Chapter is slightly modified, and a parametric analysis is carried out in order to study the effect of the fillet radius at the edge tip.

[1] Prof. Mike Hill (University of California) told the author these exact words when discussing about the preliminary results referred in this Chapter

3 radii are considered for the fillet, namely 10 µm, 25 µm and 40 µm, in order to have a direct comparison with the previously seen model of the sharp notch and move progressively toward the condition of a blunt edge.
Given the very small with the previous model (if the absolute value of the dimensions is considered), the modification is introduced only in the FEM analysis and not in the DEM model, which is considered still valid.
As for the former case, the results are compared to the reconstructed RS field mentioned in Section 3.3. The second part of this Chapter is devoted to the simulation of SP on a notch. Extending the previous analyses to the condition of a sharp notch is the last step that will be taken towards the simulation of the treatment on a notch. As seen in Section 3.3, the specimen used to reproduce the condition of SP on a notch is shown in Figure 3.3 (c).
As highlighted in Chapter 5 and the analysis of the fillet radius effect, the exact representation of the substrate from the geometrical point of view is maybe more important than the exact modelization of the peening condition in order to achieve a reliable simulation, in particular if the main focus of the simulation is the study of the RS field generated in the substrate as in the case of the present study. For this reason, in a first attempt to study the process on a notch, no DEM simulation is performed, and the simplified approach with orthogonally impacting shots, named (c) in Section 5.3 is applied.
In the following sections, the model and the results are presented; the results are compared to the reconstructed RS field seen in Section 3.3.

6.1 Morphology of the edge

The surface morphology in correspondence of the edge on peened samples is aquired with a confocal optical profilometer Sensofar Plu Neox, on an assessment area 1739x1305 µm^2. The 3D rendering and the profile scanning of the edge are shown in Figure 6.1.

Since no measurements were taken on the unpeened samples, it is not possible to compare the unpeened and peened condition of the edge mophology. Nontheless, the 3D scan suggests that the surface modifications due to the indents may be much smaller than the ap-

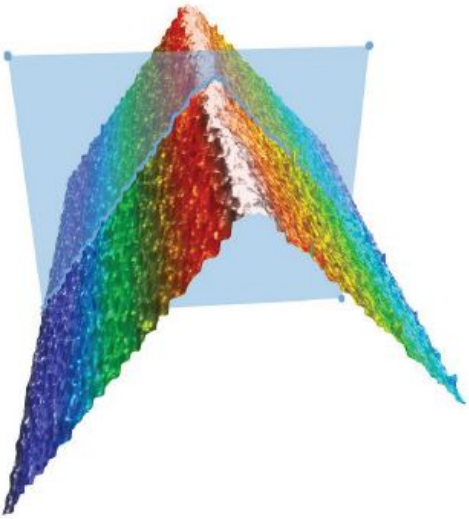

(a)

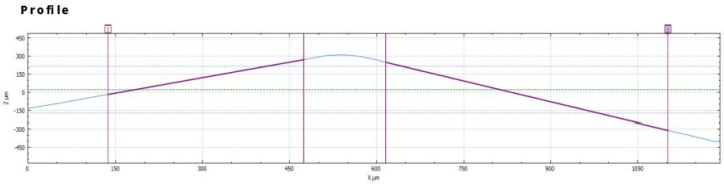

(b)

Figure 6.1: 3D scanning of the edge in peened sample (a) and section profile of the edge (b).

parent fillet radius of the edge. Thus, the original fillet radius in the non-treated sample is supposedly not much smaller than the one observed on the treated specimen. Therefore, a $\sim$40 µm fillet radius, which can be observed in the aforementioned scan, can be assumed as a reasonable value for the fillet radius of the edge after electro-discharge machining.

6.2 Edge fillet: the FEM model

As mentioned in the introduction to this Chapter, since the changes in the model concern only a very small geometrical part, the results of the DEM simulations are assumed to be valid also in the case of bigger fillet radii. The very only modification in the model is in the fillet radius of the target body. 2 more models are devised, with a 25 µm and 40 µm fillet radius. The models are shown in Figure 6.2.

No other changes are made to the model. Material model for shots and target, elements, mesh, solution options are kept from the previous model seen in detail in Section 5.3.

Only two most promosing models identified in the previous Chapter 5 are used for the analysis, namely the 214 impacts model and the 85 orthogonal impact model, denoted as (a) and (c). Details on the models can be find in Secton 5.3, and they are shown in Figure 5.12 and in Figure 5.16, respectively.

6.3 Edge fillet: the results

The results are obtained as in the case of the previous analysis, seen in Section 5.4. Also in this case, 6 simulations are carried out for each model, and the resulting average RS field is presented.

In this case, it is not possible to show the normalized deviation with the reconstructed RS field. This latter, indeed, was computed using a sharp edge FEM model, with nofillet radius. The effect of the increase in fillet radius dimension, seen in the models shown in this Chapter, is not clear on the reconstruction of the RS field presented in Section 3.3. Thus, in order to avoid the compariso between unconsistent set of data, the computation of the normalized deviation is

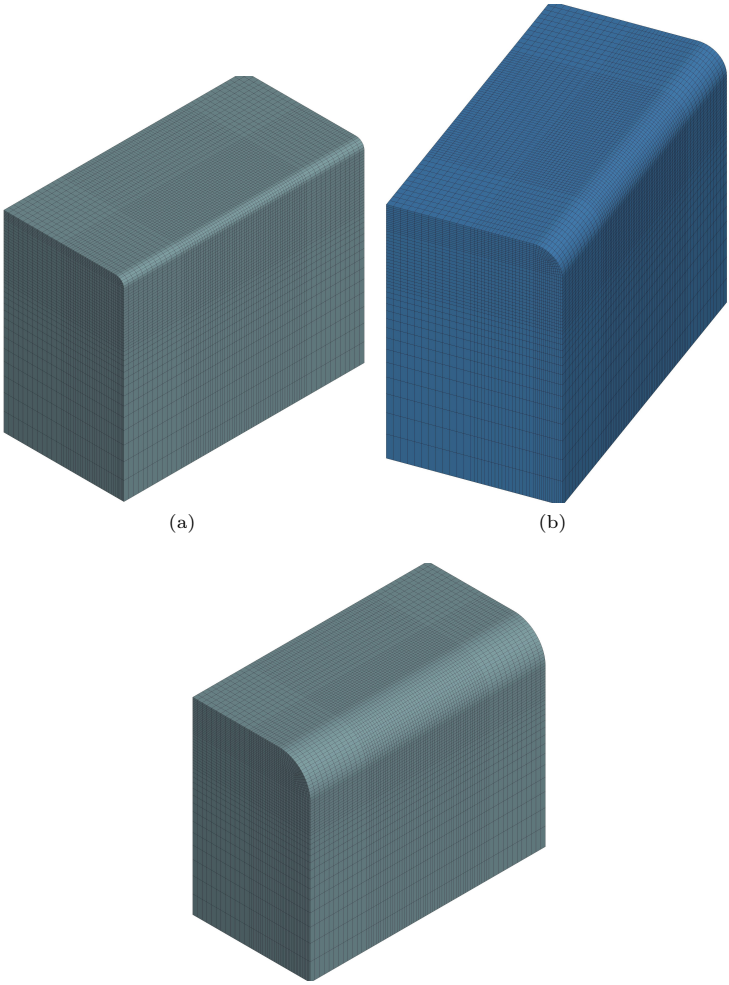

Figure 6.2: FEM model with 10 µm (a), 25 µm (b) and 40 µm (c) fillet radius on the edge tip.

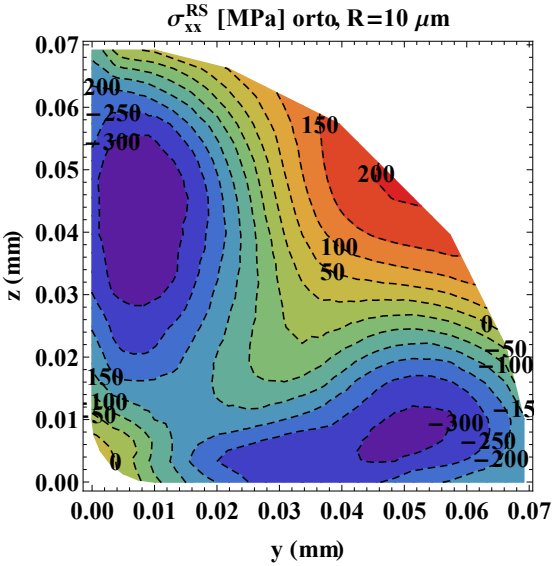

(a)

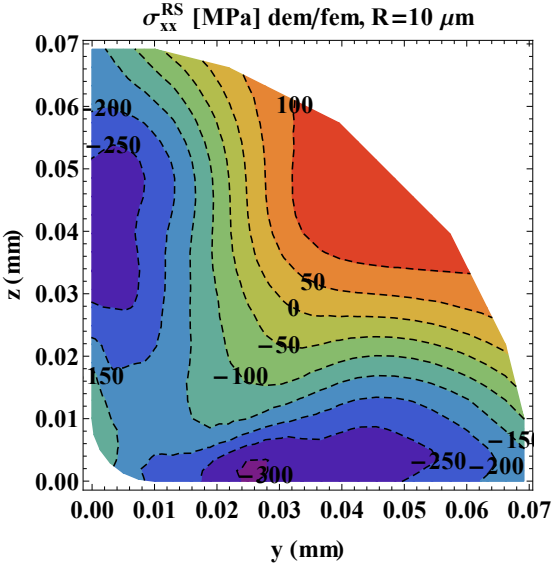

(b)

Figure 6.3: RS field from simulations with (a) 85 orthogonal shots, (b) 214 shots in DEM/FEM approach, on a 10 µm fillet radius model.

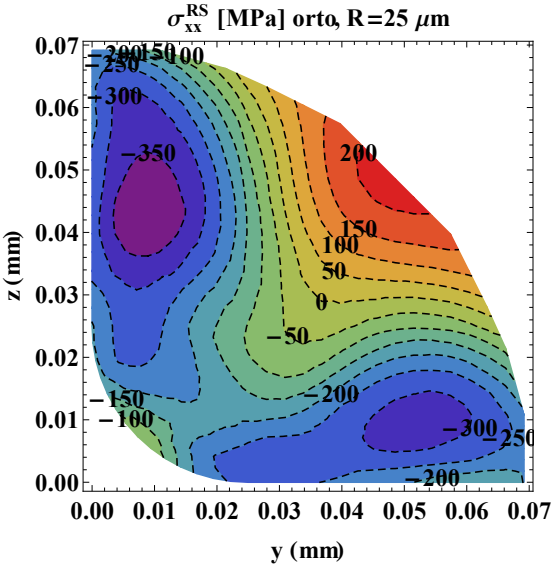

(a)

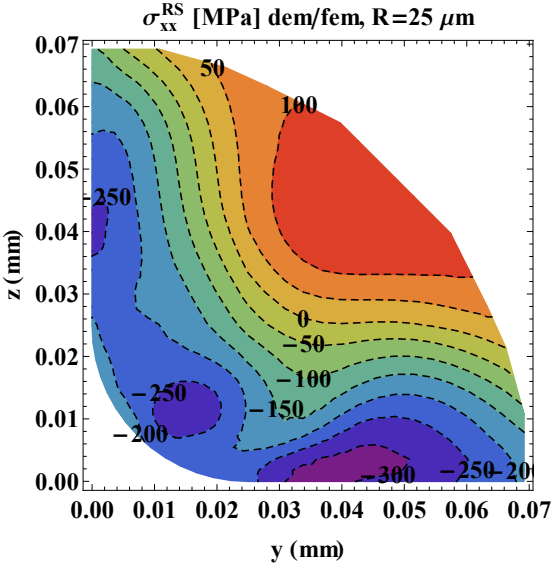

(b)

Figure 6.4: RS field from simulations with (a) 85 orthogonal shots, (b) 214 shots in DEM/FEM approach, on a 25 µm fillet radius model.

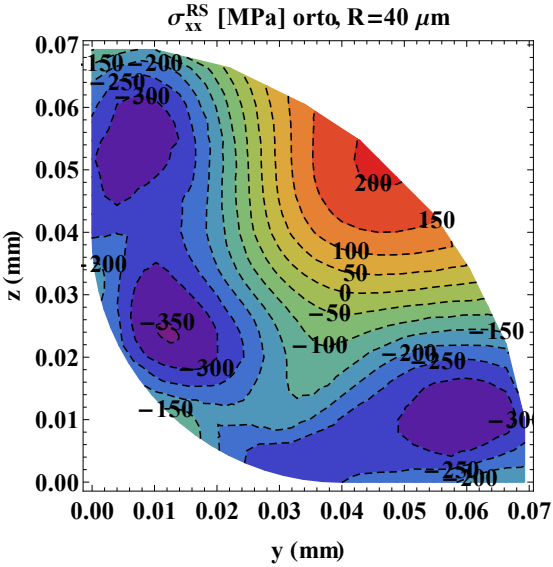

(a)

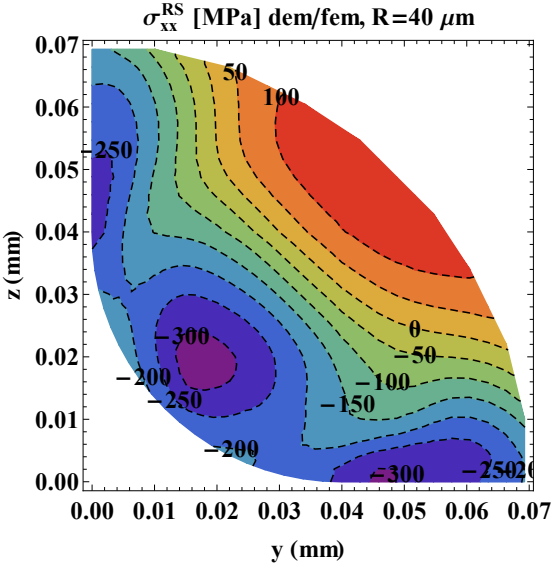

(b)

Figure 6.5: RS field from simulations with (a) 85 orthogonal shots, (b) 214 shots in DEM/FEM approach, on a 40 µm fillet radius model.

temporarily postponed.

It is interesting to observe that, for all the values of the fillet radius, the resulting RS field is always more uniform and smooth if the DEM/FEM approach is used. This is probably due to the micrometric dimension of the peening media, which helps the uniformity of the surface treatment even in the case of discontinuities.
Besides that, the differences are more qualitative than quantitative in all cases, since the variations is limited in a range of $\sim$50 MPa over much higher RS peaks. Some discrepancies can be noted in the case of the DEM/FEM approach for a 25 µm fillet radius, but this is ascribed to the stochastic approach to the simulation with randomly arranged impact and random velocities.
Most of all, it is interesting to notice that clear trend outlined with the increasing fillet radius. As mentioned in Section 5.4, the "squeezing" effect exerted by the impacting shots on the edge is strongly diminished by a (still small) increase in the fillet radius. For a bigger and, in the light of the data referred in Section 6.1, more realistic value of the fillet radius, the RS field results to be much smoother, uniform and presumably effective in enhancing the fatigue resistance of the component.
In the end, one last observation needs to be raised. The results obtained with the two simulation approaches are essentially the same. Some munor differences are present, but the effect of the target geometry is in any case much stronger than the effect of the simulation approach. It is worth to remember one more time that these simulation are aimed at studying the RS field and not the resulting surface roughness of the edge, which could require some more care in evaluating the best simulation approch. In light of these considerations, it is not inappropriate to assert that, if the RS are the subject of the study, a simplified simulation approach can give very satisfactory results, wich much less effort spent in modelization and computation, as long as the exact geometry of the target is used in the model.

6.4 SP on a notch: the FEM model

The FEM model used for the simulation of SP on a notch is shown in Figure 6.6. Two stacks of shots impact in the vicinity of the notch

root, which is similar to the target body used in the case of the edge (Section 5.3), in a curved shape.
The target body is shown in Figure 6.7. The revolved section has a 150x150 µm^2 dimension, similarly to the model used in the case of the edge. The length of the internal arch described by the revolution of the section is 240 µm^2, which is assumed to be enough to avoid perturbations of the RS field to to the borderd effects, according to the observation reported in Section 4.1.3. A 10 µm fillet radius is introduced in the model, as in the case of the edge, in order to have a better stability of the solution. Despite the results obtained in Section 6.3, only the 10 µm fillet radius configuration is considered, in order to make possible the comparison with the reconstructed RS field.

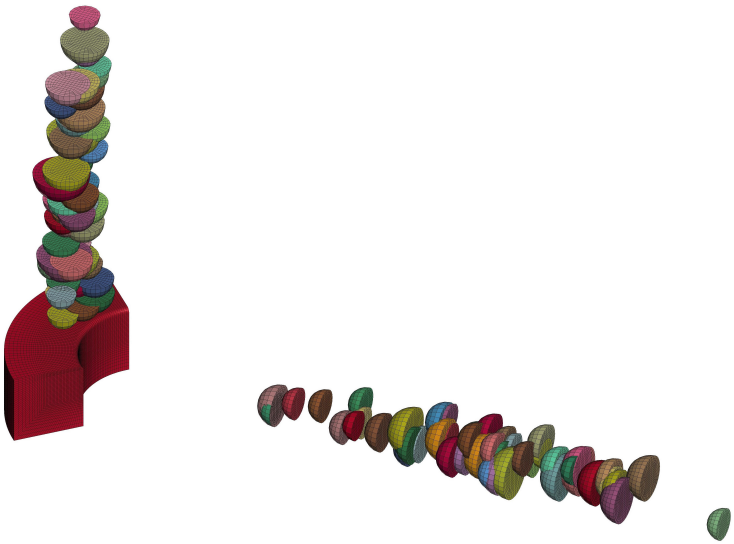

Figure 6.6: FEM model used to simulate the SP treatment on the notch.

Since Ansys/LS-Dyna does not support a radial reference system for the application of constraints, only the lateral and inferior surfaces are constrained in order to avoid normal displacement of nodes. On the external cylindrical surface of the target body, nodes are constrained in all the (translational) degrees of freedom. These constraint are not coherent with the ones applied until now to the target body, still they are the only way to emulate the constraint exerted by the

surrounding material, even if in a hard way.
As in the previous cases, 4 nodes brick elements SOLID164 with reduced integration and hourglassing control are used. The elements used to mesh the target body have a characteristic dimension of 3 µm at the root of the notch. The Lemaitre-Chaboce material is used to simulate the mechanical behavior of the target body, and the bilinear elasto-plastic model is applied to the ceramic shots, as seen in Section 4.1.1.

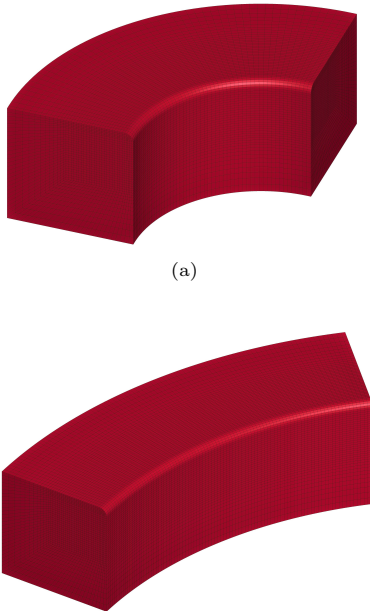

(a)

(b)

Figure 6.7: FEM models of the target body for the 150 µm notch root radius (a) and the 500 µm notch root radius (b).

The Erosion Surface-to-Surface algorithm seen in Section 5.3 is introduced for the contact between shots and target.
In order to make easier the analysis of the resulting RS, the impact area in this case in slightly expanded and is shown in Figure 6.8. Impact are randomly arranged in the impact area, and the number of impact is the average number required to achieve full coverage computed according to the MatLab routine seen in Section 4.1.2 with

the impact velocity distribution obtained by the DEM simulation on a flat surface (Section 5.1.1). 57 shots are assumed to impact on the Front Surface (see Figure 3.11) and 54 shots are arranged on the Lateral Surface.
As in the previous cases, 6 simulations are carried out for each one of the two models, in order to have some statistical representativity of the results. The RS field is obtained as an average over the simulations.

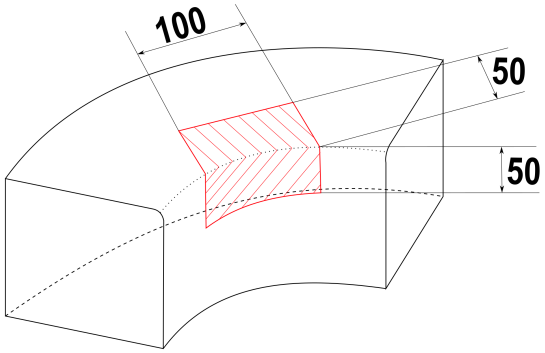

Figure 6.8: Schematic representation of the impact area for the simulation of SP on a notch. The impact area is hatched in red. Dimensions are in µm

6.5 SP on a notch: the results

Figure 6.9 shows the resulting RS field obtained from FEM simulations, for the 150 µm notch radius (a) and for the 500 µm notch radius (b). Observations similar to the one made for the ege can be raised, in particular for what concerns the RS state on the bisector line of the notch, which is also in this case ascribable to the "squeezing" effect exerted by the shots impacting on the Front and Lateral Surface on the sharp edge. Particularly for the sharp notch, this effect is very marked, up to nullify the RS on the tip of the notch.
As in the case iof the edge, the influence of the fillet radius may be worth of being analyzed, but will not be considered in this work since no reconstructed RS field on bigger fillet radii is available for validating the results of the FEM simulations.

The RS field appear to be very similar in the two cases, and no

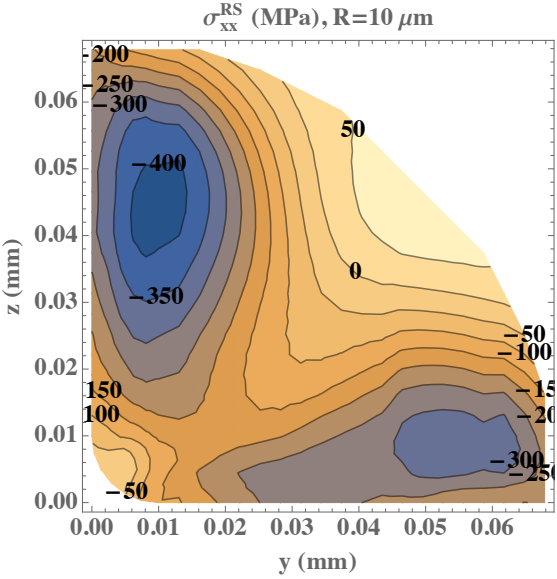

(a)

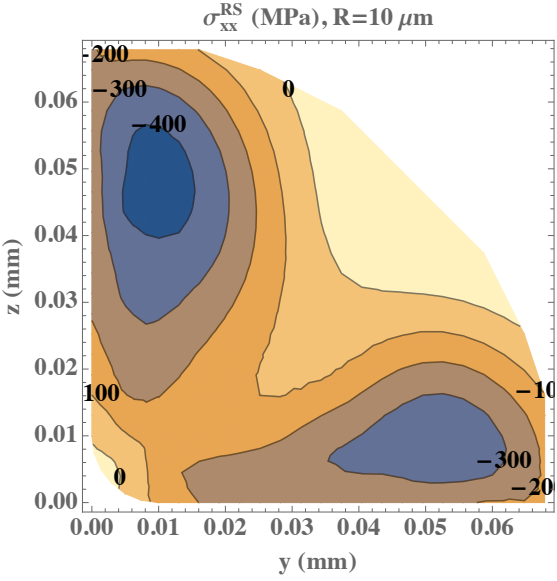

(b)

Figure 6.9: RS state computed from the simulations for 150 µm notch root radius (a) and 500 µm notch root radius (b).

great influence seems to be exterted by the difference in the notch root radius.
It is worth noting the higher compressive RS peak in the inner side of the notch, despite the lower number of impacts. This is supposed to be caused by the geometry of the notch itself: the effect of the surrounding material the concentration of the RSs, and this would explain some difference between the RS in the notch and in the edge, even when the simulation approach is very similar.
Some effect was expected to be exerted by the dimension of the notch root, which is not evident from the results of the simulations, despite the smaller ratio between the impact area dimension and the dimension notch root. The resulting RS field, instead, appears to be very comparable in both cases, and (apart from the slight concentration of Rs in the inner part of the notch, symmetric with respect to the bisectin line of the map.
This is not the case in the reconstruced RS (see Section 3.3), where marked differences are observed in the two conditions, with an remarkably higher stress in the inner part of the notch, and a very weak RS on the Front Surface is observed in the case of a sharp notch, and a more symmetric RS field is computed for the blunt notch.
This observation is more evident if the normalized deviation is considered. Figure 6.10 shows the deviation between the RS field obtained from the FEM simulation and the reconstructed ones (see Section 3.3, for the 150 µm notch radius (a) and for the 500 µm notch radius (b). First of all, it is worth to notice that the areas of the RS field where the magnitude of the stress is lower are the ones with higher deviation (up to 100%). On the other hand, the higher the RS magnitude, the lower the deviation. In this case, the deviation is even lower than in the case of the edge (Section 5.4), in particular for the wider notch. Where the RS peaks are predicted by the simulation, the RS field duplicated almost perfectly the reconstructed one with lessa than 10% difference in the RS magnitude. In the case of the sharp notch, the overall deviation of the RSs is affected by the discrepancy in predicting the RS peak unders the Front Surface.
This confirms the supposition of the greater influence of the geometry, over the peening conditions simulated. Due to this observation, it might be expectable some influence due to the RS field in the surrounding material, which would be worth to be studied.

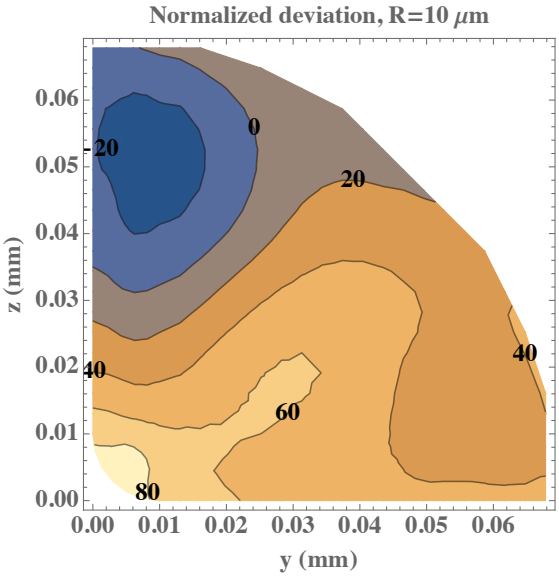

(a)

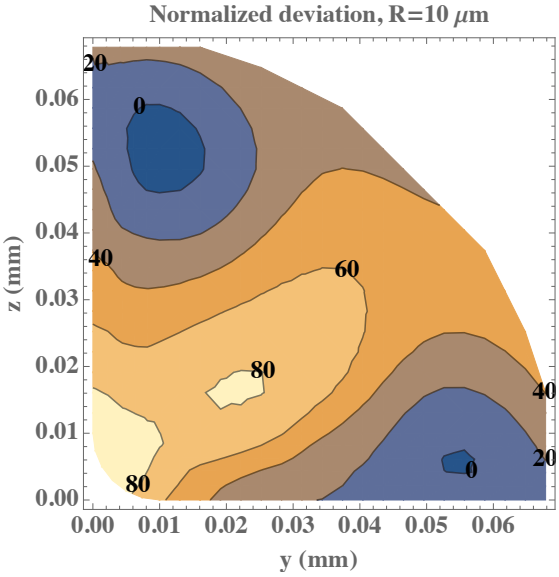

(b)

Figure 6.10: Normalized deviation of the RS field comparing the reconstructed map (Section 3.3) and the results of the simulations for for 150 µm notch root radius (a) and 500 µm notch root radius (b).

6.6 Conclusions

In this Chapter, we aimed at exploring the inflence of the fillet radius on the RS field in the vicinity of an edge, through FEM simulations. The model used is the same as in the previous Chapter, but three values of the fillet radius are considered for the edge tip, namely 10 µm, 25 µm and 40 µm. The latter value is supposed to be the closest to the true dimension of the fillet radius in the real specimens. Two simulation approaches are used, mutuated from the ones devised in the previous Chapter 5. A realistic approach obtained from the DEM simulations with 214 impacting shots and a simplified approach with 85 orthogonally impacting shots are used.
The results of the simulations could not be compared to the reconstructed RS field seen in Section 3.3 due to the increasing discrepancy in the existence domain of RS due to the fillet radius and the reconstruction being carried out on an ideally sharp edge. Nonetheless, some interesting observations can be raised through the comparison of the results with the two simulation approaches and with the different fillet radii:

- an increase in the fillet radius makes the peening condition more similar to the process being carried out on a flat surface. Removing the sharper part of the edge avoids the "squeezing effect" on the bisector line of the edge where the RS is very weak or even in positive;

- the bigger the fillet radius, the better the situation, at least in the range considered in this study. Bigger fillet radius make the RS field more uniform, and presumably effective in enhancing the fatigue resistance of the treated component even in critical locations like gemetrical features;

- the former two observation are well known in the SP practice, where filleting edges before the process is always recomended to obtain the best results from the treatment;

- the two considered simulation approaches gave similar results, in the range of the uncertainty in the RS field and the peening conditions. Some differences can be observed, and will be studied in more detail in future works. Nonetheless, the most influencing

factor in the developement of the RS field, seems to be the exact true geometry of the substrate. In order to achieve a satisfactory prediction of the peening results, the exact knowledge of the substrate geometry is more important than the modelization of the process itself.

As a further development of the analysis, the FEM simulation of SP on a notch has been presented. Two dimension for the notch root radius are considered, namely 150 µm and 500 µm. The simplified simulation approach with orthogonally impacting shots is used, with a number of shots equivalent to the average number of shots required to achieve full coverage on the impact area. The resulting RS fields are compared to the reconstructed RS fields based on experimental measurements.
The resulting RS field is very satisfactory, in particular for the wider notch, and shows very good accordance with the reconstructed RSs.
In relation to what already observed when the SP process on the edge was simulated, some observations can be raised:

- the intense compressive RS peak in the internal part of the notch is very well catched by the simulation. Thus, is appears reasonable to suppose that the concentration of RS in this locations is to be ascribed more to gemetrical arrangement of the substrate material tan to the peculiar peening conditions in this region;

- some resemblances can be observed in the RS field, with subsurface RS peaks under the Front and Lateral Surfaces, and the strongly attenuated RS on the bisector line of the edge;

- the influence of the dimension of the impact area compared to the overall dimension of the geometrical feature may need to be studied. A wider impact area, or an alternative tool to take into account the RS field geenrated by SP in the surrounding material and presumably exterting some influence on the fina RS field in the critical point of the notch are worth to be studied;

- as seen in the case of the edge, the radius of the fillet on the intersection of the Front end the Lateral Surface may exert an effect on the RS field generated; this aspect will not be subject of this study, but seems to be a natural progression of the work.

In conclusion, the simulation of SP on the notch, even if in a simplified approach, shows interesting aspects of the process and promising development for the FEM simulation applied to study of the RS generated in correspondence of geometrical features. In order to devise realistic models and have realible reference RSs to compare with the simulation results, some more experimental data need to be aquired. Nonetheless, as is evident from the results shown in the previous Sections, this is presumably the last obstacle to overcome in order to have a reliable prediction of RSs generated by SP on geometrical features, eligible to be implemented directly into the design process.

Chapter 7

Conclusions and future developments

7.1 Conclusions

In this thesis, the numerical simulation of SP was addressed. The study is focusedon the the B120 micro SP treatment, with micrometric ceramic beads, performed in aeronautical grade Al7075-T651 aluminum alloy substrate. Apart from the specific aspects of the process, which was chosen mainly for the availability of experimental data to compare the result of the numerical simualtion with, is worth to highlight once more that each and every this study has been aimed to the devlopment and validation of a procedure for the numerical simulation of SP in general, nore than to the attainment of new quantitative results.

At first, the simulation of SP on a flat surface has been addressed. A MatLab routine is used to predict the coverage level prior to the simulation linearization, given the dimeter and the velocity of the impacting shot and thus to assess the number of shots to full coverage. Sets with different numbers of shots characterized by stochastic variability in their dimension, velocity and impact location are generated and used to set up the FEM simulations. The Lemaitre-Chaboche model calibrated on cyclic strain tests has been used to simulate the realistic mechanical behavior of the substrate. 30 explicit dynamic FEM simulations has been carried out to account for the statistical nature of the process. Results have been obtained in terms of final

roughness of the treated surfce and in-depth RSs, which have been compared to the experimental data. Moreover, a purposely devised procedure has been used to account for the effect of surface roughness and radiation penetration in the RS field. Then, the deformed target bodies have been imported into static finite element simulations, in order to assess the stress concentration effect exerted by the increased surface roughness.

Then, the simulation of on an edge is addressed. A synergistic DEM-FEM approach has been used to study the true process conditions in correspondence of geometrical featrues. The DEM model of the nozzle has been tuned using preliminary simulations on a flat surface and nominal process parameters. Then, DEM simulations of SP on an edge has been carried out, to assess the number of impact in the area of interest, as well as the impact velocity distribution. The results has been used to set up FEM simulations of SP on an edge. In addition to the realistic simulations, based on DEM simulations, simulations considering only the shots blown by the nozzle in its tilting phase has been carried out. Moreover, two simplified simulation approaches based on simple coverage considerations, have been devised. The results in all cases have been obtained in terms of RS fields, and compared among themselves and with the reference RS field reconstructed using experimental RS measurements.

Then, the effect of the radius of the fillet on the edge tip has been studied, by applying the realistic and one simplified simulation approaches to models in which the target body has been modified in the fillet dimension, according to some new experimental observations on the edge real morphology.

Lastly, the simplified simulation approach has been extended to the simulation of SP on a notch, and the resulting RS field,a s in the case of the edge, is compared to the reconstructed reference one.

Conclusions have been drawn step by step during the study, nonetheless it is worth to recall some of them, together with some more observations hereafter. As regards the simulation of SP on a flat surace:

(i) the numerical simulations are in good agreement with the experimental results. Some underestimation in the surface roughness may be ascribable to the overestimation of the average impact velocity of shots (as later suggested DEM simulations) and the

consequent underestimation of the number of impacts required to achieve full coverage. Nonetheless, quite good agreement with the experimental data is found;

(ii) in-depth RSs from FEM simulations and experimental measurements are very well-matching, in particular as regards the magnitude and position of the compressive RS peak. Moreover, if the penetration effect of the X-radiation as well as the effect of the surface roughness on XRD measurements are considered, interesting improvements are obtained on the surface RS magnitude. This is due to the thickness of the layer subject to compressive RSs being the same order of magnitude as the radiation penetration, and only slighlty thicker than the maximum peak-to-peak distance on the indented surface. Better results could be achieved with some improvements in the in-depth resolution of the XRD measurements, and in the experimental data processing for measurements on not flat surfaces;

(iii) implicit static FEM simulations on the deformed model are a valid tool for the assessment of the stress concentration factor. Improvements in the predicted surface roughness (as mentioned at point (i)) may be beneficial for the prediction of the stress concentration. Nevertheless, according to the chosen failure criterion, this simulation approach is a valid tool for fatigue life prediction;

(iv) no clear general correlation has been identified relating the parameters governing the dynamics of the peening media and the final effects, apart from some correlation between the surface roughness and the overall kinetic energy of the bead stream. Nonetheless, the study of a wider range of peening varieties is to be studied prior to giving a final vewpoint.

The study of the simulation on an edge makes possible to raise some more observations:

(i) the DEM simulation on a flat surface shows the actual peening conditions to be relatively different from the nominal one, in particular as regards the impact velocity of shots, which has a remarkable improtance in the process. This highlights the

importance of a realistic and complete DEM simulation of the process, as an alternative to more detailed and expensive experimental observations of the actual treatment operations;

(ii) the used DEM-FEM synergistic approach gave results in good agreement with the reconstructed RS field based on experimental measurements. When actual peening conditions are found, orthogonally impacting shots are shown to exert a prevalent effect on the generation of RSs. Thus, even simplified approaches based on the unperturbed SP parameters can be an eligible alternative for the prediction of the final RS field in a more practical and easy-to-implement way;

(iii) in the volume of material encompassing the edge and its immediate surroundings, the RS field is strongly perturbed RS state. This confirms the well known weakness of these points for the structural integrity of the components under fatigue loads.;

(iv) in order to the integration of the effects of SP into the design process, it is *mandatory* to carefully keep into account the perturbation of RSs in the vicinity of geometrical details. The correct knowledge of the RS state in these locations is the only way for an effective and safe assessment of the significant effects introduced by SP to be considered for the optimization of the component design.

Two main observations can be raised on the results of the parametric analysis of the edge fillet radius. First of all, the importance of some rounding on edge (and geometrical features in general) is clearly assessed from the simulations for the first time, despite it being well known in practice since a long time. Then, a critical aspect of the simulation is highlighted by the results of the analysis. The realistic DEM-FEM approach and the simplified simulation approach gave comparable results, but the geometry of the substrate was shown to exert a remarkable effect of the final RS field. The correct knwoledge and the precise modelization of the target geometry is as important as (or maybe even more important than) the realistic modelization of the process. This is particularly clear in the case of the chosen SP treatment, which generates a compressive RS state whose characteristic dimension is the same order of magnitude of the micrometric

geometrical details. Nonetheless, this highlights an important aspect for the extension of the SP simulation to the study of the RS state in manufacturing components. The precise knowledge of the *exact* shape of the substrate is indeed fundamental for the success of the study.
Finally, the extremely good agreement achieved between the numerical simulations results and the reference RS field in the case of the notch, despite the use of a simplified simulation approach, opens to interesting perspectives in the future of the simulation of SP. Nonetheless, the study has not pushed to the study of the effect of SP in the notch at longer distances from the specimen surface, due to the lack of experimental data to be compared with the numerical simulation results. In this locations, the peening media stream is expected to be slighlty more perturbed by the substrate geometry, and the contribute of the DEM simulation to be substancial as well.

7.2 Future developments and perspectives

In conclusion to this dissertation, some line for the development of the research in the near future will be seen, as well as some general observations on the future perspective of the simulation of SP.
The first step for the advancement of the research will be the DEM simulation of SP in the case of the notch. The DEM-FEM approach will then be applied, and the results are going to be compared to the ones of the simplified simulation approach. In this way, the reliability of the simplified simulation approach is going to be definitively validated. In order to move a further step towards the realistic modelization of the process, the true dimension of the fillet on the edge tip (even in the case of notched sample) will be taken into account with new, purposely aquired measurements. The reconstruction of the RS field through thermal strains (Section 3.3) will be performed on adequately filleted models, in order to have a suitable reference RS field.
Moreover, it is worth to remember that, in order to achieve some results in a reasonable computation time, the simulation of SP on geometrical features has been focused quite only on the RS field. Intense deformations in the target, as mentioned in Chapter 5, pushed towards the choice of bigger elements with erosion, which needs to be carefully tuned if the final surface topology is to be studied. To this

regard, the use of the Arbitrary Lagrangian-Eulerian (ALE) formulation of elements may be a great improvement for its capability to hold up with high strain level also on fine meshes. Nonetheless, the heavy increse in computing cost required by this kind of models make this approach manageable only if power computing resources are available. Similarly, wider impact areas might be interesting to be studied, both on a flat surface and in the vicinity of geometrical features. Nonetheless, computing resorces much higer than the ones used in this work would be required to achieve this task.

The simulation of SP in the root of "deep" notches may be one of the near future developments of simulating SP. Nonetheless, as already mentioned, experimental data in the vicinity of any geometrical features are currently very few. This is due not only to the high cost of experimental measurements, but also (and even more) to the unfeasibility of XRD measurement in narrow spaces. Thus, it would difficult to validate the results of the simulations ad unwise to trust them straightforwardly. Some advancement in the XRD technology would be unexpected but unbelievably desirable, since it could expand significantly the range of reliability of the simulations.

In the end, it is worth to move the focus to some observations that go beyond the scope of this study. The FEM simulation, by its nature, is not suitable for the direct simulation of the process on an entire component, no matter the extent of the computing resources available. The FEM or DEM-FEM simulations are based on model having small dimension, also in consideration of the high level of detail required to catch the most important aspects of the process. Thus, if the overall RS state in a component is required for the integrations of the effects of SP in the design process, a mathematical method for the "assembly" of the RS fields in specific locations is needed in order to infer the general RS field. In the first instance, the choice falls over the manipulation of eigenstrains, but also other methods can be considered. Surface roughness can be considered introducing empirical coiefficients or, maybe, automatically generated surface topology modifications in the models. It is exciting to point out that, one this issues have overcame, the way is clear towards the use of the SP simulation in the industrial practice.

Bibliography

[1] H. Maryon, "Metal Working in the Ancient World," *American Journal of Archaeology*, vol. 53, no. 2, pp. 93–125, 1949.

[2] G. Leghorn, "The story of shot peening," *Journal of the American Society for Naval Engineers*, vol. 69, no. 4, pp. 653–666, 1957, ISSN: 15593584. DOI: 10.1111/j.1559-3584.1957.tb03244.x.

[3] J. J. Bush, R. L. Mattson, and J. G. Roberts, *Shot-peening treatments*, 1963. DOI: 10.1017/CBO9781107415324.004. arXiv: arXiv:1011.1669v3.

[4] L. Wagner, Ed., *Shot Peening*. Wiley-VCH Verlag GmbH & Co. KGaA, 2003, ISBN: 9788578110796. DOI: 10.1017/CBO9781107415324.004. arXiv: arXiv:1011.1669v3.

[5] M. Kobayashi, T. Matsui, and Y. Murakami, "Mechanism of creation of compressive residual stress by shot peening," *International Journal of Fatigue*, vol. 20, pp. 35–357, 1998, ISSN: 01421123. DOI: 10.1016/S0142-1123(98)00002-4.

[6] A. B. Edward, P. S. Heyns, and F. Pietra, "Shot Peening Modeling and Simulation for RCS Assessment," *Procedia Manufacturing*, vol. 7, pp. 172–177, 2017, ISSN: 23519789. DOI: 10.1016/j.promfg.2016.12.044.

[7] G. Nachman, *Shot Peening - Past, Present and Future*, 1999. [Online]. Available: www.google.com.

[8] G. A. Fett, "Understanding Shot Peening: A Case History," *Modern Casting*, no. June, pp. 29–31, 1983.

[9] Y. Mutoh, G. H. Fair, B. Noble, and R. B. Waterhouse, "The effect of Residual Stresses induced by shot-peening on fatigue crack propagation in two high strength aluminium alloys," *Fatigue & Fracture of Engineering Materials & Structures*, vol. 10, no. 4, pp. 261–272, 1987, ISSN: 14602695. DOI: 10.1111/j.1460-2695.1987.tb00205.x.

[10] D. W. Hammond and S. A. Meguid, "Crack Propagation Shot-Peening Residual Stresses," *Engineering Fracture Mechanics*, vol. 37, no. 2, pp. 373–387, 1990.

[11] J. C. Villegas, L. L. Shaw, K. Dai, W. Yuan, J. Tian, P. K. Liaw, and D. L. Klarstrom, "Enhanced fatigue resistance of a nickel-based hastelloy induced by a surface nanocrystallization and hardening process," *Philosophical Magazine Letters*, vol. 85, pp. 427–438, 2005, ISSN: 09500839. DOI: 10.1080/09500830500311705.

[12] S. Bagherifard and M. Guagliano, "Fatigue behavior of a low-alloy steel with nanostructured surface obtained by severe shot peening," *Engineering Fracture Mechanics*, vol. 81, pp. 56–68, 2012, ISSN: 00137944. DOI: 10.1016/j.engfracmech.2011.06.011. [Online]. Available: http://dx.doi.org/10.1016/j.engfracmech.2011.06.011.

[13] L. Wagner, M. Mhaede, M. Wollmann, I. Altenberger, and Y. Sano, "Surface layer properties and fatigue behavior in Al 7075-T73 and Ti-6Al-4V Comparing results after laser peening; Shot peening and ball-burnishing," *International Journal of Structural Integrity*, vol. 2, no. 2, pp. 185–199, 2011, ISSN: 17579864. DOI: 10.1108/17579861111135923.

[14] L. Wagner and M. Wollmann, "Shot Peening of Non-Ferrous Alloys To Enhance Fatigue Performance," in *ICSP10 the 10th International Conference on Shot Peening*, Tokyo, 2008.

[15] A. Zammit, "Shot Peening of Austempered Ductile Iron," in *Advanced Surface Engineering Research*, London: InTechOpen, 2018, pp. 25–44. DOI: 10.1016/j.colsurfa.2011.12.014. [Online]. Available: http://dx.doi.org/10.1039/C7RA00172J%7B%5C%%7D0Ahttps://www.intechopen.com/books/advanced-biometric-technologies/liveness-detection-in-biometrics%7B%5C%%7D0Ahttp://dx.doi.org/10.1016/j.colsurfa.2011.12.014.

[16] S. Bagherifard and M. Guagliano, "Review of shot peening processes to obtain nanocrystalline surfaces in metal alloys," *Surface Engineering*, vol. 25, no. 1, pp. 3–14, 2009, ISSN: 02670844. DOI: 10.1179/026708408X334087.

[17] J. Badreddine, E. Rouhaud, M. Micoulaut, and S. Remy, "Simulation of shot dynamics for ultrasonic shot peening: Effects of process parameters," *International Journal of Mechanical Sciences*, vol. 82, pp. 179–190, 2014, ISSN: 00207403. DOI: 10.1016/j.ijmecsci.2014.03.006.

[18] L. Wang and D. Y. Li, "Mechanical, electrochemical and tribological properties of nanocrystalline surface of brass produced by sandblasting and annealing," *Surface and Coatings Technology*, vol. 167, pp. 188–196, 2003, ISSN: 02578972. DOI: 10.1016/S0257-8972(02)00894-0.

[19] S. Bagherifard, I. Fernndez Pariente, R. Ghelichi, and M. Guagliano, "Fatigue properties of nanocrystallized surfaces obtained by high energy shot peening," *Procedia Engineering*, vol. 2, pp. 1683–1690, 2010, ISSN: 18777058. DOI: 10.1016/j.proeng.2010.03.181.

[20] S. Bagherifard, D. J. Hickey, S. Fintová, F. Pastorek, I. Fernandez-Pariente, M. Bandini, T. J. Webster, and M. Guagliano, "Effects of nanofeatures induced by severe shot peening (SSP) on mechanical, corrosion and cytocompatibility properties of magnesium alloy AZ31," *Acta Biomaterialia*, vol. 66, pp. 93–108, 2018, ISSN: 18787568. DOI: 10.1016/j.actbio.2017.11.032.

[21] K. Lu and J. Lu, *Surface nanocrystallization (SNC) of metallic materials-presentation of the concept behind a new approach*, 1999.

[22] K. Dai and L. Shaw, "Comparison between shot peening and surface nanocrystallization and hardening processes," *Materials Science and Engineering A*, vol. 463, pp. 46–53, 2007, ISSN: 09215093. DOI: 10.1016/j.msea.2006.07.159.

[23] K. Lu and J. Lu, "Nanostructured surface layer on metallic materials induced by surface mechanical attrition treatment," *Materials Science and Engineering A*, vol. 375-377, pp. 38–45, 2004, ISSN: 09215093. DOI: 10.1016/j.msea.2003.10.261.

[24] E. S. Statnikov, V. O. Muktepavel, and A. Blomqvist, "Comparison of ultrasonic impact treatment (UIT) and other fatigue life improvement methods," *Welding Research Abroad*, vol. 50, no. 5, pp. 28–40, 2004, ISSN: 00432318.

[25] B. N. Mordyuk and G. I. Prokopenko, "Ultrasonic impact peening for the surface properties' management," *Journal of Sound and Vibration*, vol. 308, pp. 855–866, 2007, ISSN: 10958568. DOI: 10.1016/j.jsv.2007.03.054.

[26] K. K. Liu and M. R. Hill, "The effects of laser peening and shot peening on fretting fatigue in Ti-6Al-4V coupons," *Tribology International*, vol. 42, no. 9, pp. 1250–1262, 2009, ISSN: 0301679X. DOI: 10.1016/j.triboint.2009.04.005. [Online]. Available: http://dx.doi.org/10.1016/j.triboint.2009.04.005.

[27] R. Foschino, C. Picozzi, A. Civardi, M. Bandini, and P. Faroldi, "Comparison of surface sampling methods and cleanability assessment of stainless steel surfaces subjected or not to shot peening," *Journal of Food Engineering*, vol. 60, no. 4, pp. 375–381, 2003, ISSN: 02608774. DOI: 10.1016/S0260-8774(03)00060-8.

[28] G. Lucchetta, F. Marinello, and P. F. Bariani, "Aluminum sheet surface roughness correlation with adhesion in polymer metal hybrid overmolding," *CIRP Annals - Manufacturing Technology*, vol. 60, no. 1, pp. 559–562, 2011, ISSN: 00078506. DOI: 10.1016/j.cirp.2011.03.073.

[29] P. Kaestner, J. Olfe, J. W. He, and K. T. Rie, "Improvement in the load-bearing capacity and adhesion of TiC coatings on TiAl6V4 by duplex treatment," *Surface and Coatings Technology*, vol. 142-144, pp. 928–933, 2001, ISSN: 02578972. DOI: 10.1016/S0257-8972(01)01214-2.

[30] J. Champaigne, *Shot Peening of orthopaedic implants for tissue adhesion*, 2006.

[31] S. Bagherifard, D. J. Hickey, A. C. de Luca, V. N. Malheiro, A. E. Markaki, M. Guagliano, and T. J. Webster, "The influence of nanostructured features on bacterial adhesion and bone cell functions on severely shot peened 316L stainless steel," *Biomaterials*, vol. 73, pp. 185–197, 2015, ISSN: 18785905. DOI: 10.1016/j.biomaterials.2015.09.019. [Online]. Available: http://dx.doi.org/10.1016/j.biomaterials.2015.09.019.

[32] N. R. Tao, M. L. Sui, J. Lu, and K. Lua, "Surface nanocrystallization of iron induced by ultrasonic shot peening," *Nanostructured Materials*, vol. 4, pp. 433–440, 1999, ISSN: 09659773. DOI: 10.1016/S0965-9773(99)00324-4.

[33] S. Bagherifard, S. Slawik, I. Fernández-Pariente, C. Pauly, F. Mücklich, and M. Guagliano, "Nanoscale surface modification of AISI 316L stainless steel by severe shot peening," *Materials and Design*, vol. 102, pp. 68–77, 2016, ISSN: 18734197. DOI: 10.1016/j.matdes.2016.03.162.

[34] M. Benedetti, V. Fontanari, P. Scardi, C. L. A. Ricardo, and M. Bandini, "Reverse bending fatigue of shot peened 7075-T651 aluminium alloy: The role of residual stress relaxation," *International Journal of Fatigue*, vol. 31, no. 8-9, pp. 1225–1236, 2009, ISSN: 01421123. DOI: 10.1016/j.ijfatigue.2008.11.017.

[35] M. Benedetti, V. Fontanari, M. Bandini, and E. Savio, "High- and very high-cycle plain fatigue resistance of shot peened high-strength aluminum alloys: The role of surface morphology," *International Journal of Fatigue*, vol. 70, pp. 451–462, 2015, ISSN: 01421123. DOI: 10.1016/j.ijfatigue.2014.07.002. [Online]. Available: http://dx.doi.org/10.1016/j.ijfatigue.2014.07.002.

[36] M. K. Tufft, "Development of a Fracture Mechanics Methodology to Assess the Competing Mechanisms of Beneficial Residual Stress and Detrimental Plastic Strain Due to Shot Peening," in *ICSP6 the 6th International Conference on Shot Peening*, San Francisco, 1996.

[37] S. M. Gangaraj and G. H. Farrahi, "Side effects of shot peening on fatigue crack initiation life," *International Journal of Engineering, Transactions A: Basics*, vol. 24, no. 3, pp. 275–280, 2011, ISSN: 17359244. DOI: 10.5829/idosi.ije.2011.24.03a.06.

[38] M. S. Bhuiyan, Y. Mutoh, and A. J. McEvily, "The influence of mechanical surface treatments on fatigue behavior of extruded AZ61 magnesium alloy," *Materials Science and Engineering A*, vol. 549, pp. 69–75, 2012, ISSN: 09215093. DOI: 10.1016/j.msea.2012.04.007. [Online]. Available: http://dx.doi.org/10.1016/j.msea.2012.04.007.

[39] L. Trško, M. Guagliano, O. Bokůvka, F. Nový, M. Jambor, and Z. Florková, "Influence of Severe Shot Peening on the Surface State and Ultra-High-Cycle Fatigue Behavior of an AW 7075 Aluminum Alloy," *Journal of Materials Engineering and Performance*, vol. 26, no. 6, pp. 2784–2797, 2017, ISSN: 15441024. DOI: 10.1007/s11665-017-2692-9.

[40] N. Ferreira, J. S. Jesus, J. A. Ferreira, C. Capela, J. M. Costa, and A. C. Batista, "Effect of bead characteristics on the fatigue life of shot peened Al 7475-T7351 specimens," *International Journal of Fatigue*, vol. 134, no. November 2019, p. 105 521, 2020, ISSN: 01421123. DOI: 10.1016/j.ijfatigue.2020.105521. [Online]. Available: https://doi.org/10.1016/j.ijfatigue.2020.105521.

[41] T. Klotz, D. Delbergue, P. Bocher, M. Lévesque, and M. Brochu, "Surface characteristics and fatigue behavior of shot peened Inconel 718," *International Journal of Fatigue*, vol. 110, no. October 2017, pp. 10–21, 2018, ISSN: 01421123. DOI: 10.1016/j.ijfatigue.2018.01.005. [Online]. Available: https://doi.org/10.1016/j.ijfatigue.2018.01.005.

[42] P. Starker, H. Wohlfart, and E. Macherauch, "Subsurface Crack Initiation During Fatigue As a Result of Residual Stresses," *Fatigue & Fracture of Engineering Materials & Structures*, vol. 1, no. 3, pp. 319–327, 1979, ISSN: 14602695. DOI: 10.1111/j.1460-2695.1979.tb00388.x.

[43] E. R. de los Rios, A. Walley, M. T. Milan, and G. Hammersley, "Fatigue crack initiation and propagation on shot-peened surfaces in A316 stainless steel," *International Journal of Fatigue*, vol. 17, no. 7, pp. 493–499, 1995, ISSN: 01421123. DOI: 10.1016/0142-1123(95)00044-T.

[44] T. Dörr and L. Wagner, "Fatigue response of various titanium alloys to shot peening," *Transactions on Engineering Sciences*, vol. 25, pp. 589–598, 1999.

[45] M. Guagliano, E. Riva, and M. Guidetti, "Contact fatigue failure analysis of shot-peened gears," *Engineering Failure Analysis*, vol. 9, no. 2, pp. 147–158, 2002, ISSN: 13506307. DOI: 10.1016/S1350-6307(01)00002-4.

[46] T. Ludian, M. Kocan, H. J. Rack, and L. Wagner, "Residual-stress-induced subsurface crack nucleation in titanium alloys," *International Journal of Materials Research*, vol. 97, no. 10, pp. 1425–1431, 2006, ISSN: 18625282. DOI: 10.3139/146.101387.

[47] N. K. Burrell, "Controlled shot peening of automotive components," *SAE Technical Papers*, vol. 7, 1985, ISSN: 2688-3627. DOI: 10.4271/850365.

[48] A. Blarasin, M. Guagliano, and L. Vergani, "Fatigue crack growth prediction in specimens similar to spur gear teeth," *Fatigue and Fracture of Engineering Materials and Structures*, vol. 20, no. 8, pp. 1171–1182, 1997, ISSN: 8756758X. DOI: 10.1111/j.1460-2695.1997.tb00321.x.

[49] M. Benedetti, V. Fontanari, B. R. Höhn, P. Oster, and T. Tobie, "Influence of shot peening on bending tooth fatigue limit of case hardened gears," *International Journal of Fatigue*, vol. 24, pp. 1127–1136, 2002, ISSN: 01421123. DOI: 10.1016/S0142-1123(02)00034-8.

[50] M. Benedetti, V. Fontanari, C. Santus, and M. Bandini, "Notch fatigue behaviour of shot peened high-strength aluminium alloys: Experiments and predictions using a critical distance method," *International Journal of Fatigue*, vol. 32, no. 10, pp. 1600–1611, 2010, ISSN: 01421123. DOI: 10.1016/j.ijfatigue.2010.02.012.

[51] C. You, M. Achintha, B. Y. He, and P. A. Reed, "A numerical study of the effects of shot peening on the short crack growth behaviour in notched geometries under bending fatigue tests," *International Journal of Fatigue*, vol. 103, pp. 99–111, 2017, ISSN: 01421123. DOI: 10.1016/j.ijfatigue.2017.05.023.

[52] C. You, B. Y. He, M. Achintha, and P. A. Reed, "Numerical modelling of the fatigue crack shape evolution in a shot-peened steam turbine material," *International Journal of Fatigue*, vol. 104, pp. 120–135, 2017, ISSN: 01421123. DOI: 10.1016/j.ijfatigue.2017.07.017.

[53] R. Eriksson, J. Moverare, and Z. Chen, "A low cycle fatigue life model for a shot peened gas turbine disc alloy," *International Journal of Fatigue*, vol. 124, pp. 34–41, 2019, ISSN: 01421123. DOI: 10.1016/j.ijfatigue.2019.02.034. [Online]. Available: https://doi.org/10.1016/j.ijfatigue.2019.02.034.

[54] E. Salvati, A. J. Lunt, S. Ying, T. Sui, H. J. Zhang, C. Heason, G. Baxter, and A. M. Korsunsky, "Eigenstrain reconstruction of residual strains in an additively manufactured and shot peened nickel superalloy compressor blade," *Computer Methods in Applied Mechanics and Engineering*, vol. 320, pp. 335–351, 2017, ISSN: 00457825. DOI: 10.1016/j.cma.2017.03.005. [Online]. Available: http://dx.doi.org/10.1016/j.cma.2017.03.005.

[55] S. Shen and S. N. Atluri, "An analytical model for shot-peening induced residual stresses," *Computers, Materials and Continua*, vol. 4, no. 2, pp. 75–85, 2006, ISSN: 15462218. DOI: 10.3970/cmc.2006.004.075.

[56] H. Guechichi, L. Castex, and M. Benkhettab, "An analytical model to relate shot peening almen intensity to shot velocity," *Mechanics Based Design of Structures and Machines*, vol. 41, no. 1, pp. 79–99, 2013, ISSN: 15397734. DOI: 10.1080/15397734.2012.703607.

[57] H. Y. Miao, S. Larose, C. Perron, and M. Lévesque, "An analytical approach to relate shot peening parameters to Almen intensity," *Surface & Coatings Technology*, vol. 205, no. 7, pp. 2055–2066, 2010, ISSN: 0257-8972. DOI: 10.1016/j.surfcoat.2010.08.105. [Online]. Available: http://dx.doi.org/10.1016/j.surfcoat.2010.08.105.

[58] T. Chaise, J. Li, D. Nélias, R. Kubler, S. Taheri, G. Douchet, V. Robin, and P. Gilles, "Modelling of multiple impacts for the prediction of distortions and residual stresses induced by ultrasonic shot peening (USP)," *Journal of Materials Processing Technology*, vol. 212, no. 10, pp. 2080–2090, 2012, ISSN: 09240136. DOI: 10.1016/j.jmatprotec.2012.05.005. [Online]. Available: http://dx.doi.org/10.1016/j.jmatprotec.2012.05.005.

[59] A. M. Korsunsky, "On the modelling of residual stresses due to surface peening using eigenstrain distributions," *Journal of Strain Analysis for Engineering Design*, vol. 40, no. 8, pp. 817–824, 2005, ISSN: 03093247. DOI: 10.1243/030932405X30984.

[60] M. Achintha and D. Nowell, "Eigenstrain modelling of residual stresses generated by laser shock peening," *Journal of Materials Processing Technology*, vol. 2, pp. 1091–1101, 2011, ISSN: 09240136. DOI: 10.1016/j.jmatprotec.2011.01.011.

[61] X. J. Zhang, T. Wang, J. B. Wang, and C. Liu, "Analytical modeling of shot peen forming process using cross-sectional linear indentation coverage method," *International Journal of Mechanical Sciences*, vol. 133, 2017, ISSN: 00207403. DOI: 10.1016/j.ijmecsci.2017.09.055.

[62] P. A. Faucheux, F. P. Gosselin, and M. Lévesque, "Simulating shot peen forming with eigenstrains," *Journal of Materials Processing Technology*, vol. 254, pp. 135–144, 2018, ISSN: 09240136. DOI: 10.1016/j.jmatprotec.2017.11.036.

[63] M. Benedetti, V. Fontanari, and B. D. Monelli, "Numerical Simulation of Residual Stress Relaxation in Shot Peened High-Strength Aluminum Alloys Under Reverse Bending Fatigue," *Journal of Engineering Materials and Technology*, vol. 132, no. 1, pp. 11012–1–9, 2010, ISSN: 00944289. DOI: 10.1115/1.3184083.

[64] M. Benedetti, V. Fontanari, M. Bandini, and D. Taylor, "Multiaxial fatigue resistance of shot peened high-strength aluminum alloys," *International Journal of Fatigue*, vol. 61, pp. 271–282, 2014, ISSN: 01421123. DOI: 10.1016/j.ijfatigue.2013.10.020. [Online]. Available: http://dx.doi.org/10.1016/j.ijfatigue.2013.10.020.

[65] M. Benedetti, V. Fontanari, M. Allahkarami, J. C. Hanan, and M. Bandini, "On the combination of the critical distance theory with a multiaxial fatigue criterion for predicting the fatigue strength of notched and plain shot-peened parts," *International Journal of Fatigue*, vol. 93, pp. 133–147, 2016, ISSN: 01421123. DOI: 10.1016/j.ijfatigue.2016.08.015. [Online]. Available: http://dx.doi.org/10.1016/j.ijfatigue.2016.08.015.

[66] J.O. Almen, *Shot Blasting Test*, 1944. DOI: 10.16971/vd.56852.

[67] W. Cao, R. Fathallah, and L. Castex, "Correlation of Almen arc height with residual stresses in shot peening process," *Materials Science and Technology (United Kingdom)*, vol. 11, pp. 967–973, 1995, ISSN: 17432847. DOI: 10.1179/mst.1995.11.9.967.

[68] M. Guagliano, "Relating Almen intensity to residual stresses induced by shot peening: A numerical approach," *Journal of Materials Processing Technology*, vol. 110, no. 3, pp. 277–286, 2001, ISSN: 09240136. DOI: 10.1016/S0924-0136(00)00893-1.

[69] Z. Chen, F. Yang, and S. A. Meguid, "Realistic Finite Element Simulations of Arc-Height Development in Shot-Peened Almen Strips," *Journal of Engineering Materials and Technology*, vol. 136, no. 4, p. 041 002, 2014, ISSN: 0094-4289. DOI: 10.1115/1.4028006. [Online]. Available: http://materialstechnology.asmedigitalcollection.asme.org/article.aspx?doi=10.1115/1.4028006.

[70] J. Champaigne, "Almen Strip Specifications," *The Shot Peener*, vol. 11, no. 3, 1997.

[71] D. Kirk, "Shot Peening," *Aircraft Engineering and Aerospace Technology: An International Journal*, vol. 71, no. 4, pp. 349–361, 1999.

[72] Y. F. Al-Obaid, "Shot peening mechanics: experimental and theoretical analysis," *Mechanics of Materials*, vol. 9, pp. 251–260, 1995, ISSN: 01676636. DOI: 10.1016/0167-6636(94)00036-G.

[73] S. Bagherifard, R. Ghelichi, and M. Guagliano, "Numerical and experimental analysis of surface roughness generated by shot peening," *Applied Surface Science*, vol. 258, pp. 6831–6840, 2012, ISSN: 01694332. DOI: 10.1016/j.apsusc.2012.03.111. [Online]. Available: http://dx.doi.org/10.1016/j.apsusc.2012.03.111.

[74] T. Hong, J. Y. Ooi, and B. Shaw, "A numerical simulation to relate the shot peening parameters to the induced residual stresses," *Engineering Failure Analysis*, vol. 15, no. 8, pp. 1097–1110, 2008, ISSN: 13506307. DOI: 10.1016/j.engfailanal.2007.11.017. [Online]. Available: www.elsevier.com/locate/engfailanal.

[75] D. Kirk and M. Abyaneh, "Theoretical basis of shot peening coverage control," *Shot Peener (USA)*, vol. Vol.9(2), no. 2, pp.28–30, 1995.

[76] D. Kirk, "Shot Peening Coverage: Prediction and Control," *The Shot Peener*, vol. 23, no. 2, pp. 24–32, 2009.

[77] H. Y. Miao, D. Demers, S. Larose, C. Perron, and M. Lévesque, "Experimental study of shot peening and stress peen forming," *Journal of Materials Processing Technology*, vol. 210, no. 15, pp. 2089–2102, 2010, ISSN: 09240136. DOI: 10.1016/j.jmatprotec.2010.07.016. [Online]. Available: http://dx.doi.org/10.1016/j.jmatprotec.2010.07.016.

[78] H. Y. Miao, S. Larose, C. Perron, and M. Lévesque, "On the potential applications of a 3D random finite element model for the simulation of shot peening," *Advances in Engineering Software*, vol. 40, no. 10, pp. 1023–1038, 2009, ISSN: 09659978. DOI: 10.1016/j.advengsoft.2009.03.013. [Online]. Available: http://dx.doi.org/10.1016/j.advengsoft.2009.03.013.

[79] D. Lombardo and P. Bailey, "The Reality of Shot Peen Coverage," *The Shot Peener*, vol. 13, no. 4, pp. 34–37, 2009. [Online]. Available: http://www.shotpeener.com/library/pdf/1999099.pdf.

[80] G. H. Majzoobi, K. Azadikhah, and J. Nemati, "The effects of deep rolling and shot peening on fretting fatigue resistance of Aluminum-7075-T6," *Materials Science and Engineering A*, vol. 516, no. 1-2, pp. 235–247, 2009, ISSN: 09215093. DOI: 10.1016/j.msea.2009.03.020.

[81] K. Dai, J. Villegas, Z. Stone, and L. Shaw, "Finite element modeling of the surface roughness of 5052 Al alloy subjected to a surface severe plastic deformation process," *Acta Materialia*, vol. 52, no. 20, pp. 5771–5782, 2004, ISSN: 13596454. DOI: 10.1016/j.actamat.2004.08.031.

[82] T. Ludian and L. Wagner, "Coverage effects in shot peening of al 2024-T4," in *ICSP9 the 9th International Conference on Shot Peening*, Paris, 2005, pp. 296–301. DOI: EC36BFBC14F384079B57CFAA4225068D.

[83] G. H. Farrahi, J. L. Lebrijn, and D. Couratin, "Effect of Shot Peening on Residual Stress and Fatigue Life of a Spring Steel," *Fatigue & Fracture of Engineering Materials & Structures*, vol. 18, pp. 211–220, 1995, ISSN: 14602695. DOI: 10.1111/j.1460-2695.1995.tb00156.x.

[84] P. S. Prevey and J. T. Cammett, "The Effect of Shot Peening Coverage on Residual Stress, Cold Work and Fatigue in a Ni-Cr-Mo Low Alloy Steel," in *ICSP8 the 8th International Conference on Shot Peening*, Munchen, 2002. DOI: 10.1002/3527606580.ch37.

[85] A. Ghasemi, S. M. Hassani-Gangaraj, A. H. Mahmoudi, G. H. Farrahi, and M. Guagliano, "Shot peening coverage effect on residual stress profile by FE random impact analysis," *Surface Engineering*, vol. 32, no. 11, pp. 861–870, 2016, ISSN: 17432944. DOI: 10.1080/02670844.2016.1192336.

[86] S. Bagherifard, R. Ghelichi, and M. Guagliano, "A numerical model of severe shot peening (SSP) to predict the generation of a nanostructured surface layer of material," *Surface and Coatings Technology*, vol. 204, no. 24, pp. 4081–4090, 2010, ISSN: 02578972. DOI: 10.1016/j.surfcoat.2010.05.035. [Online]. Available: http://dx.doi.org/10.1016/j.surfcoat.2010.05.035.

[87] S. M. Hassani-Gangaraj, M. Guagliano, and G. H. Farrahi, "Finite element simulation of shot peening coverage with the special attention on surface nanocrystallization," *Procedia Engineering*, vol. 10, pp. 2464–2471, 2011, ISSN: 18777058. DOI: 10.1016/j.proeng.2011.04.406. [Online]. Available: http://dx.doi.org/10.1016/j.proeng.2011.04.406.

[88] M. Avrami, "Kinetics of phase change. I: General theory," *The Journal of Chemical Physics*, vol. 7, no. 12, pp. 1103–1112, 1939, ISSN: 00219606. DOI: 10.1063/1.1750380.

[89] M. Avrami, "Kinetics of phase change. II Transformation-time relations for random distribution of nuclei," *The Journal of Chemical Physics*, vol. 8, no. 2, pp. 212–224, 1940, ISSN: 00219606. DOI: 10.1063/1.1750631.

[90] S. Karuppanan, J. S. Romero, E. R. de los Rios, C. Rodopoulos, and A. Levers, "A Theoretical and Experimental Investigation into the Development of Coverage in Shot Peening," in *Shot Peening*, L. Wagner, Ed., Wiley-VCH Verlag GmbH & Co. KGaA, 2003, pp. 101–107, ISBN: 3527305378. DOI: 10.1002/3527606580.ch14.

[91] S. Bagherifard, R. Ghelichi, and M. Guagliano, "On the shot peening surface coverage and its assessment by means of finite element simulation: A critical review and some original developments," *Applied Surface Science*, vol. 259, pp. 186–194, 2012, ISSN: 01694332. DOI: 10.1016/j.apsusc.2012.07.017. [Online]. Available: http://dx.doi.org/10.1016/j.apsusc.2012.07.017.

[92] P. Sanjurjo, C. Rodríguez, I. Peñuelas, T. E. García, F. J. Belzunce, P. Sanjurjo, C. Rodríguez, T. E. García, and F. J. Belzunce, "Influence of the target material constitutive model on the numerical simulation of a shot peening process," *Surface and Coatings Technology*, vol. 258, pp. 822–831, 2014, ISSN: 02578972. DOI: 10.1016/j.surfcoat.2014.07.075. [Online]. Available: https://doi.org/10.1016/j.surfcoat.2014.07.075.

[93] S. A. Meguid and M. S. Klair, "An examination of the relevance of co-indentation studies to incomplete coverage in shot-peening using the finite-element method," *Journal of Mechanical Working Technology*, vol. 11, pp. 87–104, 1985, ISSN: 03783804. DOI: 10.1016/0378-3804(85)90114-7.

[94] M. T. Khabou, L. Castex, and G. Inglebert, "The effect of material behaviour law on the theoretical shot peening results," *European Journal of Mechanics - A/Solids*, vol. 9, pp. 1–20, 1990.

[95] Y. F. Al-Obaid, "Three-Dimensional Dynamic Finite Element Analysis for Shot-Peening Mechanics," *Computers and Structures*, vol. 36, no. 4, pp. 681–689, 1990.

[96] M. Guagliano, L. Vergani, M. Bandini, and F. Gili, "An approach to relate the shot peening parameters to the induced residual stresses," in *ICSP7 the 7th International Conference on Shot Peening*, Warsaw: Institute of Precision Mechanics, 1999, pp. 274–282.

[97] S. A. Meguid, G. Shagal, and J. C. Stranart, "Finite element modelling of shot-peening residual stresses," *Journal of Materials Processing Technology*, vol. 92-93, pp. 401–404, 1999, ISSN: 09240136. DOI: 10.1016/S0924-0136(99)00153-3.

[98] S. A. Meguid, G. Shagal, J. C. Stranart, and J. Daly, "Three-dimensional dynamic finite element analysis of shot-peening induced residual stresses," *Finite Elements in Analysis and Design*, vol. 31, no. 3, pp. 179–191, 1999, ISSN: 0168-874X. DOI: 10.1016/S0168-874x(98)00057-2. [Online]. Available: http://www.sciencedirect.com/science/article/pii/S0168874X98000572.

[99] S. A. Meguid, G. Shagal, and J. C. Stranart, "3D FE analysis of peening of strain-rate sensitive materials using multiple impingement model," *International Journal of Impact Engineering*, vol. 27, no. 2, pp. 119–134, 2002, ISSN: 0734743X. DOI: 10.1016/S0734-743X(01)00043-4.

[100] J. Schwarzer, V. Schulze, and O. Vöhringer, "Evaluation of the influence of shot peening parameters on residual stress profiles using finite element simulation," *Materials Science Forum*, vol. 426-432, no. 5, pp. 3951–3956, 2003, ISSN: 02555476. DOI: 10.4028/www.scientific.net/msf.426-432.3951.

[101] G. H. Majzoobi, R. Azizi, and A. Alavi Nia, "A three-dimensional simulation of shot peening process using multiple shot impacts," *Journal of Materials Processing Technology*, vol. 164-165, pp. 1226–1234, 2005, ISSN: 09240136. DOI: 10.1016/j.jmatprotec.2005.02.139.

[102] M. Frija, T. Hassine, R. Fathallah, C. Bouraoui, and A. Dogui, "Finite element modelling of shot peening process: Prediction of the compressive residual stresses, the plastic deformations and the surface integrity," *Materials Science and Engineering A*, vol. 426, no. 1-2, pp. 173–180, 2006, ISSN: 09215093. DOI: 10.1016/j.msea.2006.03.097.

[103] S. A. Meguid, G. Shagal, and J. C. Stranart, "Development and validation of novel FE models for 3D analysis of peening of strain-rate sensitive materials," *Journal of Engineering Materials and Technology, Transactions of the ASME*, vol. 129, no. 2, pp. 271–283, 2007, ISSN: 00944289. DOI: 10.1115/1.2712469. [Online]. Available: http://www.scopus.com/inward/record.url?eid=2-s2.0-34249872488%7B%5C&%7DpartnerID=40%7B%5C&%7Dmd5=12c3014bc9e70064a2a934ab8a48cf4c.

[104] T. Hong, J. Y. Ooi, and B. A. Shaw, "A numerical study of the residual stress pattern from single shot impacting on a metallic component," *Advances in Engineering Software*, vol. 39, no. 9, pp. 743–756, 2008, ISSN: 09659978. DOI: 10.1016/j.advengsoft.2007.10.002.

[105] M. Klemenz, V. Schulze, I. Rohr, and D. Löhe, "Application of the FEM for the prediction of the surface layer characteristics after shot peening," *Journal of Materials Processing Technology*, vol. 209, no. 8, pp. 4093–4102, 2009, ISSN: 09240136. DOI: 10.1016/j.jmatprotec.2008.10.001.

[106] T. Kim, J. H. Lee, H. Lee, and S. kyun Cheong, "An area-average approach to peening residual stress under multi-impacts using a three-dimensional symmetry-cell finite element model with plastic shots," *Materials and Design*, vol. 31, no. 1, pp. 50–59, 2010, ISSN: 02641275. DOI: 10.1016/j.matdes.2009.07.032. [Online]. Available: http://dx.doi.org/10.1016/j.matdes.2009.07.032.

[107] M. Zimmermann, V. Schulze, and J. Hoffmeister, "Finite element modelling of coverage effects during shot peening of IN718," *International Journal of Materials Research*, vol. 101, no. 8, pp. 951–962, 2010, ISSN: 18625282. DOI: 10.3139/146.110375.

[108] B. Bhuvaraghan, S. M. Srinivasan, B. Maffeo, R. D. McClain, Y. Potdar, and O. Prakash, "Shot peening simulation using discrete and finite element methods," *Advances in Engineering Software*, vol. 41, no. 12, pp. 1266–1276, 2010, ISSN: 09659978. DOI: 10.1016/j.advengsoft.2010.09.003. [Online]. Available: http://dx.doi.org/10.1016/j.advengsoft.2010.09.003.

[109] B. Bhuvaraghan, S. M. Srinivasan, and B. Maffeo, "Numerical simulation of Almen strip response due to random impacts with strain-rate effects," *International Journal of Mechanical Sciences*, vol. 53, no. 6, pp. 417–424, 2011, ISSN: 00207403. DOI: 10.1016/j.ijmecsci.2011.03.004. [Online]. Available: http://dx.doi.org/10.1016/j.ijmecsci.2011.03.004.

[110] G. I. Mylonas and G. Labeas, "Numerical modelling of shot peening process and corresponding products: Residual stress, surface roughness and cold work prediction," *Surface and Coatings Technology*, vol. 205, no. 19, pp. 4480–4494, 2011, ISSN: 02578972. DOI: 10.1016/j.surfcoat.2011.03.080. [Online]. Available: http://dx.doi.org/10.1016/j.surfcoat.2011.03.080.

[111] A. Gariépy, S. Larose, C. Perron, and M. Lévesque, "Shot peening and peen forming finite element modelling - Towards a quantitative method," *International Journal of Solids and Structures*, vol. 48, pp. 2859–2877, 2011, ISSN: 00207683. DOI: 10.1016/j.ijsolstr.2016.01.012.

[112] T. Kim, H. Lee, S. Jung, and J. H. Lee, "A 3D FE model with plastic shot for evaluation of equi-biaxial peening residual stress due to multi-impacts," *Surface and Coatings Technology*, vol. 206, no. 13, pp. 3125–3136, 2012, ISSN: 02578972. DOI: 10.1016/j.surfcoat.2011.12.042. [Online]. Available: http://dx.doi.org/10.1016/j.surfcoat.2011.12.042.

[113] A. Gariépy, S. Larose, C. Perron, P. Bocher, and M. Lévesque, "On the effect of the peening trajectory in shot peen forming," *Finite Elements in Analysis and Design*, vol. 69, pp. 48–61, 2013, ISSN: 0168874X. DOI: 10.1016/j.finel.2013.02.003.

[114] C. Nouguier-Lehon, M. Zarwel, C. Diviani, D. Hertz, H. Zahouani, and T. Hoc, "Surface impact analysis in shot peening process," *Wear*, vol. 302, no. 1-2, pp. 1058–1063, 2013, ISSN: 00431648. DOI: 10.1016/j.wear.2012.11.031. [Online]. Available: http://dx.doi.org/10.1016/j.wear.2012.11.031.

[115] V. B. Nguyen, H. J. Poh, and Y. W. Zhang, "Predicting shot peening coverage using multiphase computational fluid dynamics simulations," *Powder Technology*, vol. 256, pp. 100–112, 2014, ISSN: 00325910. DOI: 10.1016/j.powtec.2014.01.097.

[116] F. Yang, Z. Chen, and S. A. Meguid, "3D FE modeling of oblique shot peening using a new periodic cell," *International Journal of Mechanics and Materials in Design*, vol. 10, no. 2, pp. 133–144, 2014, ISSN: 15691713. DOI: 10.1007/s10999-013-9236-8.

[117] S. M. Hassani-Gangaraj, M. Guagliano, and G. H. Farrahi, "An approach to relate shot peening finite element simulation to the actual coverage," *Surface and Coatings Technology*, vol. 243, pp. 39–45, 2014, ISSN: 02578972. DOI: 10.1016/j.surfcoat.2012.03.057. [Online]. Available: http://dx.doi.org/10.1016/j.surfcoat.2012.03.057.

[118] S. Bagherifard, R. Ghelichi, and M. Guagliano, "Mesh sensitivity assessment of shot peening finite element simulation aimed at surface grain refinement," *Surface and Coatings Technology*, vol. 243, pp. 58–64, 2014, ISSN: 02578972. DOI: 10.1016/j.surfcoat.2012.04.002. [Online]. Available: http://dx.doi.org/10.1016/j.surfcoat.2012.04.002.

[119] K. Murugaratnam, S. Utili, and N. Petrinic, "A combined DEM-FEM numerical method for Shot Peening parameter optimisation," *Advances in Engineering Software*, vol. 79, pp. 13–26, 2015, ISSN: 18735339. DOI: 10.1016/j.advengsoft.2014.09.001. [Online]. Available: http://dx.doi.org/10.1016/j.advengsoft.2014.09.001.

[120] M. Jebahi, A. Gakwaya, J. Lévesque, O. Mechri, and K. Ba, "Robust methodology to simulate real shot peening process using discrete-continuum coupling method," *International Journal of Mechanical Sciences*, vol. 107, pp. 21–33, 2016, ISSN: 00207403. DOI: 10.1016/j.ijmecsci.2016.01.005.

[121] D. Gallitelli, V. Boyer, M. Gelineau, Y. Colaitis, E. Rouhaud, D. Retraint, R. Kubler, M. Desvignes, and L. Barrallier, "Simulation of shot peening: From process parameters to residual stress fields in a structure," *Comptes Rendus - Mecanique*, vol. 344, no. 4-5, pp. 355–374, 2016, ISSN: 16310721. DOI: 10.1016/j.crme.2016.02.006. [Online]. Available: http://dx.doi.org/10.1016/j.crme.2016.02.006.

[122] M. Benedetti, V. Fontanari, B. Winiarski, M. Allahkarami, and J. Hanan, "Residual stresses reconstruction in shot peened specimens containing sharp and blunt notches by experimental measurements and finite element analysis," *International Journal of Fatigue*, vol. 87, pp. 102–111, Jun. 2016, ISSN: 01421123. DOI: 10.1016/j.ijfatigue.2016.01.020. [Online]. Available: http://dx.doi.org/10.1016/j.ijfatigue.2016.01.020%20https://linkinghub.elsevier.com/retrieve/pii/S014211231600030X.

[123] B. Winiarski, M. Benedetti, V. Fontanari, M. Allahkarami, J. C. Hanan, and P. J. Withers, "High Spatial Resolution Evaluation of Residual Stresses in Shot Peened Specimens Containing Sharp and Blunt Notches by Micro-hole Drilling, Micro-slot Cutting and Micro-X-ray Diffraction Methods," *Experimental Mechanics*, vol. 56, no. 8, pp. 1449–1463, 2016, ISSN: 0014-4851. DOI: 10.1007/s11340-016-0182-x. [Online]. Available: http://dx.doi.org/10.1007/s11340-016-0182-x.

[124] M. Marini, V. Fontanari, M. Bandini, and M. Benedetti, "Surface layer modifications of micro-shot-peened Al-7075-T651: Experiments and stochastic numerical simulations," *Surface & Coatings Technology*, vol. 321, pp. 265–278, 2017, ISSN: 0257-8972. DOI: 10.1016/j.surfcoat.2017.04.054. [Online]. Available: http://dx.doi.org/10.1016/j.surfcoat.2017.04.054.

[125] J. K. Li, Y. Mei, W. Duo, and W. Renzhi, "an Analysis of Stress Concentrations Caused By Shot Peening and Its Application in Predicting Fatigue Strength," *Fatigue & Fracture of Engineering Materials & Structures*, vol. 15, no. 12, pp. 1271–1279, 1992, ISSN: 14602695. DOI: 10.1111/j.1460-2695.1992.tb01262.x.

[126] M. G. Moore and W. P. Evans, "Mathematical Correction for Stress in Removed Layers in X-Ray Diffraction Residual Stress Analysis," *SAE Transactions*, vol. 66, pp. 340–345, 1958, ISSN: 0096736X, 25771531. [Online]. Available: http://www.jstor.org/stable/44554157.

[127] I. C. Noyan and J. B. Cohen, *Residual stress*. New York: Springer, 2013.

[128] W. Lee, W. Sue, C. Lin, and C. Wu, "The strain rate and temperature dependence of the dynamic impact properties of aluminum alloy," *Journal of Materials Processing Technology*, vol. 100, pp. 116–122, 2000.

[129] L. Schwer, "Optional Strain-Rate Forms for the Johnson Cook Constitutive Model and the Role of the Parameter Epsilon_01," in *6th European LS-DYNA Users' Conference*, Gothenburg, Sweden: Livermore Software Technology Coporation (LSTC), 2007, pp. 1–17. [Online]. Available: http://www.dynalook.com/european-conf-2007/optional-strain-rate-forms-for-the-johnson-cook.pdf.

[130] N. S. Brar, V. S. Joshi, and B. W. Harris, "Constitutive model constants for Al7075-T651 and Al7075-T6," in *AIP Conference Proceedings*, vol. 1195, American Institute of Physics, 2009, pp. 945–948, ISBN: 9780735407329. DOI: 10.1063/1.3295300.

[131] M. Worsham, A. Kurtz, A. D. Shirley, and X. Xiao, "Hypervelocity Impact of Spaced Plates: Simulation and Comparison to Data," in *2010 IMPLAST Conference*, Providence, Rhode Island: Society for Experimental Mechanics, 2010.

[132] J. R. Pothnis, Y. Perla, H. Arya, and N. K. Naik, "High Strain Rate Tensile Behavior of Aluminum Alloy 7075 T651 and IS 2062 Mild Steel," *Journal of Engineering Materials and Technology*, vol. 133, no. 2, p. 021 026, 2011, ISSN: 00944289. DOI: 10.1115/1.4003113.

[133] K. C. Jørgensen and V. Swan, "Modeling of Armour-piercing Projectile Perforation of Thick Aluminium Plates," in *13th International LS-DYNA Users Conference*, Detroit, Michigan: Livermore Software Technology Coporation (LSTC), 2014, pp. 1–15.

[134] D. N. Zhang, Q. Q. Shangguan, C. J. Xie, and F. Liu, "A modified Johnson-Cook model of dynamic tensile behaviors for 7075-T6 aluminum alloy," *Journal of Alloys and Compounds*, vol. 619, pp. 186–194, 2015, ISSN: 09258388. DOI: 10.1016/j.jallcom.2014.09.002. [Online]. Available: http://dx.doi.org/10.1016/j.jallcom.2014.09.002.

[135] M. Klemenz, T. Hochraine, L. Delonnoy, V. Schulze, O. Vohringer, and P. Gumbsch, "Similarity rules for the shot peening process based on finite element simulations," in *ICSP9 the 9th International Conference on Shot Peening*, Paris, 2005, pp. 94–99. DOI: 8ACEB7425C23D33B8361F41E2D79E87F.

[136] M. Zimmermann, V. Schulze, H. U. Baron, and D. Löhe, "A Novel 3D Finite Element Simulation Model for the Prediction of the Residual Stress State after Shot Peening," in *ICSP10 the 10th International Conference on Shot Peening*, Tokyo, Japan, 2008, pp. 63–68.

[137] F. Tu, D. Delbergue, H. Miao, T. Klotz, M. Brochu, P. Bocher, and M. Levesque, "A sequential DEM-FEM coupling method for shot peening simulation," *Surface & Coatings Technology*, vol. 319, pp. 200–212, 2017, ISSN: 0257-8972. DOI: 10.1016/j.surfcoat.2017.03.035. [Online]. Available: http://dx.doi.org/10.1016/j.surfcoat.2017.03.035.

[138] J. Lemaitre and J. L. Chaboche, *Mechanics of solid materials*. Cambridge, UK: Cambridge University Press, 1990, ISBN: 0521477581. DOI: 10.1139/l92-025.

[139] J. Lemaitre, *A Course on Damage Mechanics*, 2nd. Berlin,Germany: Springer-Verlag Berlin Heidelberg GmbH, 1998, ISBN: 9783540609803.

[140] E. H. Dill, *Continuum Mechanics: Elasticity, Plasticity, Viscoelasticity*. Boca Raton, Florida: CRC Press, 2013, ISBN: 9788578110796. DOI: 10.1017/CBO9781107415324.004. arXiv: arXiv:1011.1669v3.

[141] P. Mann, H. Y. Miao, A. Garie, R. R. Chromik, and M. Le, "Residual stress near single shot peening impingements determined by nanoindentation and numerical simulations," *Journal of Material Science*, vol. 50, pp. 2284–2297, 2015. DOI: 10.1007/s10853-014-8792-0.

[142] P. J. Blau, *Friction Science and Technology from concepts to applications*, 2nd ed. Boca Raton, Florida: CRC Press, 2008, ISBN: 9788578110796. DOI: 10.1017/CBO9781107415324.004. arXiv: arXiv:1011.1669v3.

[143] J. P. Davim, E. Santos, C. Pereira, and J. Ferreira, "Comparative study of friction behaviour of alumina and zirconia ceramics against steel under water lubricated conditions," *Industrial Lubrication and Tribology*, vol. 60, no. 4, pp. 178–182, 2008, ISSN: 0036-8792. DOI: 10.1108/00368790810881515. [Online]. Available: http://www.emeraldinsight.com/10.1108/00368790810881515.

[144] R. Menig, L. Pintschovius, V. Schulze, and O. Vöhringer, "Depth profiles of macro residual stresses in thin shot peened steel plates determined by X-ray and neutron diffraction," *Scripta Materialia*, vol. 45, no. 8, pp. 977–983, 2001, ISSN: 13596462. DOI: 10.1016/S1359-6462(01)01063-6.

[145] L. Susmel and D. Taylor, "The theory of critical distances to predict static strength of notched brittle components subjected to mixed-mode loading," *Engineering Fracture Mechanics*, vol. 75, no. 3-4, pp. 534–550, 2008, ISSN: 00137944. DOI: 10.1016/j.engfracmech.2007.03.035.

[146] L. Susmel and D. Taylor, "The theory of critical distances to estimate finite lifetime of notched components subjected to constant and variable amplitude torsional loading," *Engineering Fracture Mechanics*, vol. 98, no. 1, pp. 64–79, 2013, ISSN: 00137944. DOI: 10.1016/j.engfracmech.2012.12.007. [Online]. Available: http://dx.doi.org/10.1016/j.engfracmech.2012.12.007.

[147] M. Marini, F. Piona, V. Fontanari, M. Bandini, and M. Benedetti, "A new challenge in the DEM / FEM simulation of the shot peening process: The residual stress field at a sharp edge," *International Journal of Mechanical Sciences*, vol. 169, 2020, ISSN: 0020-7403. DOI: 10.1016/j.ijmecsci.2019.105327. [Online]. Available: https://doi.org/10.1016/j.ijmecsci.2019.105327.

[148] V. Smilauer, E. Catalano, B. Chareyre, and S. Dorofeenko, *Yade Documentation, 2nd edn*, 2020.

[149] A. Gariépy, H. Y. Miao, and M. Lévesque, "Simulation of the shot peening process with variable shot diameters and impacting velocities," *Advances in Engineering Software*, vol. 114, pp. 121–133, 2017, ISSN: 18735339. DOI: 10.1016/j.advengsoft.2017.06.011.

[150] P. J. Blau and C. E. Devore, "Interpretations of the sliding friction break-in curves of alumina-aluminum couples," *Wear*, vol. 129, no. 1, pp. 81–92, 1989, ISSN: 00431648. DOI: 10.1016/0043-1648(89)90281-0.

[151] T. Klotz, M. Lévesque, and M. Brochu, "Effects of rolled edges on the fatigue life of shot peened Inconel 718," *Journal of Materials Processing Technology*, vol. 263, pp. 276–284, 2019, ISSN: 09240136. DOI: 10.1016/j.jmatprotec.2018.08.019. [Online]. Available: https://doi.org/10.1016/j.jmatprotec.2018.08.019.

Ringraziamenti

A Matteo Benedetti e Vigilio Fontanari, i miei supervisori, va un ringraziamento particolare per avermi da subito gratificato della loro immeritata stima, benevolenza e simpatia, ricambiate da un affetto sincero e duraturo. La mia gratitudine va anche a Francesco Piona, senza il quale una sostanziosa parte di questo lavoro non avrebbe avuto corpo, e che è stato un collaboratore prezioso e prolifico.
A Michele Dallago, compagno di questo percorso di dottorato, un abbraccio ricolmo di amicizia e riconoscenza.
Voglio menzionare Michele Bandini e Mario Guagliano, la cui presenza e sostegno al mio esordio in una conferenza sono state fonte di incoraggiamento nel corso di tutto il lavoro.
Grazie a Matteo, Michele, Andrea, perché mi hanno dimostrato il valore della perseveranza, del lavoro e, quando serve, della leggerezza.
Ai docenti e ai collaboratori del Dipartimento, in particolare ai metallurgisti, sono cordialmente grato per avermi fatto sentire membro di un corpus di cui è un onore e un privilegio fare parte.
A Diego, grazie per avermi insegnato tante cose.
Ai colleghi, tutti, un pensiero un po' commosso: a Matteo, Marco, Silvia, Enrico, Mara, Giulia, Matteo, Francesca, Priya, Sunil, Ana, Daniel, Balanand, Michele, Alberto, Stefano, in ordine sparso. A loro, che hanno più strettamente condiviso questa esperienza con me.
Da ultimi, i più importanti. Ai miei cari: a mia madre Giovanna, a mio fratello Guido, soprattutto a Martina. Grazie, perché solo insieme a voi ho potuto farlo.
A chi ha letto fino a qui, grazie.